Glycogen regulates cellular proliferation in the context of aging, tumorigenesis, and hepatic regeneration

Claire-Alix Zapata Garin

Glycogen regulates cellular proliferation in the context of aging, tumorigenesis, and hepatic regeneration

Claire-Alix Zapata Garin

DOCTORAL THESIS / YEAR 2018

THESIS SUPERVISOR
Dr. Joan J. Guinovart

Department Molecular Medicine Research Program
Institute for Research in Biomedicine

Contents

Part I

Abbreviations

3T3	3 day transfer protocol
ADP	adenosine diphosphate
AKT	protein kinase B
AMP	adenosine monophosphate
AMPK	AMP-activated protein kinase
ATM	ataxia telangiectasia mutated
ATP	adenosine triphosphate
ATR	ataxia telangiectasia and Rad3-related protein
BGP	brain glycogen phosphorylase
BrdU	bromodeoxyuridine
CaM-PK	calmodulin and protein kinase C
CDKN2A	cyclin dependent kinase inhibitor 2A
CHK1/2	checkpoint kinase 1/2
DDR	DNA damage response
DEN	N-nitrosodiethylamine
DMEM	Dulbecco's Modified Eagle's medium
DNA	deoxyribonucleic acid
dpc	days post coitum
DSB	double stranded breaks
ECM	extracellular matrix
ER	endoplasmic reticulum
ETC	electron transport chain
FBS	fetal bovine serum
FOXO	Forkhead box O
FRTA	Free Radical Theory of Aging
G1	gap 1 phase (cell cycle)
G1P	glucose-1-phosphate

G6P	glucose-6-phosphate
GAA	alpha acid glycosidase
GAPDH	glyceraldehyde 3-phosphate dehydrogenase
GBE	glycogen branching enzyme
GDE	glycogen debranching enzyme
GK	glucokinase
GLUT	glucose transporter
GP	glycogen phosphorylase
GS	glycogen synthase
GSD	glycogen storage disease
GSK3	glycogen synthase kinase 3
GSH	glutathione
GSSG	glutathione disulfide
GYG	glycogenin
GYS1	muscle glycogen synthase, gene
GYS2	liver glycogen synthase, gene
H_2DCFDA	2',7'-dichlorodihydrofluorescein diacetate
HCC	hepatocellular carcinoma
HDAi	histone deacetylase inhibitor
HIF-1-alpha	hypoxia-inducible factor 1-alpha
HK	hexokinase
IGF-1	insulin-like growth factor 1
IIS	insulin and IGF-1 signaling pathway
HLF-1	human lung fibroblasts
KO	knockout
LGP	liver glycogen phosphorylase
LGS	liver glycogen synthase
MAPK	mitogen-activated protein kinase
MEF	mouse embryonic fibroblasts
MFI	mean fluorescence intensity
MGP	muscle glycogen phosphorylase
MGS	muscle glyogen synthase
mtDNA	mitochondrial DNA
mTOR	mechanistic target of rapamycin
NADH	nicotinamide adenine dinucleotide
NADPH	nicotinamide adenine dinucleotide phosphate
OIS	oncogene-induced senescence
OXPHOS	oxidative phosphorylation
PAS	Periodic Acid-Schiff stain
PBS	phosphate buffer solution
PCR	polymerase chain reaction

PDK1	pyruvate dehydrogenase kinase 1
Pen/Strep	penicillin streptomycin
PGM	phosphoglucomutase
PHK	phosphorylase kinase
Phx	partial hepatectomy
PI3K	phosphoinositide 3-kinase
PKA	cAMP-dependent protein kinase
PP1	protein phosphatase 1
PPP	pentose phosphate pathway
PTEN	phosphatase and tensin homolog
PTG	protein targeting to glycogen
Rb	Retinoblastoma protein
RNA	ribonucleic acid
ROS	reactive oxygen species
Ru5P	ribulose-5-phosphate
S	synthesis phase (cell cycle)
s.e.m	standard error of the mean
SA-B-Gal	senescence-associated beta galatosidase
SASP	senescence-associated secretory phenotype
siRNA	short interfering RNA
SMAD	similar to mothers against decapentaplegic
STBD1	starch binding domain-containing protein 1
TCA	tricarboxylic acid cycle
TGF-b	transforming growth factor beta
UDP	uridine diphosphate
UGP	UDP-glucose pyrophosphatase
UTP	uridine triphosphate
VHL	Von Hippel-Lindau tumor suppressor
WT	wild type

Part II

Introduction

Chapter 1

Glycogen metabolism

Brief Introduction

Metabolism is the way living organisms can extract usable energy from their environment. More specifically, energy metabolism refers to the act of generating energy in the form of ATP from available nutrients. Metabolism can either be catabolic, which refers to the breakdown of matter, or anabolic where specific nutrients, such as proteins, are generated.

Glucose metabolism, in particular, is a set of biochemical reactions which involve the manipulation of glucose. Glucose, an essential energy source for most living organisms, is a simple sugar that acts as the main energy substrate for cells. Glucose is obtained from our food, which is broken down by our digestive system and incorporated into our bloodstream, where it can then circulate around to body.

Cells can make use of this circulating blood glucose by uptaking it through specific glucose transporters present in the plasma membrane. Once inside the cell, glucose is phosphorylated to glucose-6-phosphate (G6P) by hexokinase (HK). This step is essential as it traps glucose within cells: G6P can no longer diffuse back out of the cell due to the addition of the charged phosphate group. It

is important to mention that G6P can also be produced through a process in the liver termed gluconeogenesis, which involves the formation of glucose from non-carbohydrate carbon substrates (i.e. lactate).

G6P lies at the crossroads of three major branches of glucose metabolism: glycolysis, pentose phosphate pathway (PPP), and glycogen metabolism (Figure 1.1). Glycolysis is an oxygen independent pathway that converts glucose into pyruvate, ATP and NADH. Pyruvate can then either continue on to lactic acid fermentation or the tricarboxylic acid cycle (TCA), also known as the Krebs cycle. The second possible fate of G6P is its incorporation into the PPP, thereby producing pentoses, ribose 5-phosphates, and NADPH. This pathway is mainly anabolic and is fundamental to provide precursors for DNA and RNA synthesis, in addition to reducing power in the form of NADPH. The last possible fate of G6P is its incorporation into glycogen, the main glucose depot in the body and focus of this thesis.

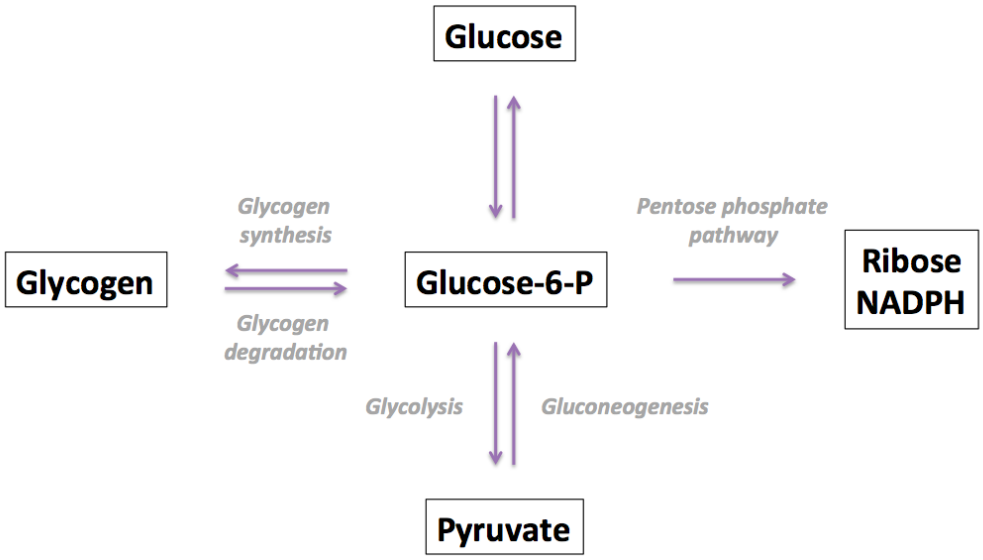

Figure 1.1: **Possible fates of glucose in the cell.** There are three possible fates for glucose once it is phosphorylated to glucose-6-phosphate: incorporation into the glycolysis pathway, pentose phosphate pathway or glycogen pathway.

1.1 Basics of glycogen metabolism

Glycogen is a highly branched polysaccharide of D-glucose units present in the cytosol, from which glucose can be rapidly released in case of demand. It serves as the main carbohydrate reserve in the human body, where the largest stores are found in the liver and skeletal muscle. In the postprandial liver, glycogen makes up about 100 grams of the total hepatic mass, whereas in the muscle, 400 grams are attributable to glycogen. In other words, glycogen makes up about 6-8% of total hepatic mass, and 1-2% of total skeletal muscle mass [Champe and Harvey, 1994]. Furthermore, glycogen plays a different role in either tissue: liver glycogen regulates and maintains blood glucose homeostasis, while muscle glycogen is consumed during muscular contraction.

Besides the well defined roles of glycogen in the liver and skeletal muscle, it is important to note that glycogen has also been described in minute quantities in the brain, in both astrocytes and neurons. Cerebral glycogen has been estimated to make up about 0.1% of the brain's total mass, or about 0.5 to 1.5 grams [Brown, 2004]. Originally, it was thought that the glycogen present in the brain was used during stress conditions, such as hypoglycemia or ischemia [Obel et al., 2012]. However, it is becoming increasingly clear that cerebral glycogen is highly dynamic and participates in important activities in the brain such as long-term memory formation, synaptic activity and tolerance to hypoxia [Gibbs et al., 2006, Duran et al., 2013, Saez et al., 2014].

There are clear advantages to storing excess glucose in the form of glycogen in the cytosol: 1) it accumulates intracellularly without increasing the osmotic pressure within the cell, 2) it provides a mean of stabilizing glucose levels within the body, 3) it is rapidly metabolized without ATP consumption, and 4) contrary to fatty acids, it can be used as an energy source in anaerobic conditions. Some of the aforementioned advantages of glycogen relate to its intricately branched structure, rendering it a dynamic molecule capable of rapidly responding to the cell's needs.

The glucose units in the linear glycogen sections are bound by alpha-1,4, glycosidic bonds. Every 8-12 glucose residues, however, alpha-1,6 branching points are introduced in order to give glycogen its characteristic branched spherical structure (Figure 1.2). Glycogen ramification increases the macromolecule's solubility within the cell, and allows for rapid glycogen degradation by introducing many non-reducing ends from which glucose units can be released. The actual size and weight of the glycogen molecule is variable, and can grow until reaching its steric

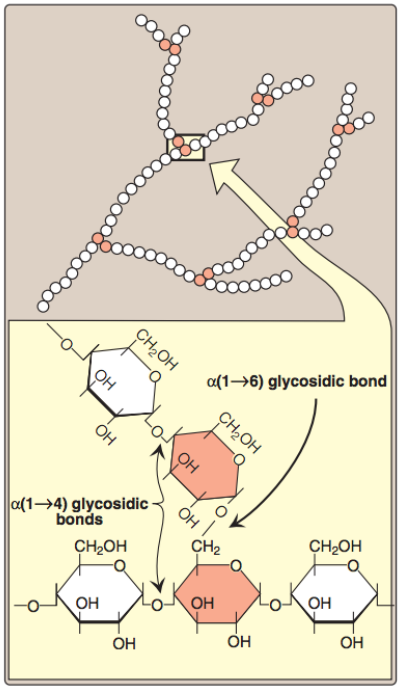

Figure 1.2: **Schematic representation of glycogen structure.** Linear segments of glycogen are formed by alpha-1,4 glycosidic bonds, whereas branching points originate from alpha-1,6 glycosidic bonds. Adapted from [Champe and Harvey, 1994]

.

limits, referred to as a beta particle [Meléndez et al., 1998]. In the liver, beta particles can further aggregate with one another in order to form alpha rosettes, which are about five times the size of a single beta particle [Sullivan et al., 2012].

Besides the glucose, which make up the bulk of the polysaccharide, glycogen has its own proteome which is composed of associated proteins that act to regulate certain aspects of glycogen, including structure, size and cellular localization. Enzymes that make up the glycogen-associated proteome include glycogen synthase (GS), glycogen phosphorylase (GP), glycogen branching enzyme (GBE), glycogen debranching enzyme (GDE), glycogenin (GYG), among others [Stapleton et al., 2010].

Covalently bound phosphate is also present in glycogen, and occurs about every 600-1500 glucose residue in the skeletal muscle glycogen [Tagliabracci et al., 2007, Tagliabracci et al., 2008]. Although the function and origin of this modification is unknown, it is thought to be a catalytic error which is resolved by the action of a specific phosphatase, Laforin [Tagliabracci et al., 2011]. The superfluous phosphates have been linked to decreased glycogen solubility and increased cytoplasmic levels, both of which occur in Lafora disease, an autosomal recessive neurodegenerative disease [Shahwan et al., 2005].

Besides Laforin, mutations in Malin, a E3 ubiquitin ligase, can also lead to Lafora disease. It has been suggested that Malin forms a complex with Laforin, thereby promoting the ubiquitination of certain proteins involved in the glycogen metabolism pathway [Romá-Mateo et al., 2012]. Dysregulation of this ubiquitination process is believed to lead to Lafora body (LB) formation which are insoluble polyglucosan inclusions present in the brain and other affected tissues.

1.2 Glycogen synthesis

Once glucose enters the cell through tissue-specific glucose transporters (GLUTs) and is phosphorylated to G6P by hexokinase (HK), G6P is isomerized to glucose-1-phosphate (G1P) by the action of phosphoglucomutase (PGM). Next, G1P reacts with UTP, catalyzed by UDP-glucose pyrophosphorylase (UGP) in order to produce UDP-glucose, the glycosyl unit donor. UDP-glucose then participates in the formation of a new alpha-1,4 glycosidic linkage by the action of GS (Figure 1.3).

The formation of a new glycogen granule begins by the action of GYG which transfers the glucose residue from UDP-glucose to a specfic tyrosine on its side

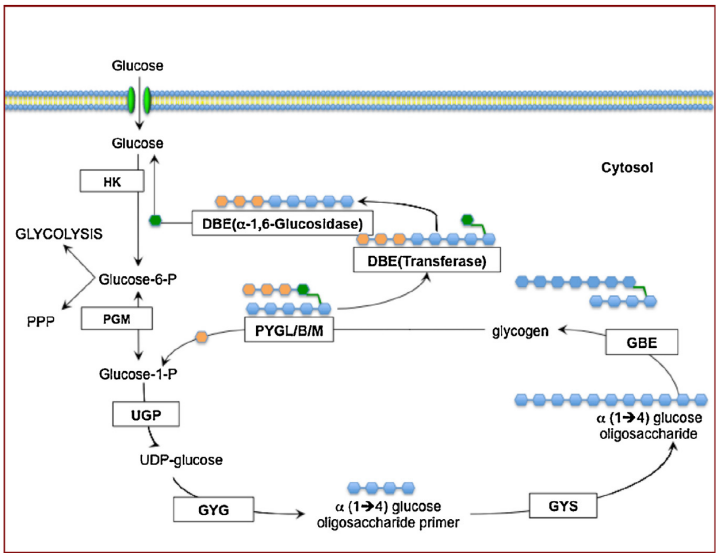

Figure 1.3: **Schematic representation of glycogen metabolism.** **HK**: hexokinase, **PGM**: phosphoglucomutase, **UGP**: UDP-glucose pyrophosphatase, **GYG**: glycogenin, **GYS**: glycogen synthase, **GBE**: glycogen branching enzyme, **PYGL/B/M**: glycogen phosphorylase, liver/brain/muscle, **DBE**: debranching enzyme, **PPP**: pentose phosphate pathway. Adapted from [Zois et al., 2014].

chain. From there, GYG continues to catalyze its proper self-glycosylation until forming an oligomer of about 8 glucose residues. GS then takes over chain elongation by catalyzing the formation of alpha-1,4 glycosidic bonds between the carbon 1 on the glycosyl group of UDP-glucose and the carbon 4 of the glycosyl acceptor on the growing glycogen chain. During glycogen synthesis, UDP is released and recycled back into UTP to restart the process.

If all glucose residues were added to glycogen by GS, linear polymers would ensue, as occurs in plants in the form of amylose. Consequently, the action of GBE is essential to give glycogen its characteristic branched structure in order to increase solubility. Once the linear chain reaches about 12 residues, GBE transfers about half of the residues to an adjacent chain through an alpha-1,6 glycosidic bond between the carbon 1 on the glucose molecule and the carbon 6 of the glucose residue located within the polymer. Ultimately, this creates a branch point which contributes to the elaborate structure of glycogen.

1.3 Glycogen degradation

When glucose is needed in the cell, glycogen can be degraded by the action of glycogen phosphorylase (GP). GP cleaves alpha-1,4 bonds thereby releasing G1P, which can either enter glycolysis or the PPP once converted back to G6P by phosphoglucomutase (PGM). GP only acts on non-reducing ends of a glycogen chain that are at least 4 glucoses away from a branch point. A second enzyme, glycogen debranching enzyme (GDE), is necessary to transfer a trisaccharide from an alpha-1,6 branch point onto an adjacent alpha-1,4 linear chain, leaving a single glucose at the original branch point. GDE then catalyzes the hydrolysis of the remaining glucose, thereby also releasing free glucose.

Glycogen can also be degraded through the less characterized lysosomal pathway in a process termed glycophagy or glycogen autophagy [Zirin et al., 2013], whereby the polysaccharide is transferred to the autophagosome and delivered to the lysosome. Ultimately, alpha-acid glycosidase (GAA) hydrolyzes the glycogen polymer to glucose. It is believed that glycogen is delivered to the lysosomal component by anchoring through the starch binding domain-containing protein 1 (STBD1), a protein recently identified in the glycogen proteome [Stapleton et al., 2010]. Mutations in the GAA gene causes Pompe's disease, also known as glycogen storage disease type II, which is characterized by the accumulation of large lysosomes full of undegraded glycogen. The aberrant lysosomal accumulation of glycogen eventually leads to myopathy, hypotonia, hepatomegaly and cardiac defects [Chen and Weinstein, 2016].

1.4 The regulation of glycogen metabolism

Glycogen synthesis and breakdown are reciprocally regulated as a control mechanism to avoid synthesis occurring at the same time as degradation. The glycogen shunt is an exception to the rule and has been observed in both muscle and brain metabolism [Shulman and Rothman, 2001, Obel et al., 2012].

The mechanisms in place to regulate glycogen metabolism are either through covalent modifications (phosphorylation), allosteric regulation or by the cellular localization of enzymes. Furthermore, differences in regulation exist between different tissue isoforms, most notably muscle and liver isoforms.

1.4.1 Regulation of glycogen synthase

Glycogen synthase is the only enzyme capable of synthesizing glycogen in the body, and two isoforms have been reported: muscle glycogen synthase (MGS) and liver glycogen synthase (LGS). MGS is expressed in most tissues of the body, including the brain, whereas LGS expression is limited to the liver, as the name suggests. Additionally, LGS is about 70% identical to its muscular counterpart. The N- and C- terminal extremes, however, are only about 50% homologous [Ros et al., 2009]. Since GS is the rate limiting enzyme in glycogen synthesis, it is highly regulated through various mechanisms, including through phosphorylation, allosteric regulation and cellular localization.

Regulation by phosphorylation
An important regulatory control of GS is its inactivation by phosphorylation, where in MGS, for instance, nine serine residues are subject to phosphorylation at both the N and C terminals. The phosphorylation of different serine residues leads to inactivation of the enzyme by decreasing its affinity for its substrate: UDP-glucose and its allosteric activator, G6P.

There are various kinases known to participate in GS inactivation by phosphorylating different serines and include calmodulin and protein kinase C (CaM-PK), cAMP-dependent protein kinase (PKA), AMP-activated protein kinase (AMPK), glycogen synthase kinase 3 (GSK3), among others [Zois and Harris, 2016]. By phosphorylating different combination of serine residues, the kinases are able to fine tune the inactivation of GS depending on cellular conditions.

The main enzyme that dephosphorylates GS in order to initiate glycogen synthesis is protein phosphatase 1 (PP1). Simultaneously, PP1 also dephosphorylates GP causing its inactivation in parallel to GS activation. Furthermore, protein targeting to glycogen (PTG) acts as a scaffold by facilitating molecular interactions between PP1 and other regulatory proteins involved in glycogen metabolism, thereby leading to an accumulation of glycogen in the cell [Printen, 1997].

The presence of insulin also plays an important role in regulating glycogen synthesis. In the postprandial state, blood glucose rises which leads to the release of insulin into the circulatory system. Insulin, in turn, binds to its receptor located in the plasma membrane which then activates downstream effectors, eventually stimulating glycogen synthesis through either GSK3 inactivation or by increasing intracellular G6P levels (an allosteric activator of GS) [Bouskila et al., 2008].

Allosteric regulation

Besides phosphorylation, GS activity can also be regulated by allosteric regulation which can either be inhibitory or activating. For instance, nucleotides (i.e. ATP, ADP, AMP and UDP) act as allosteric inhibitors, whereas G6P has been identified as the main activator (Figure 1.4). These allosteric regulators attach to an arginine residue rich region present in human MGS, which corresponds to residues 579, 580, 582, 586, 581 and 588 [Bouskila et al., 2010]. The union between the regulators and the arginine rich region induces a conformational change in MGS, rendering the catalytic center more accessible, thereby favoring synthesis.

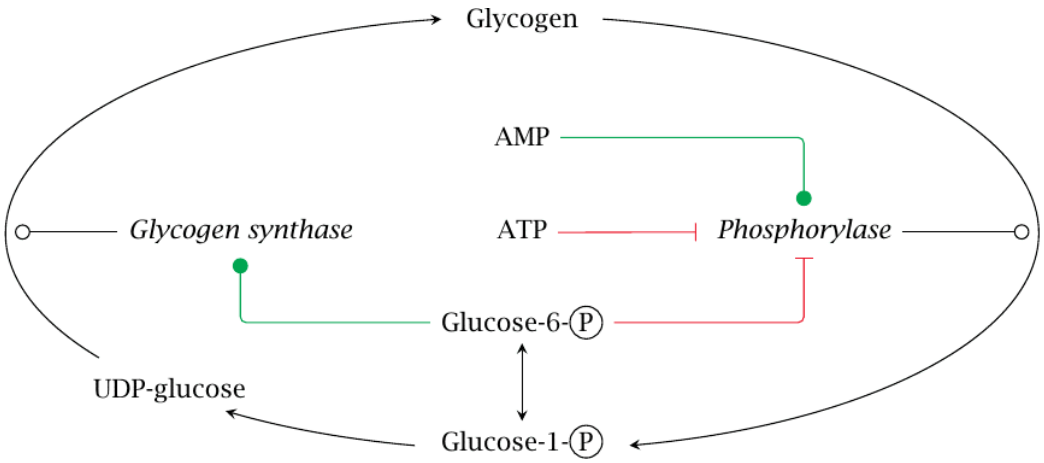

Figure 1.4: **Allosteric regulatory effects.** The allosteric regulatory effects of AMP, ATP and G6P on GS and GP. It is important to note that AMP activates glycogen phosphorylase in the muscle (MGP) but not in the liver (LGP).

Importantly, it has been shown that in response to *in vivo* insulin stimulation in the muscle, MGS is activated by allosteric activation rather than by MGS dephosphorylation [Bouskila et al., 2010]. Furthermore, when the concentration of G6P reaches a certain threshold, allosteric activation by G6P reverts inactivation by covalent phosphorylation, thereby achieving maximal activity.

Cellular localization

Glycogen synthase has a high affinity for the glycogen granule, rendering it complicated to find a physiological situation when GS is not present where glycogen is. In the muscle, when glycogen stores are low, MGS concentrates in the nucleus. But as levels increase, MGS will migrate to the cytoplasm which is where glycogen is found in physiological conditions. LGS present in hepatocytes, on the other hand, will start glycogen synthesis from the cell periphery and progress towards

the cell's interior [Ferrer et al., 1997].

It has also been speculated that the interaction between GS and GYG is important in the regulation of the former. Specifically, in the skeletal muscle, MGS translocates to an enriched actin fraction in response to glycogen depletion due to muscle contraction. In order to resynthesize glycogen, MGS must interact with GYG through associations at the actin cytoskeleton [Baqué et al., 1997].

1.4.2 Regulation of glycogen degradation

Three GP isoforms have been described in mammals and include muscle (MGP), liver (LGP) and brain (BGP) glycogen phosphorylase. As for GS, GP is also regulated by both phosphorylation and allosteric regulation. In literature, two forms of GP are often referred to and include the dephosphorylated, inactive (GP-b) and phosphorylated, active (GP-a) forms. Furthermore, both forms can either be found in a relaxed (R) or tense (T) state, where the T-state is more inactive due to its low affinity for substrate [Berg et al., 2002].

Regulation by phosphorylation
Contrary to GS, GP phosphorylation occurs only at one serine residue, serine 14, which activates the enzyme [Newgard et al., 1989]. The phosphorylation of GP is catalyzed by phosphorylase kinase (PhK), which is activated by PKA in response to increases in cAMP levels. High Ca^2+ levels can also activate PhK due to the presence of a calmodulin subunit which induces a conformational change [Berg et al., 2002]. PP1 is responsible for dephosphorylating both GP and PhK, which leads to the conversion of active GP-a to inactive GP-b.

In order to respond to extracellular conditions, such as physical activity, hormonal stimulation (glucagon, adrenaline and epinephrine) activates second messenger amplification systems that modulate glycogen metabolism through the activation of PhK leading the phosphorylation and activation of GP into its more active form, GP-a.

Allosteric regulation
Allosteric regulation of GP allows for an adequate response to the intracellular energy status: allosteric ligands which stabilize the R-state include AMP, inorganic phosphate and G1P, while glucose, ATP, purine nucleosides and G6P stabilize the T-state [Zois and Harris, 2016]. In addition, the presence of intracellular glucose triggers the dephosphorylation of GP-a to GP-b by the action of PP1.

As a specific example, MGP is responsive to nucleotide levels present in the cell, thus activation or inhibition of MGP is determined by the energy charge of the cell [Rath et al., 2000]. High levels of AMP stabilize the conformation of GP-a, while high ATP levels act as a negative allosteric effector by competing with AMP. Furthermore, the presence of G6P will also favor MGP to adopt the GP-b conformation.

1.5 Differences in glycogen metabolism between the liver and muscle

As previously mentioned, the most important glycogen depots in the body are in the liver and muscle, where glycogen metabolism in these two tissues is regulated by different glycogen synthase and phosphorylase isoforms.

When blood glucose levels are low, the **liver** breaks down glycogen in order to release free glucose into the circulatory system. Hepatic glycogen is degraded by the action of liver glycogen phosphorylase (LGP) which releases G1P, and phosphoglucomutase which then converts G1P into G6P. Next, G6P is shuttled to the endoplasmic reticulum (ER), where it is dephosphorylated by glucose-6-phosphatase and transported back to the cytosol, and eventually released to the bloodstream (Figure 1.5).

Although most of the free glucose will make it to the bloodstream, some will be phosphorylated back to G6P by the action of glucokinase (GK), resulting in a futile cycle. However, due to the low affinity of GK for free glucose, most will be transported out of the cell.

Contrary to liver glycogen, **muscle** glycogen is used locally to power muscle contraction during physical activity. In this case, the glycogen is broken down into G6P and then consumed within the muscle cell via normal catabolic pathways.

Muscle cells express hexokinase which results in the maintenance of low levels of intracellular free glucose through phosphorylation. Since intracellular glucose levels are low, this stimulates the import of extracellular glucose through glucose transporters (GLUTs). Furthermore, muscle cells are capable of converting G6P into pyruvate and then lactate which is then released into the extracellular space (Figure 1.6). Circulating lactate can be reabsorbed by the liver to participate in the **Cori Cycle**, where the lactate is reconverted into glucose through glyconeo-

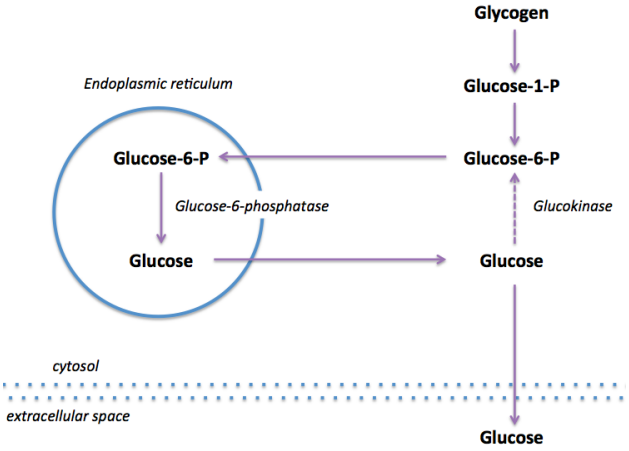

Figure 1.5: **Glycogen mobilization in the liver.** During fasting periods, the liver releases free glucose into the circulatory system in order to maintain blood glucose homeostasis.

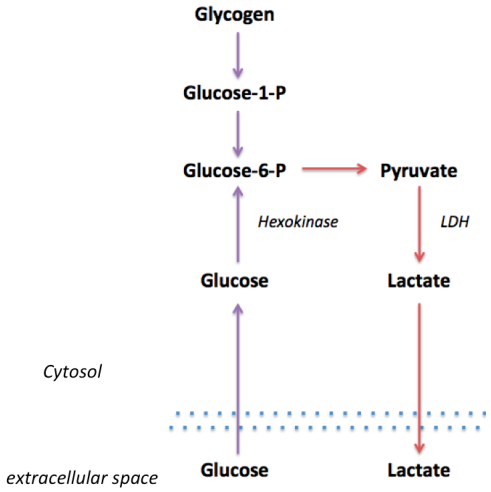

Figure 1.6: **Glycogen mobilization in the muscle.** Muscle glycogen can contribute to blood glucose levels via lactate release and subsequent integration into the Cori Cycle in the liver.

genesis.

1.6 Glycogen-related pathologies

Glycogen storage diseases (GSD) encompass diseases that are due to defects in different genes which encode enzymes required for glycogen synthesis or degradation. These metabolic diseases can either be divided into those with hepatic or neuromuscular involvement, or a mixture of both [Chen and Weinstein, 2016]. GSDs are detected through a combination of clinical symptoms, biochemical assays, histological findings and more recently, through DNA testing. GSDs have been instrumental in furthering knowledge of glycogen metabolism, and have clarified the role of individual enzymes and their importance in the grand scope of glycogen metabolism.

To date, 15 distinct diseases are commonly considered GSDs, and each involves a different affected gene (Table 1.1). In general, GSDs result in a pathological accumulation of glycogen in various tissues, including the liver, muscle and brain. The only exception is GSD type 0, caused by a homozygous or compound heterozygous mutation in the glycogen synthase gene (liver isoform, GYS2), which results in the absence of glycogen. In this case, the main presentation is hepatic and the main clinical symptom is fasting hypoglycemia and low lactate levels. On the other hand, feeding in these patients results in hyperglycemia and hyperlactatemia. Histologically, glycogen is not present in liver biopsies due to the lack of the main glycogen-synthesizing enzyme.

1.7 The role of glycogen metabolism beyond energy storage

To date, most glycogen metabolism research has focused on the characterization of its biochemical properties, regulatory pathways, and systemic effects. Only recently, however, has there been increased interest in its roles beyond just serving as a glucose depot in the body [Greenberg et al., 2006].

Glycogen in the brain, for instance, has been considered an emergency glucose store for a long time. Our laboratory, however, has demonstrated that brain glycogen is essential in other physiological functions that include hypoxia tolerance,

Number	Enzyme deficiency	Eponym	Affected organ	Glycogen in the affected organ
GSD type 0	Glycogen synthase	-	Liver (LGS), muscle and heart (MGS)	Null/low level
GSD type 1	Glucose-6-phosphatase	Von Gierke's disease	Liver and kidney	Increased amount, normal structure
GSD type II	Acid alpha-glucosidase	Pompe's disease	all organs	Massive increase in amount, normal structure
GSD type III	Glycogen debranching enzyme	Cori's disease	Muscle and liver	Increased amount, short outer branches
GSD type IV	Glycogen branching enzyme	Andersen disease, Adult Polyglucosan Body Disease (APBD)	Liver, spleen and nervous system	Increased amount, very long unbranched chains
GSD type V	Muscle glycogen phosphorylase	McArdle disease	Muscle	Moderately increased, normal structure
GSD type VI	Liver glycogen phosphorylase	Hers' disease	Liver	Increased amount
GSD type VII	Muscle phosphofructokinase	Tarui's disease	Muscle	Increased amount, normal structure
GSD type VIII	Liver phosphofructokinase	-	Liver	Increased amount, normal structure
GSD type IX	Phosphoglycerate mutase	-	Muscle	Increased amount
GSD type X	Phosphorylase kinase, PHKA2	-	Liver and muscle	Increased amount
GSD type XI	Lactate dehydrogenase	-	Muscle, blood	-
GSD type XII	Aldolase A	Red cell aldolase deficiency	Blood	-
GSD type XIII	Beta-enolase	-	Muscle	Increased amount
GSD type XV	Glycogenin	-	Muscle, heart	Increased amount
-	Laforin or Malin	Lafora disease	Nervous system, muscle, heart	Increased amounts, lafora bodies

Table 1.1: **Glycogen storage diseases (GSDs).**

long-term memory formation and learning [Duran et al., 2013, Saez et al., 2014].

Glycogen metabolism has also been implicated in pathological conditions. For instance, alterations in glycogen metabolism have been demonstrated to be a characteristic feature of certain cancers, including breast, bladder, brain and liver, among others [Rousset et al., 1981]. Energy reprogramming allows neoplastic cells to adapt and survive under adverse nutrient and oxygen conditions in tumors. Thus, the role of glycogen in tumorigenesis and, more specifically, in metabolic reprogramming has become a topic of interest in oncology.

Recent studies are also starting to uncover new roles for glycogen in the normal aging process in species ranging from *Saccharomyces cerevisiae* to humans [Lin et al., 2001, Sinadinos et al., 2014, Houtkooper et al., 2011, Gusarov et al., 2017]. Therefore, in the following chapter, we will delve into the specifics of aging, with an emphasis on senescence, a hallmark of aging.

Chapter 2

Aging and metabolism

Brief Introduction

Increased longevity and decreased fertility are dramatically changing the composition of today's society, leading to an increasingly aged population in developed and developing nations [Northridge, 2012]. Concretely, by 2050, the number of old and young will be the same worldwide: 2 billion people will be aged 60 or over, while 2 billion will be under 15 [Harper, 2014]. The implications of an aging population on public health, healthcare and families are considerable, specifically in socioeconomic terms. Aging populations impose more of a burden on healthcare systems due to chronic ailments that appear with age. Therefore, one approach to lighten the financial and societal implications of aging on society is to maintain health among older individuals, in order to lessen future costs on society. Consequently, aging-related research is becoming increasingly important in today's world. As with cancer, aging is heterogeneous in nature and its complicated aetiology converges on the progressive loss of organismal function, which eventually leads to death. This decreased fitness leads to a plethora of age-associated pathologies with include cancer, diabetes, cardiovascular disorders, neurodegenerative diseases, among others [López-otín et al., 2013]. Therefore, a better scientific understanding of aging and its associated processes, will relieve our societies from unnecessary spending and suffering.

2.1 Hallmarks of aging

Aging has been characterized by a number of proposed hallmarks that include essential criteria of normal aging [López-otín et al., 2013]. The nine hallmarks are stratified into 3 tiers which include *primary*, *antagonistic* and *integrative* hallmarks (Figure 2.1). Primary hallmarks are thought to be the primary cause of cellular damage which leads to aging and include **genomic instability**, **telomere attrition**, **epigenetic alterations** and **loss of proteostasis**. Antagonistic hallmarks, on the other hand, are compensatory responses to the primary hallmarks and act on a gradient: initially these responses are beneficial, but if they become chronic they eventual lead to worsened aging phenotypes. These hallmarks include **deregulated nutrient sensing**, **mitochondrial dysfunction** and **cellular senescence**. Lastly, integrative hallmarks are proposed on the basis that they directly affect tissue function and homeostasis and encompass **stem cell dysfunction** and **altered intercellular communication**.

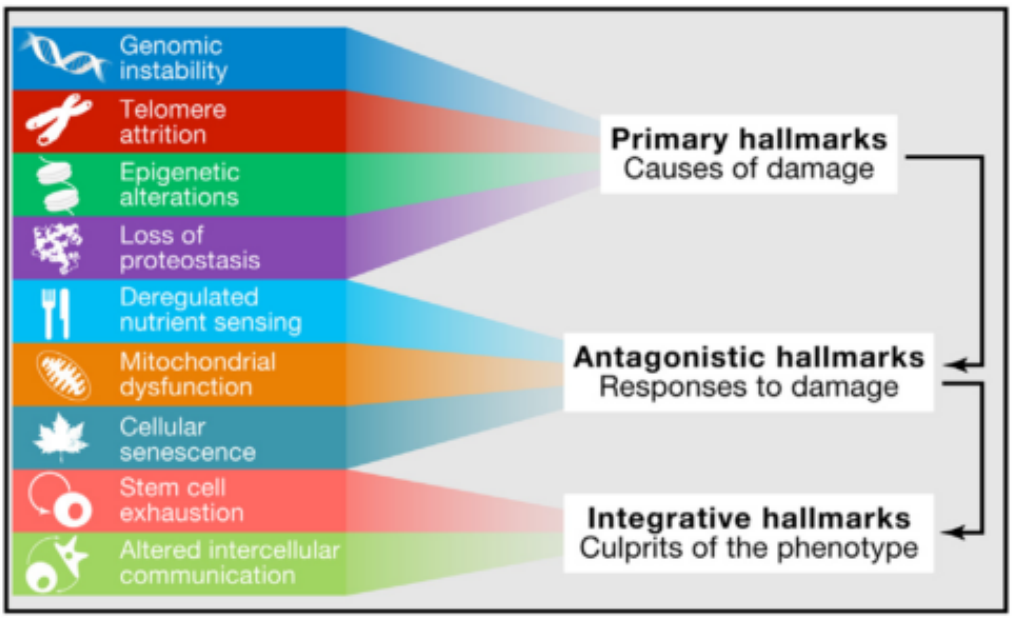

Figure 2.1: **The hallmarks of aging.** Adapted from [López-otín et al., 2013].

Primary aging hallmarks
Primary aging hallmarks cause the damage that eventually leads to aging. The **accumulation of genomic damage**, and the resulting genomic instability, is a

classical source of cellular dysfunction during aging. DNA lesions arise due to the exposure to endogenous and exogenous sources of genomic damage, that accumulate with time, and eventually lead to decreased fitness of the organism. Genomic lesions are highly heterogeneous and arise from various genetic aberrations including chromosomal abnormalities, copy number variations, and translocations, among others. DNA repair mechanisms are essential to detect and resolve genomic issues, but with time the response is less effective and the accumulation of DNA lesions leads to sub par cellular function.

Telomeres, the protective end-caps of chromosomes, are considered a molecular clock as they shorten with every cell division due to inefficient DNA replication. Somatic cells, in general, lack the ability to fix end replication issues due to the fact that they do not express telomerase. Thus, with each cellular division, **telomeric attrition** results and eventually leads to the activation of the DNA damage response. Therefore, normal aging is intrinsically linked to telomere shortening and associated phenotypes.

A cell's DNA is subjected to **epigenetic alterations** which offer an additional dynamic control of gene expression. Epigenetic DNA control can range from histone modifications to chromatin remodeling. In addition, the epigenome is very sensitive to environmental conditions, thereby allowing this response to be dynamic and responsive to the immediate needs of the cell. These chemical DNA modifications have been shown to constitute an important aging hallmark, as they can alter the accessibility of genetic information which leads to aberrant gene expression and genomic instability [Pal and Tyler, 2016].

Besides genome-related issues, aging has also been characterized by **impaired protein homeostasis**, a process essential to maintain protein stability and turnover. With age, however, it has been demonstrated that cells are no longer capable of maintaining normal proteostatic functions which can lead to abnormal protein aggregates, as is the case in Alzheimer's disease. Furthermore, experimentally perturbing proteostasis leads to the induction of age-related pathologies. On the other hand, certain genetic manipulations regarding protein homeostasis pathways have been shown to improve aging phenotypes [Zhang and Cuervo, 2008].

The aforementioned primary aging hallmarks are important to understand where the underlying causes of aging originate. However, once the damage or loss of homeostasis is sensed, the tissue will act accordingly and activate responses that attempt to reverse or, at least, maintain the damage.

Antagonistic aging hallmarks

When damage is sensed, a cell will attempt to resolve the issue by activating compensatory programs. At first, this response is beneficial as the damage will be effectively repaired. However, when the trigger or the response becomes chronic, the compensatory response can become deleterious.

This is the case with **nutrient sensing** in many organisms. Nutrient sensing pathways have been demonstrated to play an important role in determining lifespan in various species. The insulin and insulin-like growth factor 1 (IGF-1) pathway (IIS), an important glucose-sensing mechanism in cells via insulin action, is the most conserved aging-controlled pathway in evolution. Specifically, downstream effectors including AKT, mTOR and members of the Foxo family have been shown to play a role in longevity. Furthermore, dietary restriction, defined as a reduction of nutrient intake without malnutrition, has repeatedly been linked to an extended lifespan in many different organisms, including yeast, flies, worms, rodents and primates [Fontana et al., 2010]. Accordingly, the AMPK pathway signals nutrient scarcity, and its upregulation favors lifespan extension via an integrated signaling network [Salminen and Kaarniranta, 2012].

Mitochondria have been suspected of playing an important role in aging considering they are the cell's powerhouse where most ATP is produced. As such, when mitochondrial function declines, so does the ability of the cell to generate energy for basic cellular functions. Furthermore, mitochondria have been shown to be a major source of ROS. These oxidative species have been directly associated to aging when they overwhelm the cell's redox capacity.

When cells sense either environmental or endogenous stress, depending on cues, they may become **senescent**, or in other words, enter a non-reversible growth arrest. This mechanism is thought to protect the organism, by filtering out possibly oncogenic or defective cells from proliferating. As an organism ages, this response may become less effective, thereby leading to an accumulation of senescent cells that can generate a localized chronic inflammatory response. This particular hallmark of aging is central to this thesis, and we will further address this in the next section.

Integrative aging hallmarks

Lastly, integrative aging hallmarks are those that arise when overall tissue homeostasis is lost, which eventually leads to loss of tissue function. An important part of tissue homeostasis is its ability to regenerate tissue through the action of stem cells. However, with age, organisms have an overall decreased capacity to regenerate due to **stem cell exhaustion**, a key aging hallmark. For instance, with age, the number of hematopoietic stem cells progressively decreases, which results in

a decreased production of adaptive immune cells (immunosenescence).

Besides the progressive loss of stem cells, aging also affects normal **intercellular communication**, which can include changes at the endocrine or neuronal level. Inflammation, for instance, is a common phenotype of aging and it reflects abnormal communication between cells. More specifically, inflammation during aging can result from a weakened immune system, in addition to a growing population of senescent cells with a pro-inflammatory secretory phenotype (SASP) [Campisi, 2013].

Although the aforementioned aging hallmarks have only recently been described, they serve as a starting point to better define aging research. In the next section, we will be focusing on cellular senescence, an antagonistic hallmark of aging, which lies at the crossroads of cancer and aging. Senescence exerts an important tumor-suppressive function in the face of oncogenic stress, but it also engenders characteristic aging phenotypes.

2.2 Cellular Senescence

Cellular senescence was first observed over half a century ago by Hayflick and Moorhead. The two scientists realized that after a certain number of passages, primary cell cultures were no longer capable of proliferation and remained indefinitely arrested [Hayflick and Moorhead, 1961]. Five years later, Hayflick hypothesized that 'the finite lifetime of diploid cell strains *in vitro* may be an expression of aging or senescence at the cellular level' [Hayflick, 1965].

Since Hayflick and Moorhead's original observations, we now know that with each passage, the telomeres of primary cells lacking telomerase are progressively shortened, eventually reaching their 'Hayflick limit'. In other words: time's up on their molecular clock. Once telomeres reach a critical length, the DNA damage response (DDR) is activated which leads to senescence or apoptosis, depending on whether DNA damage reaches a certain threshold [Kaul et al., 2012].

Senescence triggered by a high number of *in vitro* passages is now referred to as **replicative senescence**. To date, three other types of senescence have been described, including: **stress-induced premature** senescence (SIPS), **oncogene-induced** senescence (OIS), and **developmental** senescence. Each type activates different sets of signaling cascades, that all converge on the hypo-phosphorylation of the Retinoblastoma (Rb) protein, thereby inhibiting cell cycle progression.

2.2.1 The causes of senescence

Senescence is now viewed as a mechanism to prevent possible oncogenic transformation in at-risk cells, in other words, a tumor-suppressive mechanism. To date, many causes of senescence have been described and range from inadequate culture conditions to genomic damage.

In vitro culture conditions, for instance, can lead to SIPS: cells are routinely cultured in supraphysiological oxygen levels (21% O_2, ambient oxygen levels), thereby inducing oxidative damage. It has been shown that by culturing cells at physiological levels of 3% O_2, oxidative stress is mitigated, allowing primary cells to significantly extend their lifespan [Dolivo et al., 2016]. Along the same lines, inappropriately supplemented culture medium can also stress cells and lead to growth arrest. Besides culture conditions, an extensive range of different exogenous and endogenous stressors can induce cellular senescence (i.e. proteasome inhibitors, ROS inducing drugs, among others).

Genomic damage is another well-known cause of cellular senescence, and can be induced by a myriad of factors, including UV light, ionizing radiation, chemical DNA damage inducers, including certain chemotherapeutic drugs. DNA damage-inducing stimuli incurring severe DNA damage such as double stranded breaks (DSBs) in the genome, cause cells to senesce by activating the DDR. It is important to note that only persistent activation of the DDR leads to senescence, while transient DDR activation due to mild DNA damage will induce DNA repair mechanisms (Ref). Furthermore, perturbations in chromatin and histone modifications, which determine the activity of genes, can also lead to senescence induction. Treating cells with chemical histone deacetylase inhibitors (HDAi), for instance, will promote the aberrant formation of euchromatin (gene activation) and senescence, making HDAis potentially powerful allies in anti-cancer treatments [Ogryzko et al., 1996].

In 1983, Land et al. demonstrated that two steps are required for the oncogenic transformation of primary cells: first, immortalization and then transformation. This seminal research identified that *myc* and *ras* have to be introduced in parallel in order to correctly transform primary fibroblast cultures [Land et al., 1983]. By 1997, Serrano et al. observed that the activation of one oncogene in primary cells, in this case *ras*, led to a G1 cell cycle arrest indistinguishable from senescence [Serrano et al., 1997]. This phenomenon is now referred to as **oncogene-induced** senescence (OIS), which is now an umbrella term for the activation of an onco-

gene or the silencing of tumor suppressor genes which also lead to a senescent response.

As discussed, senescence can be induced by a plethora of different stressors and damage-inducing stimuli, which makes senescence a complex phenomenon. Furthermore, a number of senescence markers have been characterized and are used to establish the senescence state. Senescence is considered a heterogeneous state driven by multiple effector programs, thereby a combination of markers usually have to be considered. In the next few sections, we will be exploring which markers are currently being used, as well as deepening our knowledge about how different effector programs activate different signaling cascades.

2.2.2 Senescence Markers

Senescent cells are identified *in vitro* and *in vivo* through either phenotypic or molecular markers, which are detailed in Table 2.1. Senescence markers are not present in all forms of senescence and can be context-dependent. Therefore, the presence of a combination of multiple markers is required to establish senescence in a system. Furthermore, it is postulated that different combinations of effector programs will lead to a spectrum of senescence, such as early and late senescence [Salama et al., 2014].

The most recognized hallmark of senescent cells is that they are irreversibly growth arrested, and no known physiological stimulus can rescue senescent cells. Logically, one would assume that senescence only affects mitotic cells, which are those that may face potential aberrant oncogenic signals due to their proliferative nature. However, recent evidence is suggesting that post-mitotic cells, such as neurons and cardiomyocytes, can display certain signs of senescence. Specifically, it has been demonstrated that Purkinje neurons exhibit a p21-dependent senescent-like phenotype *in vivo* driven by DDR [Jurk et al., 2012]. Post-mitotic cellular senescence is currently a debated concept in the senescence field. We therefore center our definition on classical senescence observed in mitotic cells.

Growth arrest arises from the action of cell cycle inhibitors, notably p21 and p16. In addition to cell cycle arrest, senescent cells are known to resist apoptotic signals, thereby making them stable and long-lived in culture and in tissues [Childs et al., 2014].

Besides growth arrest, senescent cells exhibit a flattened cell morphology due to the lack of cell divisions. Additionally, senescent cells usually manifest senescence-

Phenotypic markers
Lack of cell proliferation
Large and flat cellular morphology
Lack of response to growth factors
SA-B-Gal (senescence-associated B-galactosidase activity)
PML nuclear bodies
SAHF (senescence-associated heterochromatic foci)
SASP (senescence-associated secretory phenotype)
TIF (telomere dysfunction-induced foci)
TAF (telomere-associated foci)
DNA-SCARS (DNA segments with chromatin alterations reinforcing senescence
Molecular markers
CDKIs (p16, p21, etc)
p53
ARF
DEC1 (BHLHE40)
DCR2 (TNFRSF10D)
DDR (ATM, 53BP1, gamma-H2AX, etc)
SASP factors and receptors (IL6, IL8, IL1, MMPs, etc)
HMGA proteins
Heterochromatin markers (HP1, H3K9me3, etc)
Lamin B1 reduction

Table 2.1: **General overview of phenotypic and molecular markers of senescence.** Adapted from [Salama et al., 2014].

associated beta-galactosiadase activity (SA-Bgal), which most likely occurs due to the increased lysosomal biogenesis and beta-galactosiadase [Dimri et al., 1995].

The pro-inflammatory senescence-associated secretory phenotype (SASP), another marker of senescence, is an important mechanism which allows for additional signaling: the SASP exerts both autocrine and paracrine activities, which are thought to create an inflammatory microenvironment. It is important to note that, unlike apoptotic and quiescent cells, senescent cells remain highly metabolically active in order to maintain a strong and robust secretory phenotype [Campisi, 2013]. The secretome of senescent cells is complex and is composed of soluble signaling factors (chemokines, growth factors, interleukins, etc), secreted proteases, and secreted insoluble proteins/extracellular matrix (ECM) components [Coppé et al., 2010]. Depending on the context and cell type, the SASP is thought to induce, interestingly, both pro-tumorigeneic and tumor-suppressive effects, as well as pro- and anti-inflammatory signaling. The specific SASP signature will lead to a local inflammatory response, where senescent cells are cleared by phagocytosis. The SASP also allows for paracrine signaling, where secreted TGF-b, for

instance, will lead to the senescence of surrounding cells, through ROS generation and DNA damage [Munoz-Espin and Serrano, 2014].

2.2.3 Signaling cascades of senescence

Different senescence stressors and triggers can activate various signaling pathways that eventually converge on the activation of cell cycle inhibitors and the hypophosphorylation of the Retinoblastoma (Rb) protein, resulting in the proliferative arrest of affected cells (Figure 2.2). To date, senescence can either be categorized as **non pathological**, such as senescence associated to physiological embryonic development, or **pathological** when it is induced by damage-inducing stimuli. Consequently, these two types of senescence rely on different signaling cascades activated by various triggers, which eventually converge on growth arrest.

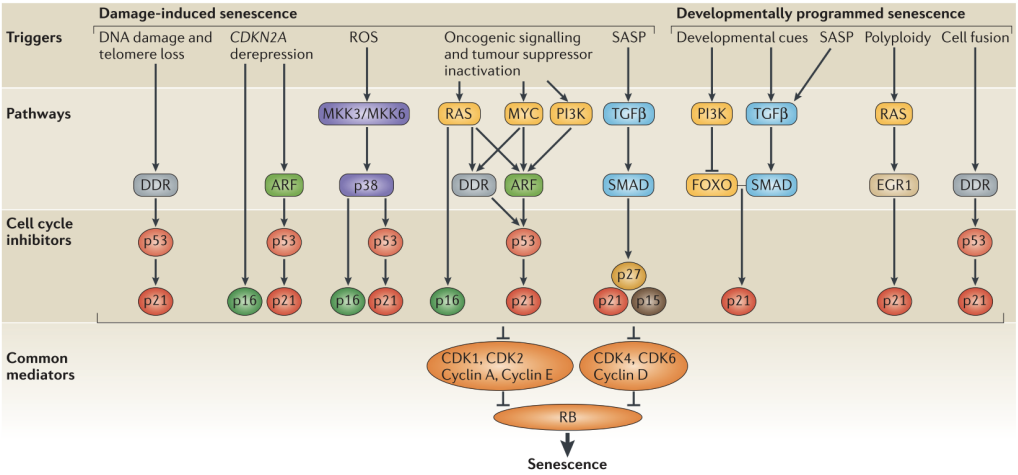

Figure 2.2: **Molecular pathways associated to senescence** Senescence can be induced through various molecular pathways depending on the type of trigger. Eventually, the molecular pathways converge on the activation of cell cycle inhibitors and the Retinoblastoma (Rb) tumor suppressor. Adapted from [Munoz-Espin and Serrano, 2014]

Within the realm of **non pathological** senescence, normal developmental signaling converges on p21 upregulation controlled by both the TGFb-SMAD and PI3K-Foxo pathways. TGFb is known to activate p21 transcription by establishing the SMAD complex. Therefore, in order to causally link the TGF-b pathway

to developmental senescence, pregnant mice were treated with a TGF-b pathway inhibitor (LY2152799), which inhibits the TGF-b receptor. Through immunohistochemistry, phospho-SMAD2, p21 and SA-Bgal were shown to be substantially decreased in both the mesonephros and endolymphatic sac, key developmental structures known to undergo senescence in normal developmental conditions [Munoz-Espin et al., 2013]. Furthermore, the same authors show that the PI3K-Foxo pathway is also implicated in developmental senescence through the use of mice with genetic alterations of the PI3K/Foxo pathway, and through the administration of a small compound inhibitor of PI3K. Importantly, developmental senescence is not characterized by DNA-damage markers or DNA-damage signaling kinases, such as ATM or ATR, thereby setting it apart from other types of senescence.

Depending which damage-inducing stimuli cells are subjected to, different signaling cascades are activated, constituting a **pathological** senescence response. Senescence induced by telomere attrition, as is the case during replicative senescence, will result in the activation of the DDR. The DDR is mediated by the action of the DNA damage kinases which include ATM, ATR, CHK1 and CHK2. Eventually, this results in the phosphorylation and activation of p53, an important cell cycle protein, which eventually activates p21. It is important to note that treating cells with DNA-damaging agents such as ionizing radiation or certain chemotherapeutic drugs will also produce DNA lesions that will eventually lead to the activation of the DDR and senescence-onset. Furthermore, replicative senescence and aging are linked to CDKN2A locus derepression, which encodes both p16 and ARF tumor suppressors. ARF, in turn, induces p53 stability by inactivating MDM2, an important E3 ubiquitin protein which normally degrades p53.

Besides DNA damage, cells can also face with high oxidative stress levels, which can originate from various sources (i.e. drugs, oncogene activation, DNA damage, among others). In this case, kinases MKK3 and MKK6 activate their downstream kinase effector, p38 MAPK. Subsequently, p38 MAPK activation leads to an increased transcriptional activity of both p53 and p16, eventually inducing growth arrest.

OIS will also activate certain signaling cascades that converge on the inhibition of the cell cycle. As we have seen, OIS can either be due to the activation of different oncogenes (i.e. RAS, MYC), or rather, by the loss of certain tumor suppressors (i.e. PTEN, VHL). The activated signaling cascade to induce senescence can depend on which oncogene is activated or which tumor suppressor is lost, thereby making this type of senescence quite complex and context-dependent. Generally, OIS will induce the DDR due to DNA damage incurred by OIS, as well as in-

creased ROS levels. However, in the case of PTEN loss, for instance, the DDR is not activated. Furthermore, differences between species seems to exist: OIS in humans relies mostly on the DDR-p53 pathway, whereas OIS in mice is more dependent on the ARF-p53 pathway.

Lastly, senescent cells release a pro-inflammatory SASP composed of cytokines, chemokines and other components which are known to modulate the behavior of neighboring cells in a paracrine manner. A notable component of the SASP is TGF-b which can induce senescence in surrounding cells through the generation of ROS and DNA damage. Growth arrest is mediated by the upregulation of cell cycle inhibitors p21, p27 and p15 through the SMAD complex.

Although different senescence triggers lead to the activation of different signaling cascades, the end result remains the same: the activation of cell cycle inhibitors and Rb tumor suppressor leads to a growth arrest phenotype. We will now add another level of complexity to the senescence response by analyzing how cellular metabolism comes into play in the context of senescence.

2.2.4 Metabolic control of senescence

Metabolism plays an important role in senescence induction and maintenance. Although senescent cells are no longer actively proliferating, they still play an active role in signaling and tissue remodeling through the SASP.

In 1984, Bittles and Harper observed that as cells enter a senescent state, they exhibit a more glycolytic metabolism [Bittles and Harper, 1984]. Today, we still ignore why glycolysis is preferred, however, it has been postulated that since the SASP requires macromolecule biosynthesis, this favors glycolysis due to its ability to provide precursors for protein and lipid biosynthesis [Vander Heiden et al., 2009]. Furthermore, increased ADP:ATP and AMP:ATP ratios are frequently associated with the senescent state. This can further be evidenced by the fact that the addition of exogenous AMP to the culture medium results in senescence induction [Zwerschke et al., 2003].

The low energy status of senescent cells activate AMPK, the cell's nutrient and energy sensor, which causes growth arrest via two different mechanisms: (1) constitutive activation of AMPK leads to the phosphorylation of p53 on multiple sites resulting in cell cycle arrest [Jones et al., 2005], and (2) AMPK inhibits the degradation of p16 and p21 encoding mRNAs, both of which are cyclin-dependent kinase inhibitors that promote growth arrest [Wang et al., 2003].

Besides inducing cell cycle arrest, p53 has also been shown to transcriptionally antagonize glycolysis, while encouraging mitochondrial respiration [Wiley et al., 2016]. Therefore, p53 acts to balance metabolism between glycolysis and respiration, maintaining the senescent state.

Specific metabolic phenotypes, however, seem to depend on the type of senescence. Oxidative respiration in cells undergoing OIS, for instance, has been shown to be favored over glycolysis [Kaplon et al., 2013]. It is believed that the increased oxygen consumption in OIS senescent cells leads to increases in ROS, which allows OIS maintenance. In addition, it has been shown that when PDK1 is overexpressed in BRAF(V600E)-expressing cells, senescence is bypassed, revealing the importance of balancing glycolysis and oxidative phosphorylation in senescence maintenance [Aird and Zhang, 2013].

2.2.5 The *in vivo* function of senescence: tissue remodeling

Up until recently, aging research has focused on the senescent response associated to pathological states, with little emphasis on the physiological role of senescence. In 2013, however, **developmentally-programmed senescence** was described as a physiological response that supports embryonic growth and patterning [Storer et al., 2013, Munoz-Espin et al., 2013]. During normal development, the senescent response induces macrophage infiltration, clearance of senescent cells and, ultimately, contributes to tissue remodeling. This morphologic process occurs at multiple embryonic stages and in various locations within the developing embryo, including the mesonephros, endolymphatic sac of the inner ear, interdigital webs and the apical ectodermal ridge, among others [Storer et al., 2013, Munoz-Espin et al., 2013]. For instance, as the senescent cells present in the interdigital webs of the growing embryo are removed through macrophage-mediated clearance (Figure 2.3), the digits of the embryo will become more defined.

Phenotypic and molecular senescence markers have been detected during developmentally-programmed senescence and include positive SA-B-gal staining, absence of proliferation, increased heterochromatin markers and increased expression of cell cycle inhibitors (i.e. p15, p21 and p27) [Munoz-Espin and Serrano, 2014]. Importantly, developmental senescence has been shown to occur independently of DNA damage, and is regulated by the TGF-b/SMAD and PI3K/Foxo pathways which converge on p21. Accordingly, development in p21 null embryos is partially compensated by an increased apoptotic response. However, embryos still display significant developmental abnormalities, notably an increased incidence of vaginal

septa in females leading to decreased fertility [Munoz-Espin et al., 2013].

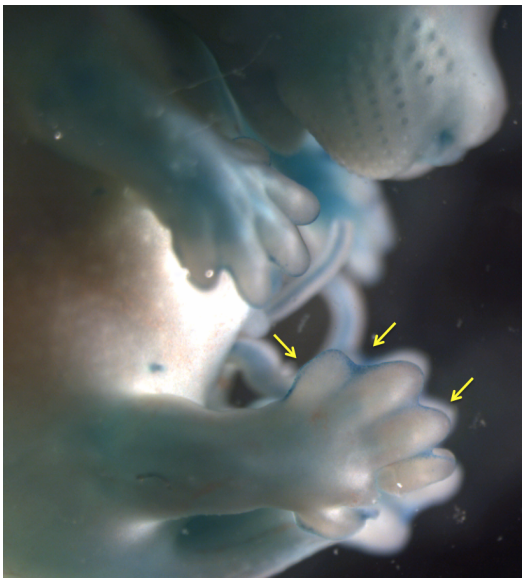

Figure 2.3: **Interdigital webs and developmental senescence.** Senescent cells (blue stain, highlighted with yellow arrows) are present in the interdigital webs of wild type embryos at day E14.5.

Besides the newly described physiological role of senescence in embryonic patterning, senescence has also been shown to play a role in many diseases *in vivo* (Figure 2.4). Specifically, the association between cancer and senescence is the most well studied implication of senescence in disease. Somatic cell hybridization studies were the first concrete indication that senescence was a tumor suppressor mechanism: hybrid cells generated by fusing immortal cancer cells to normal cells always results in senescence entry [Smith and Pereira-smith, 1996]. Furthermore, the discovery of OIS was another important step in clarifying the link between senescence and cancer: the increased expression of oncogenic *ras* in primary cells results in senescence [Serrano et al., 1997].

Today, we know that when normal cells reach a certain threshold level of oncogenic signaling, they can respond by entering a senescent state activated by the p16 and p53 tumor suppressor pathways. As a result, senescent cells are often detected in the earlier pre-malignant stages of tumorigenesis, whereas malignant tumors are required to evade the senescent process [Collado and Serrano, 2010]. However, in response to either tumor suppression restoration (i.e. *Trp53*) or oncogenic inactivation (i.e. *Myc*), malignant tumors rapidly regress and show

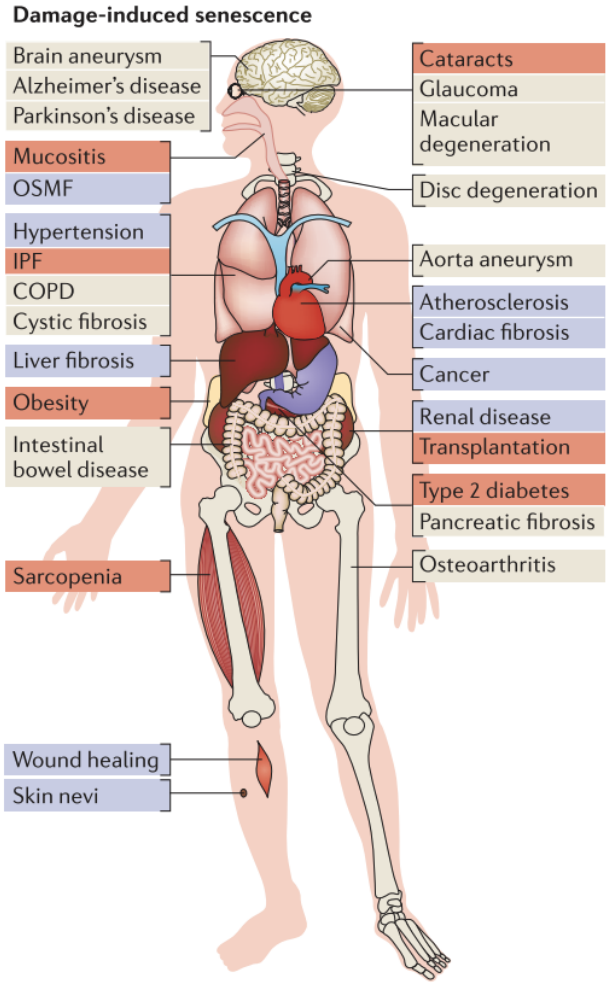

Figure 2.4: ***In vivo* senescence in disease** Senescence has been shown to play either a beneficial (blue) or detrimental (red) role in a variety of diseases. There are some diseases, however, where the role of senescence has not yet been established (beige). Adapted from [Munoz-Espin and Serrano, 2014]

evidence of cellular senescence [Ventura et al., 2007, Wu et al., 2007]. Moreover, from a therapeutic standpoint, chemotherapy-induced tumor regression has been associated with both apoptosis and senescence-induction of malignant cells *in vivo* [Roberson et al., 2005]. Globally, senescence plays a beneficial role in cancer by suppressing tumor growth. However, certain SASP components, such as WNT16B, released by senescent cells have been proposed to potentially promote disease progression [Collado and Serrano, 2010].

Senescence has also been shown to play a beneficial role in certain liver diseases. Liver fibrosis is due to the excessive accumulation of extracellular matrix proteins that lead to cirrhosis and eventually liver failure. Specifically, activated hepatic stellate cells proliferate and respond to fibrogenic cytokines, which stimulates them to depose collagen, senesce and form fibrotic scars [Bataller and Brenner, 2005]. The senescent hepatic stellate cells release a SASP that attracts immune cells that clear the senescent cells and partially eliminate the fibrotic scar [Kong et al., 2012].

In other diseases, however, senescence has been shown to play a detrimental role, as is seen in the context of obesity and diabetes. Type 2 diabetes is a metabolic disorder that is characterized by insulin resistance which induces a chronic overcompensation of insulin production in beta cells. Eventually, pancreatic beta cell failure occurs due to the proliferative exhaustion of these cells. Senescent cells that accumulate during diabetes contribute to inflammation, insulin resistance, metabolic dysfunction and progenitor cell dysfunction through the SASP. Specifically, senescent pancreatic beta cells could be a good target for senolytic agents, drugs that remove senescent cells, in order to prevent beta cell dysfunction [Palmer et al., 2015].

Generally speaking, a transient senescent response that removes damaged cells is considered beneficial to organisms. On the other hand, a chronic and faulty senescent response that does not correctly clear damaged cells is considered detrimental to organisms [Munoz-Espin and Serrano, 2014]. This leads to the unified model of senescence proposed by Munoz-Espin et al, which states that the senescent response contributes to the *in vivo* tissue remodeling process by recruiting immune cells through the SASP (Figure 2.5). In turn, macrophages clear senescent cells and progenitor cells repopulate the region and contribute to tissue regeneration. If a tissue is exposed to persistent damage during either aging or pathological conditions, the recruitment-clearance-regeneration chain of events becomes less effective, eventually leading to tissue dysfunction due to the accumulation of senescent cells and chronic inflammation.

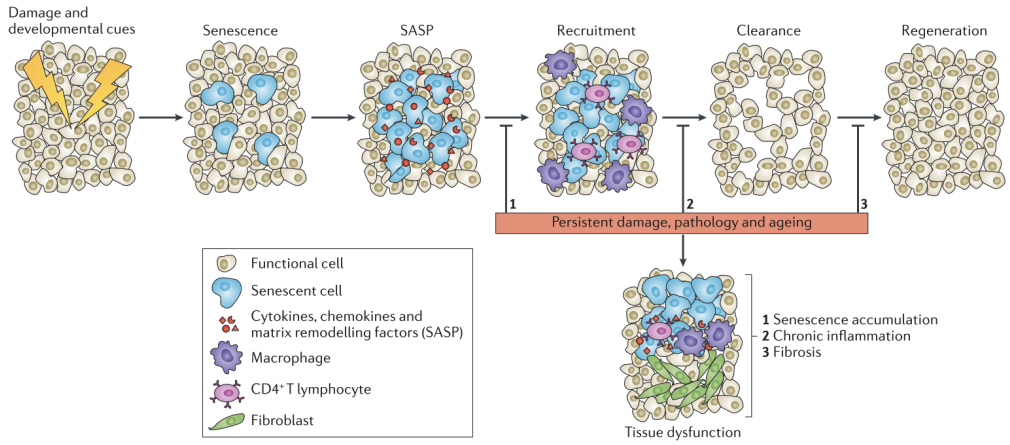

Figure 2.5: **Senescence contributes to tissue remodeling.** Adapted from [Munoz-Espin and Serrano, 2014]

Chapter 3

Cancer and metabolism

Brief Introduction

Cancer is a worldwide public health issue that has become more prevalent due to the increase in global life expectancy. Ergo, most cancers are recognized as an age-related hyperproliferative disease whose incident exponentially increases as a species reaches a certain age, about 50-60 years for humans [Campisi, 2013]. According to the World Health Organization (WHO), cancer is the second leading cause of deaths worldwide: globally, 1 in 6 deaths are due to cancer. The most deadly cancers are as follows, in order: lung, liver, colorectal, stomach and breast cancer. It has been reported that most cancers are due to environmental factors (i.e. lifestyle), whereas only about 5-10% are attributable to genetic mutations [Anand et al., 2008].

Cancer is a multi-step microevolutionary process that arises from a single clonal origin: it takes one abnormally proliferating cell to initiate a neoplasm [Alberts

et al., 2002]. Through repeated rounds of unrestrained cellular proliferation, the tumoral seed expands into a population. With time, as selection forces act on the cells, the tumor will progress as it acquires additional characteristics favoring proliferation, survival, invasion and metastasis. This process of clonal selection continues throughout the tumor's lifetime, as it becomes more aggressive with the addition of mutations conferring a selective advantage.

Although cancer is complex and multi-etiological in nature, there are some attributes inherent to the definition of cancer. Accordingly, in an attempt to logically categorize the underlying principles of cancer, Hanahan and Weinberg proposed the hallmarks of cancer, a list that was later revisited to include two new emerging hallmarks [Hanahan and Weinberg, 2000, Hanahan and Weinberg, 2011]: (i) evading immune detection, and (ii) metabolic reprogramming.

3.1 Hallmarks of cancer

A cell has to undergo several essential alterations in its molecular, biochemical and cellular biology in order to evolve from normalcy to a tumorigenic cell [Hanahan and Weinberg, 2000]. In this section, we will visit the traits considered essential for a cell's path to tumorigenesis (Figure 3.1).

While normal cells require external growth signals to initiate their mitogenic cellular programs, cancer cells are known to be **self-sufficient** in this aspect. The decreased dependency on external mitogenic signaling is due to the fact that these cells can generate many of their own growth signals and induce alterations in the intracellular transducers of growth signaling. These important changes, in turn, cause an upset in tissue homeostasis, as tumorigenic cells no longer respond normally to mitogenic growth signals from other cells.

In addition to mitogenic stimulation, cells also normally respond to anti-proliferative signaling, which further contributes to proliferative homeostasis within a healthy tissue. A normal cell can respond to anti-growth signals in one of two ways: 1) it may either enter a quiescent state by exiting the cell cycle, with the possibility of re-entering the cycle when growth signaling permits, or 2) become post-mitotic and permanently exit the cell cycle.

Tumor cells, however, are **insensitive to anti-growth signals**, another fundamental trait of cancer. Neoplastic cells can evade anti-growth signaling by perturbing essential Gap 1 phase (G1) cell cycle signaling, the phase when cells either com-

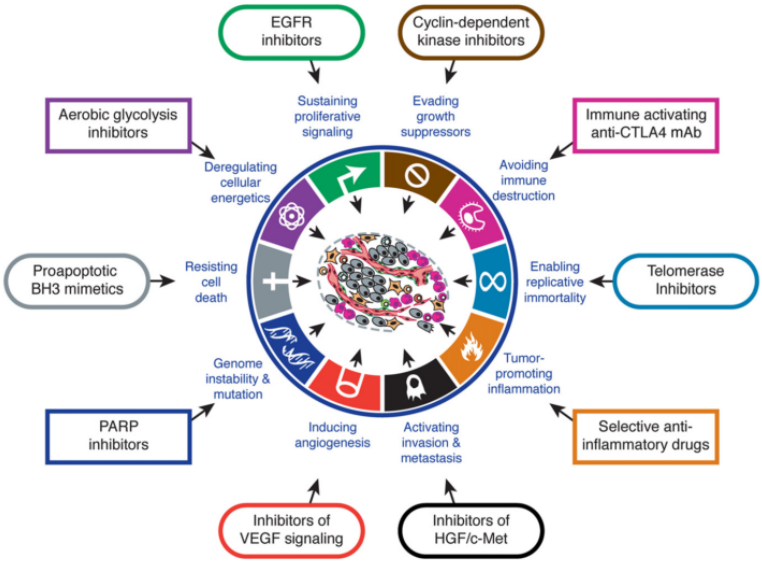

Figure 3.1: **The hallmarks of cancer and possible therapeutic targets.** Adapted from [Hanahan and Weinberg, 2011].

mit to cell division or leave the cell cycle. The tumor suppressor Retinoblastoma (Rb) protein is a regulator of the progression from G1 to synthesis (S) phase: when Rb is hypo-phosphorylated, it blocks cellular proliferation by sequestering E2F transcription factors which are essential for G1 to S progression. Therefore, cells with disrupted pRb signaling become insensitive to anti-growth factors that act on cells, most notably the cytokine transforming growth factor beta (TGF-b).

As we have seen, disruptions in homeostatic growth signaling are indispensable when it comes to requirements for tumorigenesis. However, the ability of malignant cells to **evade apoptosis** is just as crucial. Apoptosis, also known as programmed cell death, is a highly regulated and complex mechanism to eliminate dysfunctional cells. When cells sense abnormal external or internal stimuli, the apoptotic pathway is initiated, leading to the elimination of defective cells. In cancer, however, cells can adopt various mechanism to avoid apoptosis, including: a disrupted balance of pro- and anti-apoptotic proteins, impaired death receptor signaling and reduced caspase expression [Wong, 2011].

Growth and apoptosis signaling aberrations lead to the uncoupling of normal signaling and environmental cues in malignant cells, thus permitting tumor growth. However, in order to defy normal proliferative laws, cancer cells also have to demonstrate **limitless replicative potential**. Non-malignant cells have a limited

replicative potential, in other words, they will stop proliferating after a certain number of *in vitro* passages, and eventually enter a non-proliferative phase termed cellular senescence. However, a variant can acquire a mutation that confers the ability to proliferate without limit, a process referred to as immortalization. Cells isolated from *in vivo* tumors demonstrate immortalization in culture, thereby suggesting that malignant cells must acquire the capacity to replicate without limit. Telomere maintenance partly accounts for the ability of tumoral cells to immortalize, and they do so by upregulating the expression of telomerase, an enzyme crucial for maintaining telomere length. Another key component of limitless replicative potential, is the ability of pre-malignant cells to circumvent the activation of the senescent response, a recognized protective mechanism against cancer which responds to abnormal oncogenic signaling within a cell. We will revisit this important tumor suppressive response in detail in the next chapter.

Nutrients and oxygen are essential for any cell to survive, as is an effective waste disposal system, making vasculature an essential part of tissues and organs. Accordingly, tumors are able to activate and **sustain angiogenesis** in order to boost neoplastic growth. Tumors essentially hijack the angiogenic system by shifting the balance of pro- and anti-angiogenic signaling in favor of the former. As a result of the loss of homeostasis, tumors generally exhibit aberrant vasculature which includes excessive branching, precocious capillary sprouting, leakiness and aberrant blood flow, among others [Carmeliet, 2003]. Although tumors demonstrate aberrant angiogenesis, the blood flow to malignant cells is sufficient to deliver nutrients and remove waste, thereby allowing tumors to propagate.

All of the previously described hallmarks of cancer are considered essential for cancer progression, however it is the acquired ability of a tumor to **invade healthy tissues and metastasize** which makes tumors deadly, and cause about 90% of cancer deaths [Seyfried and Huysentruyt, 2013]. Invasion and metastasis involve a series of discrete steps which are now collectively referred to as the invasion-metastasis cascade [Fidler, 2003, Fidler et al., 2010]. Generally, in order for metastasis to occur, cancer cells must locally invade, enter the circulatory system (either blood or lymphatic systems), escape the circulatory system (extravasation) in a distant tissue, form micrometastases which will eventually colonize the new environment and grow into macroscopic tumors.

The six aforementioned hallmarks were recognized as the essential properties a cancer cell had to display in order to be considered oncogenic. By 2011, the authors revisited their original cancer hallmarks to include two emerging cancer properties: **evading immune destruction** and the **reprogramming of energy metabolism** [Hanahan and Weinberg, 2011].

In normal conditions, the immune system acts to protect the organism from invaders and incipient neoplasias. However, it is becoming increasingly apparent that cancer cells somehow are able to evade immune detection, but the mechanism remains unclear. One possibility is that tumor cells secrete certain immunosuppressive factors such as TGF-b [Yang et al., 2010].

The second emergent hallmark, **metabolic reprogramming** is the most pertinent to our present work. In order for a tumor cell to be able to proliferate beyond normal levels, it must readjust its metabolic capability in order to feed this uncontrolled proliferation. Therefore, the next section is dedicated to further deepen our knowledge on how cancer cells rewire normal metabolic signaling to their advantage.

3.2 Tumor metabolic reprogramming

Cancer cell metabolism is one of the oldest branches of oncology research, and actually predates more recent disciplines, such as cancer genomics, by more than half a century (Cantor 2012). Altered metabolic activity in cancer cells supports the gain and maintenance of malignancy. As previously mentioned, metabolic reprogramming is now a recognized characteristic of cancers due to its generality across different tumor types [Hanahan and Weinberg, 2011].

To survive, cells need a way to extract usable energy from their surroundings in order to synthesize ATP and cellular building blocks. The intricate network of pathways that lead to energy production and macromolecular synthesis is generally referred to as metabolism. Metabolism is a delicately regulated process that requires the activation and inhibition of enzymes to either release energy (catabolic metabolism) or generate macromolecules (anabolic metabolism). Interestingly, metabolism is closely linked to cellular proliferation pathways (i.e. PI3K/Akt), and in times of nutrient excess, cells can choose to shunt macromolecules and metabolites towards biomass generation (Figure 3.3). In an oncogenic context, however, activated oncogenes and/or inactive tumor suppressors contribute to metabolic rewriting and imbalances that eventually lead to uncontrolled and rapid proliferation (Figure 3.2). Ultimately, tumor metabolic reprogramming due to aberrant oncogenic activation, or loss of tumor suppression, contributes to tumorigenesis.

Although a variety of metabolic pathways are affected during tumorigenesis, we

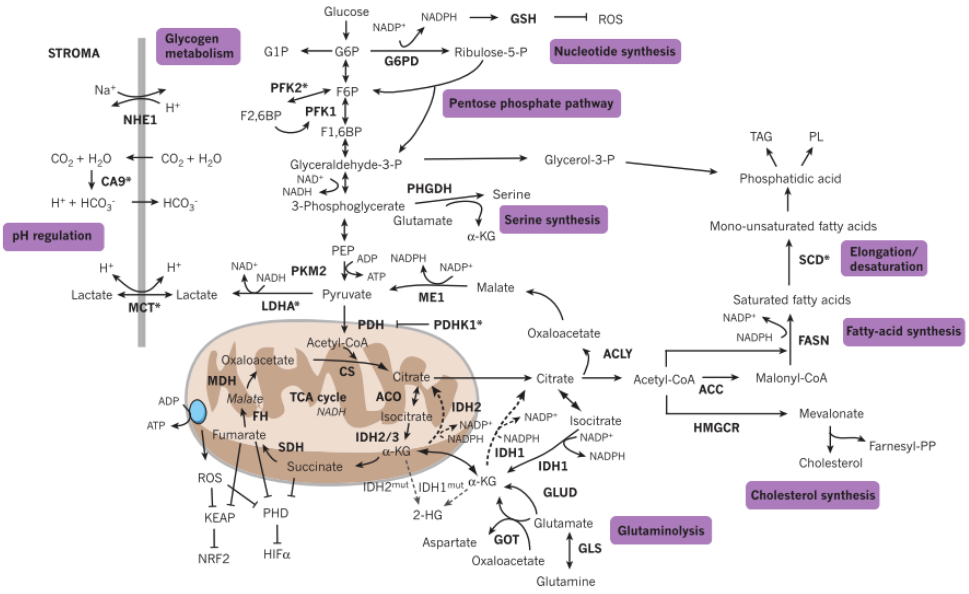

Figure 3.2: **Metabolic activities affected during metabolic reprogramming in cancer cells** An overview of metabolic pathways that contribute to macromolecule synthesis, which include nucleotide synthesis, pentose phosphate pathway, serine synthesis, glutaminolysis, cholesterol synthesis, fatty-acid sythesis and elongation/desaturation. Glycogen metabolism and pH regulation contribute to cellular bioenergetics. Asterisks denote enzymes that are induced during hypoxia. Adapted from [Schulze and Harris, 2012].

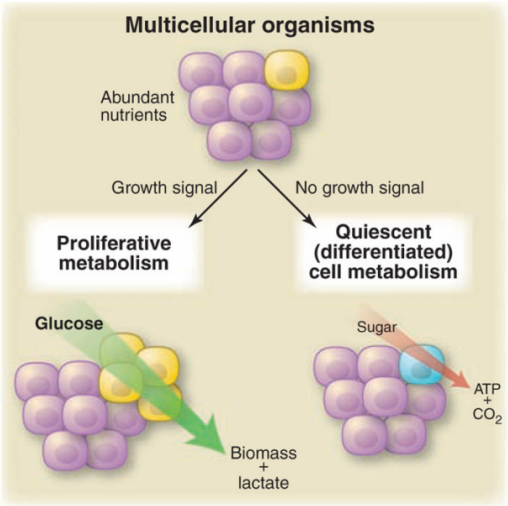

Figure 3.3: **Metabolic phenotype of actively proliferating cells in conditions of abundant nutrients.** Depending on extracellular nutrient conditions, multicellular organisms will either be stimulated to proliferate or remain quiescent. During proliferative metabolisms, organisms will be stimulated to metabolize glucose through glycolysis in order to increase biomass and produce lactate. During limiting conditions, however, oxidative metabolism will be favored in order to maximize ATP production, as no increase in biomass is required. Adapted from [Vander Heiden et al., 2009].

focus our attention on pathways directly pertaining to glucose metabolism, namely glycolysis, the pentose phosphate pathway and mitochondrial metabolism.

3.2.1 Glycolysis and the Warburg Effect

Glycolysis, literally translated into the breakdown of glucose, is the main oxygen-independent pathway in carbohydrate metabolism, which results in the production of pyruvate, ATP and NADH. This central pathway is compromised of 10 enzyme-dependent steps, and each provides an alternative entry point to glycolysis (i.e. 5-carbon sugar entry).

The end product of glycolysis, pyruvate, can either be converted into lactate, or can continue on to feed the tricarboxylic (TCA) cycle and produce ATP through oxidative phosphorylation (OXPHOS) in the mitochondria. An important difference between shuttling pyruvate into lactate production or through OXPHOS is that the former is oxygen-independent, while the latter strictly relies on the presence of oxygen as a proton acceptor at the end of the electron transport chain (ETC). In addition to oxygen reliance, there is a large discrepancy when it comes to the amount of ATP that can be extracted from pyruvate when a cell chooses between either pathway: OXPHOS produces a total of 36 ATP, while converting pyruvate to lactate only produces 2 ATP per molecule of glucose.

One of the first, and arguably most important, metabolic observations in cancer cells is aberrant glyolysis. In 1930, Otto Warburg was the first to describe the peculiar characteristic of cancer cells to favor glycolysis, regardless of ambient oxygen concentrations. This metabolic reprogrammed state in tumor cells is now referred to as the **Warburg effect**, or **aerobic glycolysis** (Figure 3.4). Warburg originally believed that cancer cells were reliant on glycolysis due to defective mitochondria, however, subsequent work has shown that most cancer cells have normal, functional mitochondria [Zong et al., 2016].

As previously mentioned, glycolysis is less efficient than OXPHOS on a per glucose molecule basis. Therefore, cancer cells have to compensate by fluxing glucose at a higher rate to keep up with energy demands. To do this, cells upregulate plasma membrane glucose transporters, such as GLUT 1 [Hsu and Sabatini, 2008]. Medical oncology has exploited the fact that cancer cells flux glucose at higher rates to detect, visualize and grade tumors using Positron Emission Tomography (PET) which uses radio-labeled glucose analogs as *in vivo* metabolic tracers.

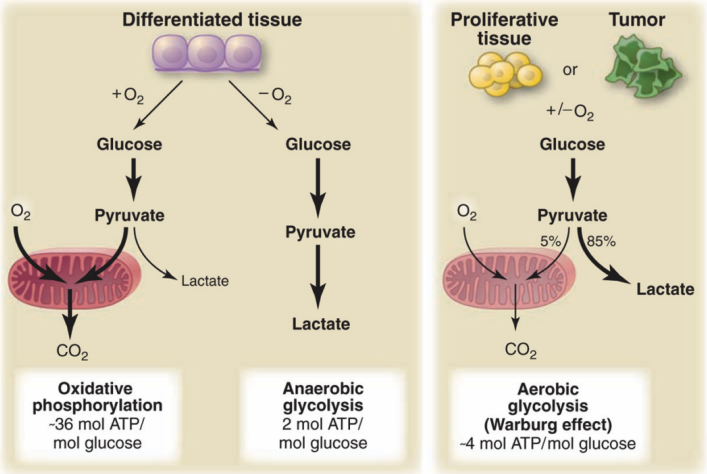

Figure 3.4: **Global differences between oxidative phosphorylation, anaerobic glycolysis and the Warbug effect.** Adapted from [Vander Heiden et al., 2009].

It was previously thought that the hypoxic environment present in tumors selects for cancer cells dependent on aerobic glycolysis. However, recent studies have demonstrated that cancer cells actually exhibit aerobic glycolysis before both aberrant tumor vasculature and the onset of a hostile hypoxic environment. For instance, leukemic cells present in the bloodstream of patients are exposed to higher oxygen levels than in most other parts of the body, but continue to show a preference for aerobic glycolysis [Shanmugam et al., 2009]. Furthermore, lung tumor cells derived from tumors originating in airways, where oxygen levels are equal to ambient levels, have also been shown to favor aerobic glycolysis [Christofk et al., 2008]. Therefore, the hypoxic environment within tumors cannot explain the dependency of cancer cells on aerobic glycolysis.

At first glance, aerobic glycolysis may seem disadvantageous for tumoral cells due to the large discrepancy in ATP production. In order to remain viable, cells must be able to generate ATP, whereas cells that cannot produce ATP will undergo apoptosis. However, as we will see, in order to proliferate, cells need more than just ATP: cellular building blocks and macromolecules are essential as they contribute to biomass generation. It is worth mentioning that in abundant nutrient conditions, aerobic glycolysis is not limiting in the amount of ATP produced when compared to oxidative phosphorylation. Rather, glucose will flux at higher levels and can surpass the energy generation capability of OXPHOS. Additionally, by favoring aerobic glycolysis, cancer cells generate high levels of lactate which is excreted to the extracellular environment through monocarboxylate transporters

(MCTs). In turn, neighboring cells, irrespective of whether they are cancerous or normal, can make use of the lactate in order to feed the TCA cycle to produce energy. The resulting symbiotic relationship between cells is referred to as the 'Reverse Warburg Effect', and illustrates the metabolic heterogeneity present within tumors [Pavlides et al., 2009].

Besides energy considerations, cancer cells require nucleotides, amino acids and lipids to keep up with biomass demands resulting from active proliferation. If the totality of glucose was converted to CO_2 through OXPHOS to generate the maximum ATP possible, this would severely limit the available carbon for macromolecular synthesis. For instance, amino acid synthesis requires more carbons and NADPH equivalents from glucose than ATP. Therefore, it becomes rapidly clear that for biomass generation, the bulk of glucose must be destined to carbon catabolism than to ATP production. Moreover, maintaining a high ATP/ADP ratio would impair glucose flux thereby limiting the availability of precursors for macromolecular synthesis.

The phosphoinositide 3-kinase (PI3K) signaling pathway represents a fundamental link between growth control and glucose metabolism, and is often upregulated in many types of cancer. The PI3K signaling pathway can either shuttle amino acids into protein synthesis through mTOR, or alternatively, regulate glucose flux through AKT. In addition, PI3K activation is the most important event that drives glycolysis, lactate production and macromolecular synthesis in tumoral cells [de Souza et al., 2011].

Although cancer cells rely on a steady carbon and energy source originating from aerobic glycolysis, reactive oxygen species (ROS) are another reason to favor glycolysis. Oxidative phosphorylation in the mitochondria is the major source of cellular ROS production due to proton leakage. When ROS levels exceed the antioxidant capacity of cells, macromolecules and organelles can suffer from oxidative damage, eventually leading to senescence-induction. Therefore, if a cell were to mainly rely on oxidative phosphorylation in nutrient-rich conditions without making the switch to glycolysis, excessive ROS levels would eventually induce either apoptosis or senescence. In addition, glycolysis generates reducing equivalents which also keeps the redox state in balance within the cell. In oncogene-induced senescence (OIS), for instance, RAS upregulation drives glucose uptake, but will eventually lead to OIS due to excessive ROS and the missing cooperating oncogene [Gitenay et al., 2014].

3.2.2 The pentose phosphate pathway

Cells mostly oxidize glucose through glycolysis, however, the remaining glucose is oxidized through the pentose phosphate pathway (PPP) (Figure 3.5) [Stincone et al., 2015]. The PPP is essential to generate 5-carbon sugars used in nucleotide and nucleic acid synthesis [Wamelink et al., 2008]. Another important product of the PPP is NADPH which is required for fatty acid synthesis and plays a pivotal role in maintaining the cellular redox state. Specifically, NADPH is required for the reduction of glutathione (GSH), a major scavenger of ROS in cells. The amount of G6P that is diverted into either the PPP or glycolysis is dependent on the cellular requirement for NADPH, ribose-5-phosphate and ATP [Wamelink et al., 2008]. The PPP is divided into two branches: an irreversible 3 step **oxidative** branch and a reversible **non-oxidative** branch.

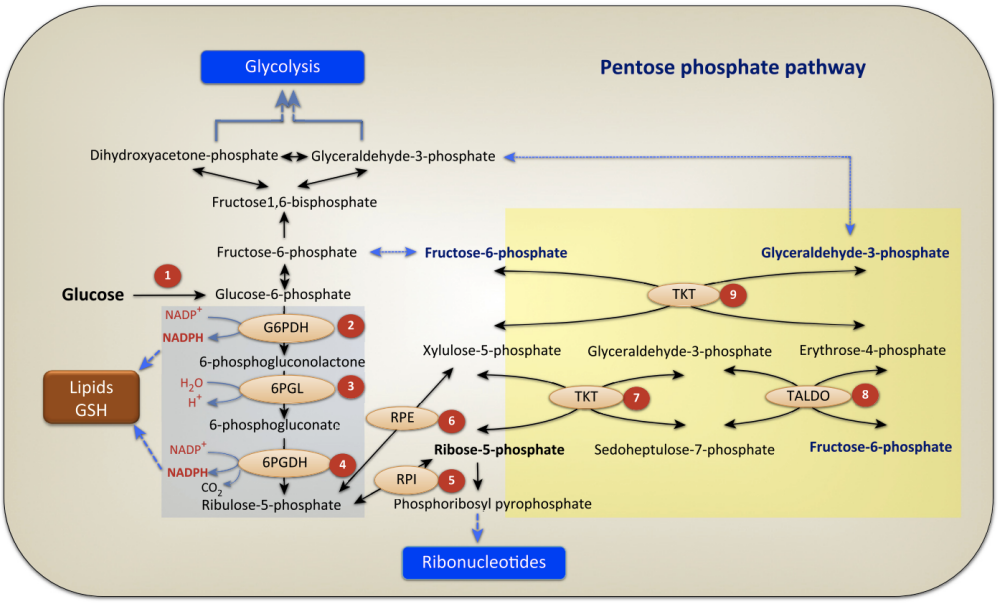

Figure 3.5: **The pentose phosphate pathway (PPP)** The PPP is a major source of ribonucleotides and NADPH, an important component of the cellular redox system. The PPP is split into two phases which include the oxidative (blue) and non-oxidative (yellow) branches. Adapted from [Patra and Hay, 2014].

The oxidative branch of the PPP produces two molecules of NADPH by harnessing the energy released from the conversion of glucose-6-phosphate into ribulose 5-phosphate (Ru5P). Subsequently, Ru5P can then be converted to ribose-5-phosphate (R5P). The non-oxidative branch, on the other hand, is comprised

of a series of reversible reactions important for generating R5P. Furthermore, the non-oxidative PPP can recruit glycolysis intermediates, notably G6P, fructose-6-phosphate and glyceraldehyde-3-phosphate to convert them into pentose phosphates according to the needs of the cell [Patra and Hay, 2014].

The PPP plays an important role in the cancer cells as increased PPP flux generates high NADPH levels to reduce damaging ROS while also producing large quantities of nucleotides for DNA synthesis and repair. It is the PPP's role in combating oxidative stress, however, that is the most well studied within an oncogenic context. Cancer cells are known to produce high ROS levels due to an accelerated metabolism. Additionally, the oxidative stress aids in promoting pro-oncogenic mutations which further promotes tumorigenesis. In turn, cancer cells can protect themselves by boosting their redox capabilites through the shuttling of G6P to the oxidative branch of the PPP to increase NADPH levels. However, when extracellular glucose levels are insufficient to promote oxidative PPP and produce NADPH, ROS levels can increase beyond a certain threshold, thereby inducing cell death [Patra and Hay, 2014]. Low glucose availability, however, induces AMPK activation that helps either maintain or generate NADPH in energetically stressed cells. For instance, AMPK activation can inhibit fatty acid synthesis in order to limit NADPH consumption, while at the same time promote fatty acid oxidation to generate more NADPH [Jeon et al., 2012].

3.2.3 Mitochondrial metabolism

Mitochondrial Basics

Mitochondria are considered the powerhouses of cells as they are in charge of breaking down carbohydrates and fatty acids into ATP through oxidative phosphorylation. Interestingly, mitochondria arose from the engulfment of an alphaproteobacterium by the precursor of an eukaryotic cell, about 2 billion years ago [Gray et al., 2001]. Accordingly, the mitochondrion is the only cytoplasmic organelle to contain its own genome that encodes 13 proteins in humans. The encoded proteins make up the core constituents of the mitochondrial respiratory complexes embedded in the inner mitochondrial membrane [Friedman and Nunnari, 2014].

Mitochondria contain both an **inner** and **outer membrane** separated by an **intermembrane space**. The inner membrane is characterized by many folds, or **cristae**, which extend into the mitochondrial **matrix**. Each structural component of the mitonchondrion plays an important part in the organelle's role as the main

cellular energy producer.

The matrix contains the mitochondrial genome as well as the necessary enzymes responsible for oxidative metabolism. Notably, pyruvate, generated during glycolysis, and fatty acids are transported into the mitochondrial matrix and converted into acetyl CoA. This represents the first step of the **tricarboxylic acid (TCA) cycle**, or the **Krebs cycle** (Figure 3.6). The complete oxidation of acetyl CoA results in CO_2 generation and is also coupled to the reduction of NAD^+ and FAD to NADH and $FADH_2$, respectively. Next, the highly charged electrons generated during the TCA cycle are shuttled to the electron transport chain (ETC) which is located in the inner membrane of the mitochondrion. As the electrons flow along the ETC, protons are actively pumped across the inner mitochondrial membrane, thereby generating an electrical potential and pH gradient across the inner membrane (Figure 3.7). The combination of these free energies generated the proton motive force that drives the synthesis of ATP through the final complex of the respiratory chain, ATP synthase [Adams and Turnbull, 1996].

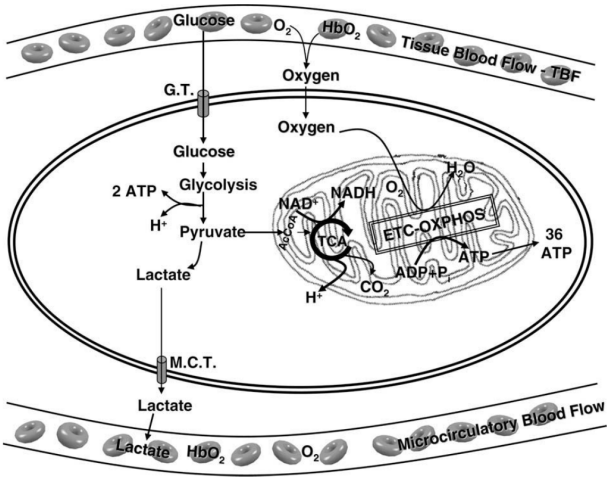

Figure 3.6: **Cellular energy metabolism** A schematic representation of how cellular energy metabolism is connected between cytosolic glycolysis and mitochondrial oxidative phosphorylation. Hb: hemoglobin, G.T.: glucose transporter, M.C.T: monocarboxylase transporter, ETC: electron transport chain, OXPHOS: oxidative phosphorylation. Adapted from [Mayevsky, 2009].

The availability of oxygen is critical for the normal functioning of oxidative phosphorylation in the mitochondrion, as oxygen acts as the final electron acceptor. Interestingly, of the 38 ATPs generated during the oxidation of a molecule of glucose, 2 ATPs are generated during glycolysis while 36 ATPs are generated during

oxidative phosphorylation. When oxygen is not available, cells will convert pyruvate to lactate and excrete it to the extracellular space.

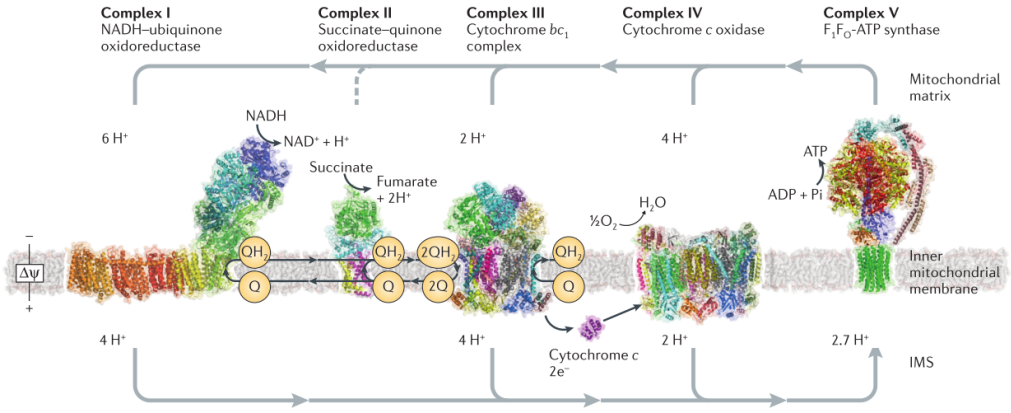

Figure 3.7: **The electron transport chain (ETC)** A schematic representation of the electron transport chain embedded in the inner mitochondrial membrane. Adapted from [Sazanov, 2015].

Mutations either in the mitochondrial genome, or in mitochondrial-associated proteins encoded in the nuclear genome, can lead to a variety of clinical abnormalities which range from mild to fatal [Adams and Turnbull, 1996]. For instance, many research groups are working on clarifying the link between mitochondrial dysfunction and aging. More specifically, causal role of apoptosis and mitochondria in neurodegenerative diseases, such as Parkinson's or Alzheimer's diseases, has been documented in detail [Mayevsky, 2009]. In addition, considering the mitochondria's critical role in cellular bioenergetics, the pivotal role of this organelle in diabetes and obesity is also becoming clear [Mayevsky, 2009].

Mitochondria also play a significant role in cancer cell metabolism, consequences of which are only starting to come to light. Otto Warburg's pioneering work on aberrant glycolysis in cancer cells, termed the Warburg effect, led to the hypothesis that this phenomenon was partially caused by defective mitochondria and oxidative phosphorylation [Zong et al., 2016]. However, more recently, research has focused on the non-energetic aspects of mitochondrial biology, such as apoptosis and ROS.

Mitochondrial ROS generation

It is widely accepted that mitochondria are the main source of reactive oxygen species (ROS) in the cell, a byproduct of normal metabolism which, in high concentrations, can contribute to oxidative stress and aging. ROS excess leads to significant cellular damage, including DNA damage, lipid peroxidation, protein oxidation and impaired respiration, among others [Nita and Grzybowski, 2016]. At low levels, however, ROS have been shown to be beneficial and participate in physiological cell signaling [Thannickal and Fanburg, 2000]. Mitochondrial-specific ROS, also known as superoxide, is produced during oxidative phosphorylation in the ETC when protons leak through mitochondrial complexes I and III. Superoxides can further react to generate other ROS in the form of hydrogen peroxide and hydroxyl radicals. These ROS, in turn, damage mitochondria and decrease the efficiency of the ETC, which results in a positive feedback loop of mitochondrial oxidative damage [Balaban et al., 2005].

Cells, however, have a natural defense system of antioxidants which include glutathione, catalase and superoxide dismutase enzyme which work to metabolize oxidative toxic intermediates. When ROS levels exceed the antioxidant capabilities of cells, however, macromolecules (i.e. DNA) can suffer from oxidative damage. In primary cells, telomeric damage due to unchecked ROS levels has been shown to promote stress-induced senescence [Correia-Melo et al., 2014]. This is the basis for the free-radical theory of aging (FRTA) proposed by Harman, which postulates that organisms age due to a lifelong accumulation of free radical damage (Harman 1954). A few decades later, the theory was extended to specifically implicate mitochondria in the production of superoxide radicals [Harman, 1972].

Part III

Objectives

Recent studies are starting to uncover new roles for glycogen besides just being a glucose depot. Importantly, glycogen metabolism has been implicated in various proliferative contexts. For instance, changes in glycogen metabolism have been associated to the normal aging process in species ranging from *Saccharomyces cerevisiae* to humans. Moreover, the metabolic reprogramming of glycogen metabolism in cancer has been also been reported among a variety of tumor types. Thus, the main objective of this thesis is to elucidate how glycogen affects cellular proliferation, in both physiological and pathological contexts.
The objectives of this thesis can be divided into the following **four** specific aims:

1.To characterize glycogen metabolism in the context of senescence

2.To characterize the senescent response in the absence of glycogen

3.To establish the metabolic phenotype of immortalized cells lacking glycogen

4.To determine how the lack of hepatic glycogen affects the proliferative capacity of hepatocytes *in vivo*

Part IV

Results

Chapter 4

Senescence and glycogen metabolism

4.1 Brief Introduction

Throughout the different kingdoms that form part of the phylogenic tree of life, we can find examples where glucose metabolism is altered as an organism ages. For instance, a study in *Saccharomyces cerevisiae*, a type of yeast which forms part of the **Fungi** kingdom, has demonstrated that glycogen levels increase during chronological aging [Lin et al., 2001]. Moreover, a yeast strain which accumulates glycogen due to a mutation in GP (glycogen phosphorylase), displays rapid aging, in addition to decreased stress resistance [Favre et al., 2008].

In the **Animalia** kingdom, glycogen metabolism has also been implicated in the normal aging process. In *Caenorhabditis elegans*, Gusarov et al demonstrate that high glycogen levels accumulated on a high glucose diet significantly shorten longevity [Gusarov et al., 2017]. Likewise, in *Mus musculus*, the metabolic footprint of aging, revealed through global metabolomics, shows a significant perturbation of carbohydrate metabolism. Specifically, the accumulation of glycogen intermediates in the liver and muscle suggests an altered glycogen metabolism during normal aging [Houtkooper et al., 2011]. Furthermore, our laboratory has recently shown that glycogen contributes directly to the aging phenotype in the

brain [Sinadinos et al., 2014]. Concretely, we demonstrate that targeted silencing of glycogen synthase (GS) in *Drosophila melanogaster* neurons leads to improved neurological functioning and an extended lifespan.

Although a through literature search portrays a strong relationship between glycogen and aging, it seems that few studies have addressed the link between glycogen metabolism and cellular senescence, a recognized hallmark of aging. Notwithstanding, two critical papers reveal an important role for glycogen metabolism during senescence [Seo et al., 2008, Favaro et al., 2012].

The first specific mention of senescence and glycogen metabolism is a study by Seo et al. where it is revealed that glycogenesis, or the biogenesis of glycogen, plays a central role in cellular senescence [Seo et al., 2008]. More specifically, they show that glycogen synthase kinase 3 (GSK3) inactivation, and consequently GS activation, leads to glycogen accumulation and induction of cellular senescence. Further direct evidence is provided when the authors demonstrate that both pharmacological inhibition and siRNA silencing of GSK3 are sufficient to induce cellular senescence with increased glycogenesis. Interestingly, knocking down GS rescues the senescent phenotype, thereby highlighting an important and direct role for glycogen metabolism in senescence.

More recently, Favaro and colleagues delve into the mechanisms of glycogen and senescence in the context of tumor hypoxia [Favaro et al., 2012]. Hypoxia, a condition of oxygen deficiency, is known to induce GS through the activity of HIF1-alpha, leading to an increase in glycogen content in normal and cancer cells [Pescador et al., 2010]. As proof, when U87 glioblastoma cells are exposed to hypoxic conditions, MGS (muscle glycogen synthase) is rapidly induced and glycogen levels increase. This occurs until LGP (liver glycogen phosphorylase) levels subsequently increase, leading to glycogen breakdown. However, when LGP is silenced, glycogen accumulates leading to increased ROS levels and p53-dependent senescence onset. Additionally, the authors demonstrate *in vivo* that tumor xenografts of U87 LGP knockdown cells are significantly smaller than WT counterparts. It is proposed that glycogen degradation is important for the proper function of the pentose phosphate pathway (PPP) in order to maintain a healthy redox balance. Interestingly, it is not experimentally addressed whether the physical accumulation of glycogen could be affecting the onset of senescence.

We dedicate this first chapter to the study of glycogen metabolism in senescence. Specifically, we first determine whether glycogen metabolism is affected during senescence *in vitro*. Next, in the second results section, we assess whether glycogen is essential for a correct entry into senescence by using a cellular model which

lacks glycogen.

4.2 Results I: Senescence and glycogen metabolism

4.2.1 Human lung fibroblasts (HLF-1) accumulate glycogen during replicative senescence

In order to determine whether, in our hands, glycogen metabolism is altered during senescence, we used commercially available human embryonic lung fibroblasts (HLF-1). HLF-1 have been previously shown to undergo replicative senescence, making them an ideal model for our preliminary exploration [Kapeta et al., 2010]. Replicative senescence refers to a limit in the number of times that primary cells can divide in culture, and in human cells, has been attributed to telomere shortening in the absence of telomerase (Figure 4.1) [Harley et al., 1990].

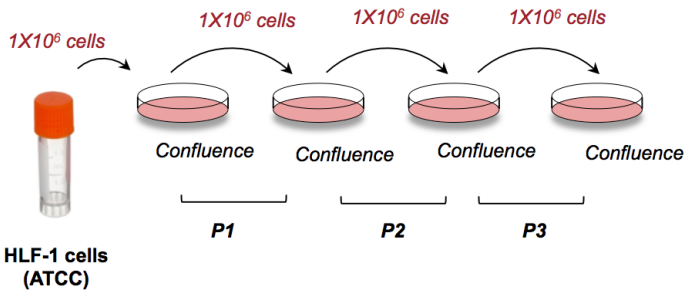

Figure 4.1: **HLF-1 Replicative senescence protocol.**

First, we compared the glycogen content of HLF-1 that were either actively proliferative (early passage), proliferative (medium passage) or senescent (late passage). As represented in Figure 4.2, we observed extremely high levels of glycogen as HLF-1 became progressively older and less proliferative. To corroborate these results, we assessed MGS protein levels, and determined that levels significantly increase as cells became less proliferative (Figure 4.3).

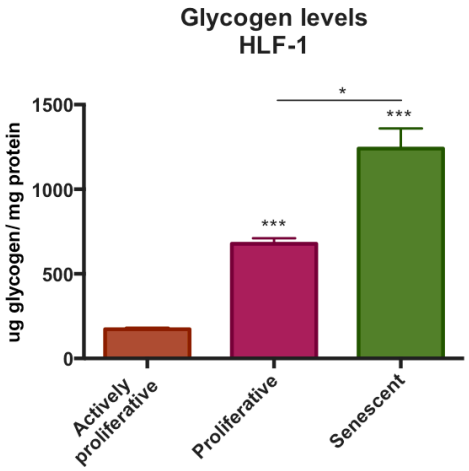

Figure 4.2: **Glycogen levels at different proliferative stages of HLF-1 cells.** Glycogen levels in HLF-1 cells that were either at an early (actively proliferating), medium (proliferating) or late (senescent) passage. Results are expressed as [ug glycogen / mg protein]. Results are presented as the mean $+/-$ s.e.m of 3 independent experiments. The following p values were considered to be statistically significant: * $p \leq 0.05$, *** $p \leq 0.001$.

In order to confirm that cells were senescent, we proceeded to determine the presence of several protein markers associated to the senescent state. The protein levels of cell cycle inhibitors, p16 and p21, steadily increased as HLF-1 became less proliferative. Furthermore, we verified CHK1 levels, a protein required for checkpoint-mediated cell cycle arrest in response to DNA damage [Patil et al., 2014]. We determined that as HLF-1 entered a senescent state through repetitive passaging, CHK1 protein levels increased significantly (Figure 4.3).

4.2.2 HLF-1 accumulate glycogen during stress-induced senescence (SIPS)

In the previous section, we were able to verify that human lung fibroblasts accumulate glycogen as they become less proliferative when subjected to a replicative senescence protocol (Figure 4.1). Consequently, we were interested in clarifying whether the significant changes in glycogen metabolism patterns observed during replicative senescence were specific to this type of senescence or whether this was true for other senescence models.

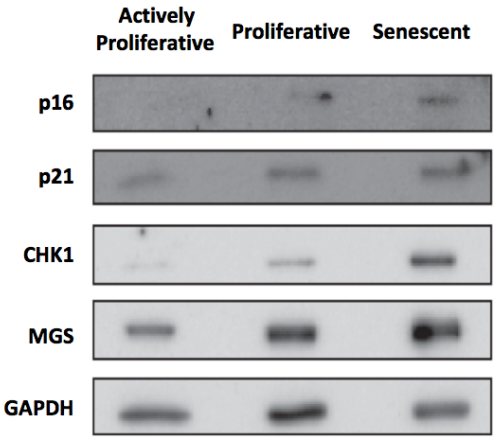

Figure 4.3: **Western blot of senescence markers in HLF-1 cells.** Total HLF-1 cell homogenates obtained at indicated proliferative stages were probed for senescent markers and muscle glycogen synthase (MGS). GAPDH was used as a loading control.

To test this, we induced SIPS by treating HLF-1 with epoxomicin, a proteasome-specific inhibitor. Proteasome-depedent degradation is essential for normal cellular homeostasis and survival, and its activation has been demonstrated to confer lifespan extension in human fibroblasts [Chondrogianni et al., 2015]. Accordingly, proteasome-inhibition due to epoxomicin treatment has been shown to induce a senescence-like phenotype in primary fibroblasts [Chondrogianni et al., 2008].

In order to determine the effect of epoxomicin on glycogen metabolism in HLF-1, we performed a time course experiment over a 14 day period. We closely monitored glycogen content in both non-treated and epoxomicin-treated HLF-1. As observed in replicative senescence experiments, glycogen content massively increased as cells became senescent due to proteasome inhibition by epoxomicin (Figure 4.4). Non-treated HLF-1 also showed a modest variation in glycogen content, which was likely due to unfavorable cell culture conditions (overly confluent plate) and the long duration of the experiment (loss of proliferative capacity).

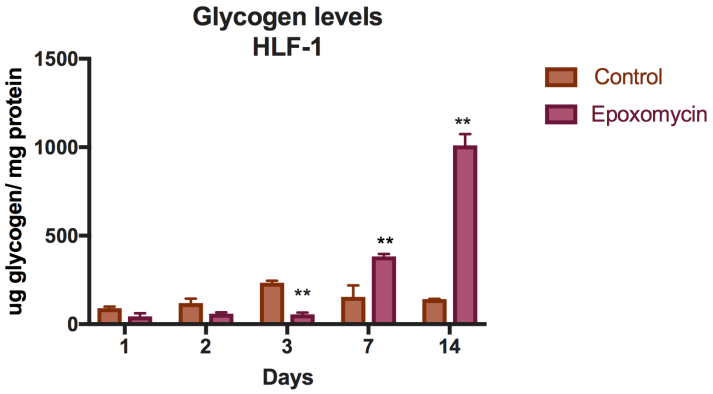

Figure 4.4: **Glycogen levels during stress-induced premature senescence (SIPS) in HLF-1 cells.** HLF-1 cells were subjected to a 14 day epoxomicin treatment which resulted in SIPS. Glycogen levels were measured at the indicated time points. Control cells were incubated with DMSO. Results are expressed as [ug glycogen / mg protein], and are presented as the mean $+/-$ s.e.m of 3 independent experiments. The following p value was considered to be statistically significant: ** $p \leq 0.01$.

4.2.3 Mouse embryonic fibroblasts (MEFs) accumulate glycogen during replicative senescence

The next step was to verify whether glycogen alterations during senescence also occurred in murine cells. For this, we isolated and subjected wild type mouse embryonic fibroblasts (MEFs) to the same replicative senescence protocol (Figure 4.5), previously performed on HLF-1.

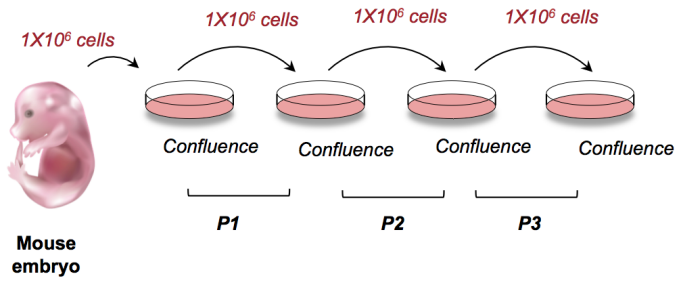

Figure 4.5: **Replicative senescence protocol using isolated mouse embryonic fibroblasts (MEFs).**

We monitored glycogen levels throughout passages and determined that they significantly increased as MEFs became progressively less proliferative. Furthermore, we also observed that MGS protein levels mirrored the increase in glycogen content as cells entered a senescent state induced by repeated passaging (Figure 4.6).

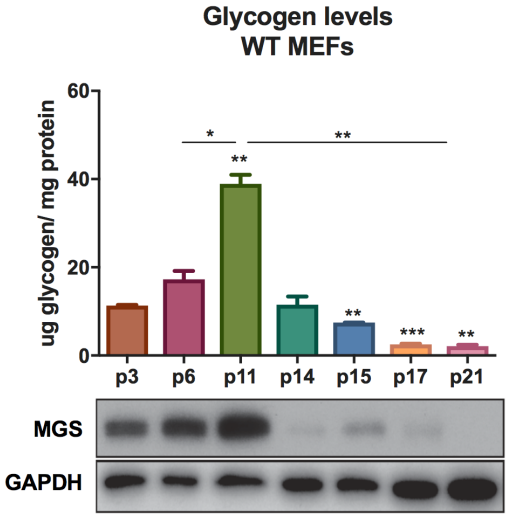

Figure 4.6: **Glycogen levels with corresponding MGS protein expression during replicative senescence in WT MEFs.** MEFs were subjected to a replicative senescence protocol, and were immortalized (passages greater than 11). We have included MGS immunoblotting for the same passages. GAPDH was used as a loading control. Results are expressed as [ug glycogen / mg protein] and presented as the mean $+/-$ s.e.m of 3 independent experiments. The following p values were considered to be statistically significant: * $p \leq 0.05$, ** $p \leq 0.01$, *** $p \leq 0.001$

It is interesting to note that once MEFs started regaining their proliferative capability as they entered an immortalized state, the cells progressively lost the ability to synthesize glycogen. At passage 14 and beyond, glycogen levels sharply decreased as did MGS protein levels.

4.3 Results II: Senescence and the absence of glycogen

From section 4.2, we can state that glycogen levels are closely associated to the proliferative state of primary cells: when cells are actively proliferative, glycogen content is low. Conversely, when cells reach a senescent state, due to either culture conditions or chemically-induced growth arrest, glycogenesis increases dramatically. Furthermore, when MEFs enter an immortalized state due to regular passaging, they lose the ability to synthesize glycogen.

Next, we determined what happens to the proliferative capacity of cells when glycogen is not readily available. For this, we took advantage of a constitutive muscle glycogen synthase (MGS) KO mouse model. Essentially, due to the absence of the glycogen synthesizing enzyme, MGS, these mice do not accumulate glycogen anywhere in the body. The only exception is the liver, since hepatic glycogen is synthesized by the liver-specific isoform, LGS.

Close to 90% of MGS KO mice die soon after birth due to cardio-respiratory failure. However, timed matings show that normal Mendelian proportions are maintained until d.p.c 18.5 [Pederson et al., 2004]. Therefore, to detour the high perinatal lethality of this model, we chose to isolate MEFs at d.p.c 14.5 in order to perform *in vitro* experiments.

4.3.1 Model verification: characterization of primary MEFs isolated from MGS KO embryos

During the MEF isolation protocol, we always kept either the head or tail tip of the embryo in order to determine the genotype. Additionally, before performing experiments with isolated MEFs, we always verified that the primary cell cultures matched the initial genotype. For this, we performed Western blots to detect the presence of MGS in cell homogenates. MGS KO primary MEFs were devoid of the MGS protein (Figure 4.7 a), while mRNA transcripts were absent for the Gys1 gene (Figure 4.7 b). We also measured whether glycogen was present in MGS KO MEFs, and we concluded that glycogen levels were non-detectable, thereby confirming the efficacy of our knockout model in isolated MEFs (Figure 4.7 c). Lastly, we did not observe any important differences between genotypes, in either viability or morphology (Figure 4.8).

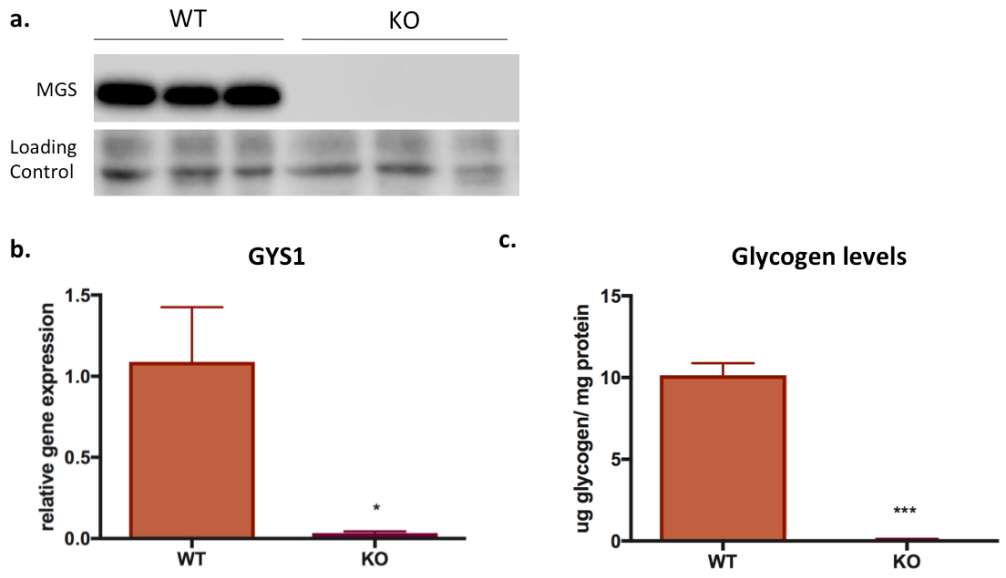

Figure 4.7: **Primary MGS KO MEF model verification.** **a)** Representative Western blot from total homogenates of cell samples obtained from both MGS WT and KO primary MEFs at p2. Loading control was performed using the REVERT total protein stain (LI-COR), **b)** GYS1 gene expression levels were measured in both genotypes at p2, and data were normalized for MGS WT MEFs relative to r18s gene expression (n=5), and **c)** glycogen levels were measured in both genotypes at p2 and expressed as [ug glycogen / mg protein] (n=5). Results are presented as the mean $+/-$ s.e.m. The following p values were considered to be statistically significant: * $p \leq 0.05$, *** $p \leq 0.001$.

4.3.2 MGS KO MEFs demonstrate a proliferative advantage during replicative senescence

First, we measured MGS protein levels as MEFs entered senescence. Similarly to the results in the previous section, we observed that MGS WT cells showed a clear increase in MGS, while MGS KO MEFs maintained their KO status (Figure 4.9).

Next, we calculated the population doubling levels (PDL) of each genotype. PDL are a measure of how long it takes for certain cell populations to double in size, and is an accurate measure of cell growth especially in proliferative arrest contexts. MGS WT and KO MEFs were subjected to the replicative senescence pro-

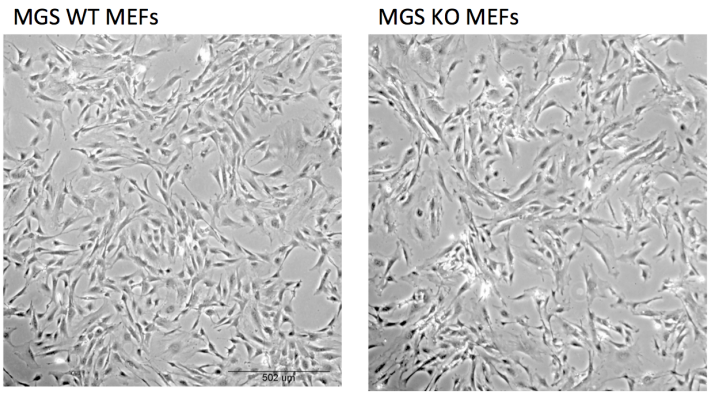

Figure 4.8: **MEF cell morphology for both MGS WT and KO MEFs at p2.** Phase contrast images of primary MGS WT and KO MEFs at passage 2. Images were taken with a 10x objective lens.

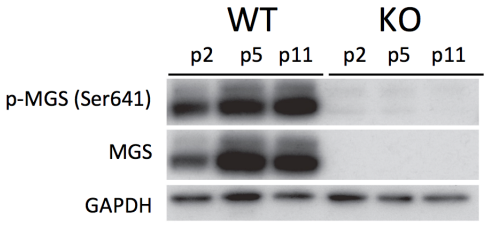

Figure 4.9: **Western blot of MGS in MGS WT and KO MEFs throughout passages to senescence.** Total MGS WT and KO MEF cell homogenates were probed for MGS and p-MGS(Ser641). GAPDH was used as a loading control.

tocol (Figure 4.5), where 10^6 cells were passed each time confluence was reached.

We drew three important conclusions from the cumulative population doubling graph (Figure 4.10). First, when cells were actively proliferating at early passages, we did not observe significant differences in proliferation rates between genotypes. Second, both MGS WT and KO MEFs entered a proliferative plateau around passage 11, suggesting that both genotypes entered a senescent phase. Lastly, MGS KO MEFs manifested faster immortalization post-growth arrest (p11) than WT counterparts. Furthermore, more population doubling calculations after immortalization were made for MGS KO MEFs because they consistently reached confluence faster than wild types, suggesting differences in proliferative capacity. These observations suggest that MGS KO MEFs demonstrate a proliferative advantage, which allows for a shorter senescent phase and faster immortalization

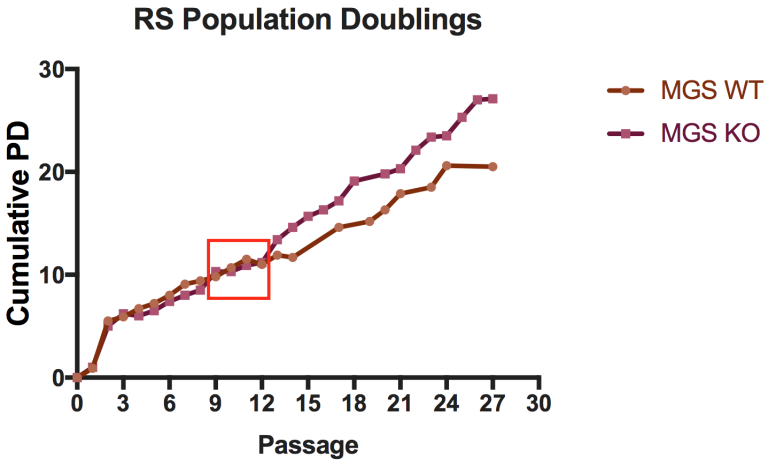

Figure 4.10: **Cumulative population doubling (PD) of MGS WT and KO MEFs during replicative senescence.** Graphical representation of cumulative PD of MGS WT and KO MEFs subjected to a replicative senescence protocol. PD refers to the time it takes for a cell population to double in size. The red box indicates passages when cells were growth arrested.

process.

4.3.3 MGS WT and KO MEFs display senescence markers

In order to verify that both MGS WT and KO MEFs were in fact senescent at passage 11, we assessed cell cultures for various senescence-associated phenotypes. Notably, we monitored cell morphology, SA-B-GAL, and certain senescence protein markers.

A visual indication of the senescent state is that cells become larger and flatter than normal proliferative cells. Passage 11 senescent MGS WT and KO MEFs were observed using a phase-contrast microscope, and it was determined that both genotypes exhibited a flattened and enlarged cell morphology (Figure 4.11), indicative of a senescent state.

Besides changes in cell morphology, positive SA-B-GAL staining is another well known biomarker of cellular senescence, and is explained by the increased presence of lysosomal beta-galactosiade in senescent cells and tissues [Dimri et al., 1995]. Passage 11 MGS WT MEFs exhibited extensive positive blue staining, while MGS KO MEFs showed significantly less staining than WT counterparts

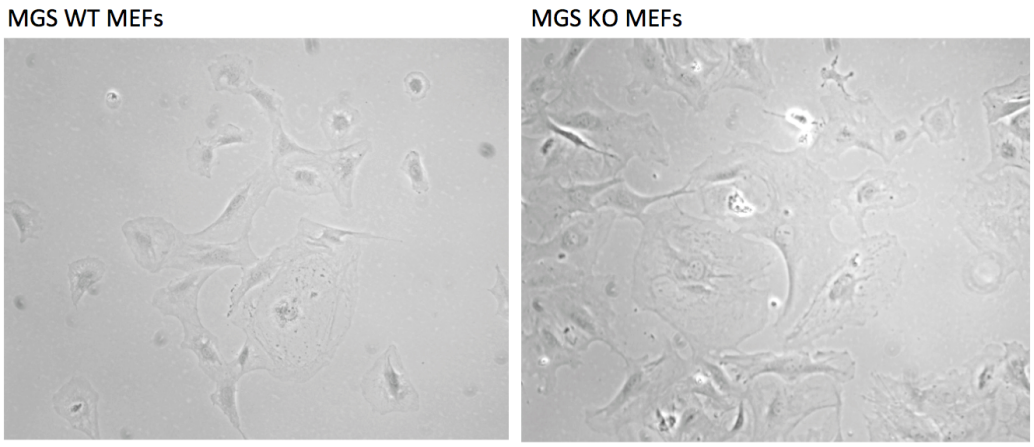

Figure 4.11: **Senescent cell morphology.** Representative phase contrast images of senescent MGS WT and KO primary MEFs at passage 11 after being subjected to replicative senescence. Images were taken with a 40x objective lens.

(Figure 4.12).

Cell cycle inhibitor proteins (p16, p21, p53) and stress-induced protein (p38), known to participate in senescence, were probed for both genotypes to determine possible mechanistic differences in senescence induction. Interestingly, we observed slightly lower protein levels of p21 and p16, while p38 anf p53 were similarly expressed in both genotypes (Figure 4.13).

4.3.4 MGS KO MEFs display a proliferative advantage during the 3T3-induced senescence

The 3T3 protocol is another established way of immortalizing primary MEFs. As for the replicative senescence protocol, primary cells enter a non-proliferative phase before becoming immortalized. Rather than passaging 10^6 cells every time confluence is reached, as is the case in replicative senescence, 10^6 cells are passaged every three days regardless of whether cells have reached confluence (Figure 4.14). In this way, spontaneously immortalized cells are established after about 15 passages. We subjected MGS WT and KO MEFs to the 3T3 protocol in order to corroborate our results from the replicative senescence experiments.

PDL was calculated the same way as for the replicative senescence protocol. How-

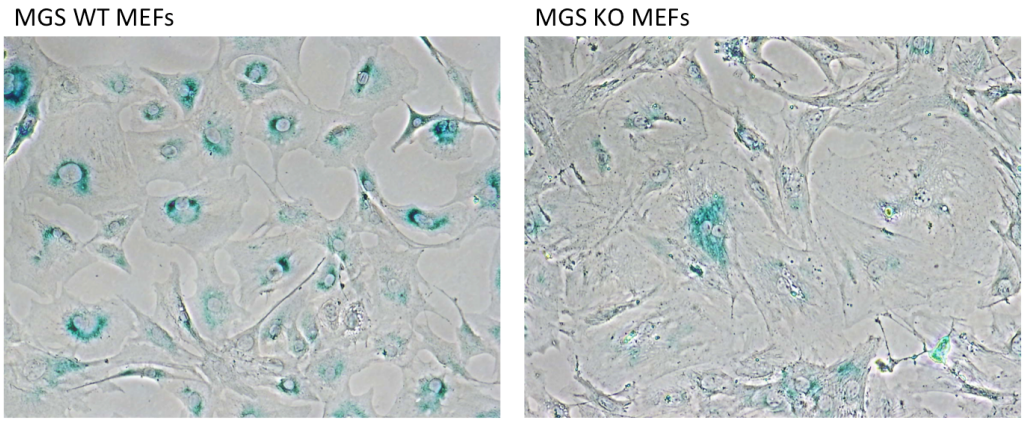

Figure 4.12: **Senescence-associated beta galactosidase (SA-B-GAL) staining of MGS WT and KO MEFs at passage 11.** Representative phase contrast images of SA-B-GAL staining of primary MEFs at passage 11 after being subjected to replicative senescence. Images were taken with a 40x objective lens.

ever, in this scenario, the same number of calculations were made for each genotype since the time factor was a constant of 3 days. Interestingly, as in the replicative senescence protocol, we observed a similar growth plateau around passage 10-11 for both genotypes. Additionally, we observed faster immortalization of MGS KO MEFs than wild type counterparts.

Overall, we drew the same conclusions by using a different protocol to induce replicative senescence in primary cells: MGS KO MEFs bypassed senescence and became immortalized faster than WT counterparts. To gain insight into the possibility that glycogen was actively modulating pathways related to senescence onset, we performed a microarray analysis comparing actively proliferative versus senescent MEFs for both genotypes.

4.3.5 Experimental setup of the transcriptomic study and preliminary results

In order to understand which pathways could be regulating senescence in the absence of glycogen, we performed a transcriptomic analysis using microarray technology. For the experimental design, we chose four different conditions which included: actively proliferating MGS WT MEFs (p2), actively proliferating MGS KO MEFs (p2), senescent MGS WT MEFs (p11), and senescent MGS KO MEFs

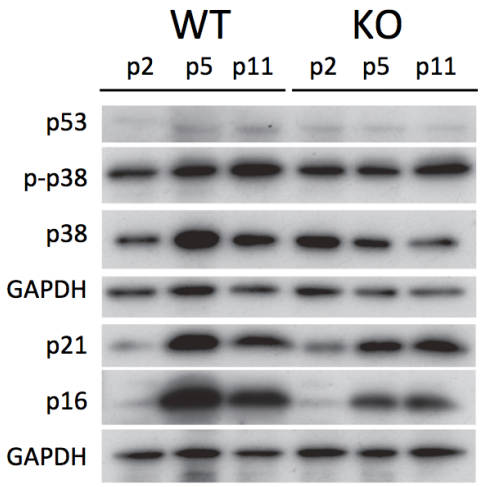

Figure 4.13: **Western blot of senescence markers in both MGS WT and KO MEFs throughout passages to replicative senescence.** Total MGS WT and KO MEF homogenates obtained at indicated passages were probed for senescent markers. GAPDH was used as a loading control.

(p11) (Figure 4.16). In essence, the comparison was made between genotypes at two different time points: p2 which represented actively proliferative MEFs, and p11 when cells were non-proliferative. In addition to the four aforementioned conditions, we included 3 biological replicates for each condition.

Strikingly, the only differentially down regulated gene in MGS KO versus WT at passage 2 is Gys1, which is the gene that encodes MGS. This serves as an internal control of our MGS KO model (Supplementary table 8.2). Furthermore, the top modulated gene lists for each comparison are included in the supplementary information (Supplementary tables 8.3, 8.4, 8.5, 8.6, 8.7, 8.8).

4.3.6 Gene Set Enrichment Analysis (GSEA) identifies the TGF-b pathway as differentially modulated in senescent MEFs lacking glycogen

In order to give meaning to the list of differentially expressed genes, we performed a gene set enrichment analysis (GSEA) that detects which genes are over- or under-represented in a specific gene set. First, GSEA revealed that there were counter-enriched senescence-related pathways that were conserved between genotypes, specifically DNA replication and cell cycle (Figure 4.17). Secondly, GSEA

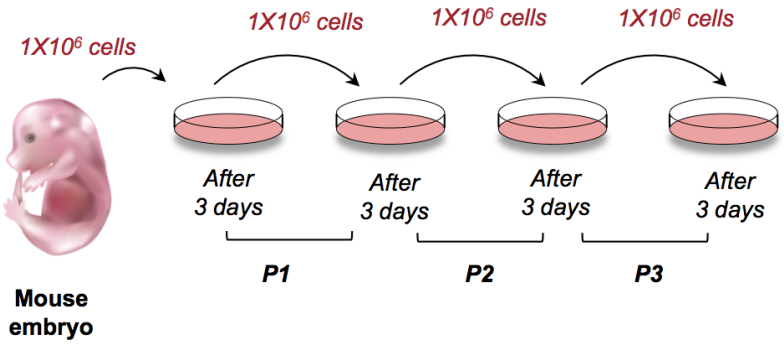

Figure 4.14: **3T3 immortalization protocol.**

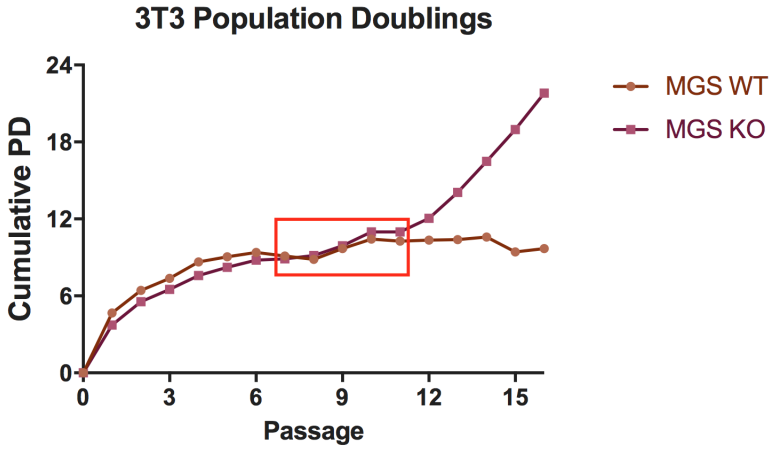

Figure 4.15: **Cumulative population doubling (PD) of MGS WT and KO MEFs during the 3T3 immortalization protocol.** Graphical representation of cumulative PD of MGS WT and KO MEFs subjected to a 3T3 immortalization protocol. The red box indicates passages when cells were growth arrested.

revealed that the TGF-b pathway was associated with WT p11 MEFs. In other words, MGS KO senescent MEFs significantly counter-enriched genes related to the TGF-b pathway (Figure 4.17).

Figure 4.16: **Experimental conditions of transcriptomic study.** We performed a transcriptomic study which included the four experimental conditions indicated in the figure. The yellow bolt represents senescence-induction through the replicative senescence protocol.

4.3.7 Functional Validation of GSEA enrichment

We experimentally validated the results from the microarray experiment by performing Western blots probing some key proteins. The TGF-b pathway was differentially enriched between p11 MGS WT and KO MEFs. Therefore, we probed SMAD2, which is the canonical TGF-b effector protein that mediates signal propagation of the TGF-b pathway. In addition, we measured FoxO1 protein expression, as it has been shown to act as a nodal point for the integration of the TGF-b and PI3K pathways, the latter which encompasses the insulin-dependent regulation of GSK3 and GS [Seoane et al., 2004]. We observed that FoxO1 levels steadily increased in MGS WT MEFs, along with a mirrored increase in SMAD2. In MEFs lacking glycogen, however, FoxO1 levels were very low, and SMAD2 levels were constant through different passages into senescence (Figure 4.18).

4.3.8 Transcriptomic signatures

Gamma-gamma hierarchical model analysis is an important tool which allows us to determine the expression pattern (hypothesis) that each gene follows. In our case, we had 4 groups (WT p2, KO p2, WT p11, KO p11) which allowed us to generate 15 hypotheses. In the simplest of cases, our hypothesis was *null* when the genes of all four groups were equally expressed (WT p2 = KO p2 = WT p11 = KO p11). In our results, 80.9% of genes were equally expressed between our four groups. From there, we proposed 14 different alternative hypotheses, numbered from 1 to 14. Most alternative patterns captured less than 0.5% of total genes, which we decided to disregard. Patterns 5 and 6, however, captured 12.1% (2993 genes) and 5.6% (1289 genes) of total genes, respectively (Table 4.1).

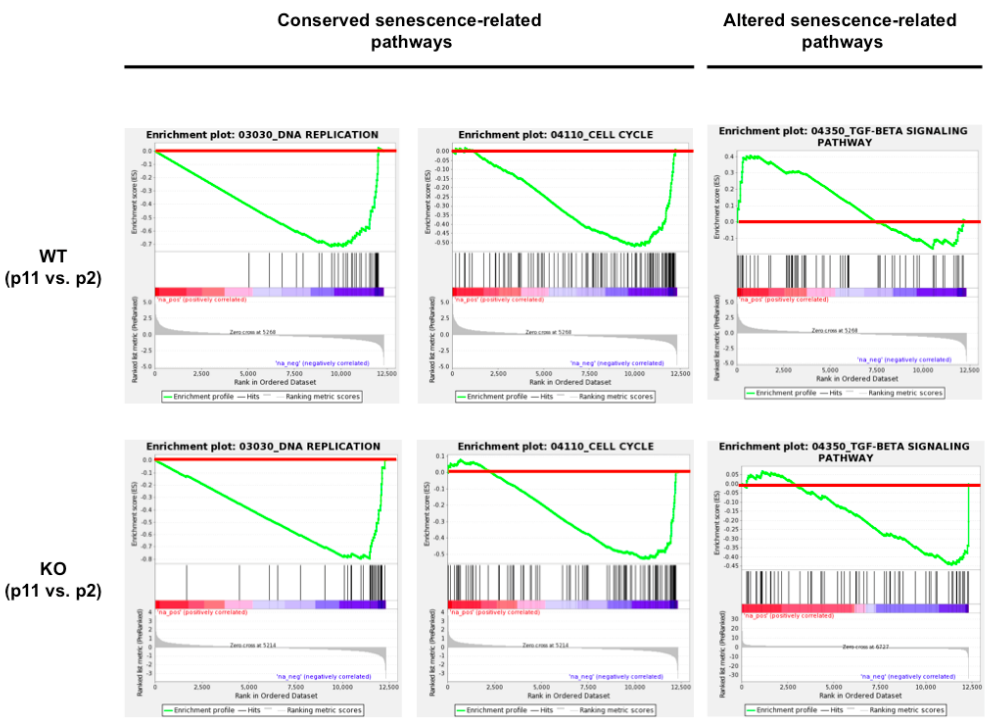

Figure 4.17: **Enrichment plots from gene set enrichment analysis (GSEA).** The enrichment plots contain profiles of the running enrichment scores (ES, green line) and positions of the gene set members on the rank ordered list in GSEA. The red lines indicate an ES of 0.

Transcriptomic signature #6 reveals gene expression differences between actively proliferating and senescent MEFs, irrespective of genotype

Transcriptomic pattern 6 was essentially a comparison between actively proliferating and senescent cells, without taking into account the genotype (WT p2 = KO p2 != WT p11 = KO p11). We took the list of 1289 genes included in this pattern, and subjected it to KEGG pathway enrichment (Figure 4.20). In Figure 4.20, we include KEGG pathways that are significantly enriched in this pattern's gene list. As expected, most KEGG pathways were related to important cellular processes that take place during senescence: the cell cycle, DNA replication, mismatch repair, among others. The enrichment of this pattern served as an internal control of our results, as our analysis was sensitive enough to expose differences between our actively proliferating and senescent cells.

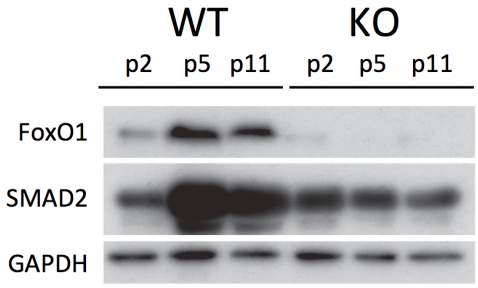

Figure 4.18: **Functional validation of microarray by Western blot.** Total MGS WT and KO MEF homogenates obtained at indicated passages were probed for FoxO1 and SMAD2 proteins. GAPDH was used as a loading control.

Pattern	# genes	% genes	Hypothesis
Pattern 0	40557	80.9% genes	WT p2 = WT p11 = KO p2 = KO p11
Pattern 1	88	0.5% genes	WT p2 = WT p11 = KO p2 !=KO p11
Pattern 2	0	0% genes	WT p2 = WT p11 = KO p11 !=KO p2
Pattern 3	2	0% genes	WT p2 = WT p11 !=KO p2 = KO p11
Pattern 4	0	0% genes	WT p2 = WT p11 !=KO p2 !=KO p11
Pattern 5	2993	12.1% genes	WT p2 = KO p2 = KO p11 !=WT p11
Pattern 6	1289	5.6% genes	WT p2 = KO p2 !=WT p11 = KO p11
Pattern 7	145	0.7% genes	WT p2 = KO p2 !=WT p11 !=KO p11
Pattern 8	0	0% genes	WT p2 = KO p11 !=WT p11 = KO p2
Pattern 9	0	0% genes	WT p2 !=WT p11 = KO p2 = KO p11
Pattern 10	0	0% genes	WT p2 !=WT p11 = KO p2 !=KO p11
Pattern 11	0	0% genes	WT p2 = KO p11 !=WT p11 !=KO p2
Pattern 12	0	0% genes	WT p2 !=WT p11 = KO p11 !=KO p2
Pattern 13	27	0.1% genes	WT p2 !=WT p11 !=KO p2 = KO p11
Pattern 14	0	0% genes	WT p2 !=WT p11 !=KO p2 !=KO p11

Table 4.1: **Overview of transcriptomic signatures.**

Transcriptomic signature # 5 indicates that senescent MGS KO MEFs are more similar to actively proliferative cells, irrespective of genotype

In Pattern 5, we were comparing all conditions against senescent p11 WT cells (WT p2 = KO p2 = KO p11 != WT p11). We took the list of 2993 genes included in this pattern, and subjected it to KEGG pathway enrichment. Figure 4.22 includes the most enriched KEGG pathways mined from this pattern's gene list. We deduced that many of these pathways play fundamental roles in proliferation and

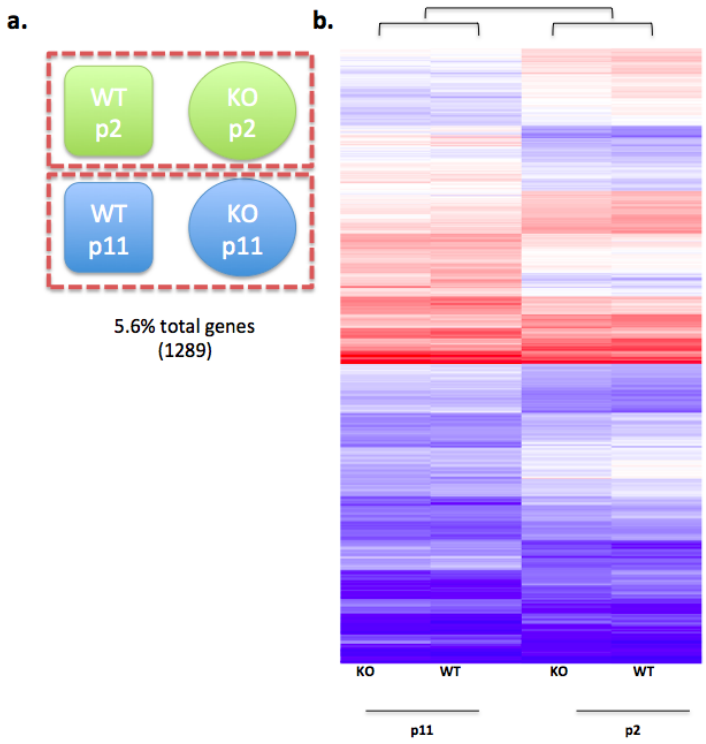

Figure 4.19: **Transcriptomic signature 6. a)** Visual representation of the comparison being made, and **b)** heatmap of pattern 6 representing the different experimental groups. Blue represents depleted genes, whereas red represents enriched genes.

cancer. Specifically, aberrant transciptional regulation, ribosome biogenesis and proteoglycan effectors are known to participate in the malignant process [Lee and Young, 2013, Pelletier et al., 2018, Iozzo and Sanderson, 2011]. Furthermore, members of the MAPK, RAS and TGF-b pathways are mutated in many different cancer types [Burotto et al., 2014, Fernández-Medarde and Santos, 2011, Massagué, 2008].

4.4 Conclusions

We showed that glycogen accumulated during senescence in both human and mouse cells. Furthermore, in the absence of glycogen, MEFs entered a pseudo-senescent state and became immortalized faster than wild type counterparts. Through transcriptomic analysis, we highlighted that the TGF-b pathway is differentially

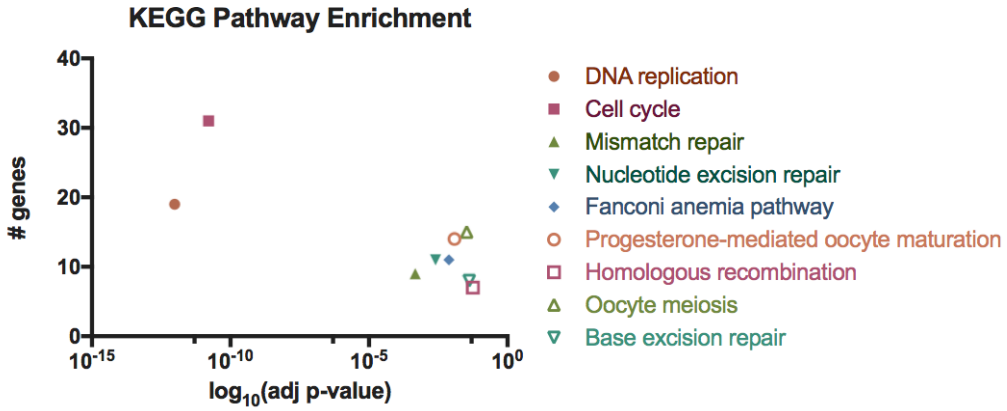

Figure 4.20: **Transcriptomic signature 6 KEGG Pathway enrichment.** Graphical representation of enriched KEGG pathways that meet the criteria of highest number of genes and most significant adjusted p-value ($\log_1 0$).

enriched in both genotypes: it is enriched in senescent MGS WT cells, while MGS KO MEFs showed a counter-enrichment of the same pathway. Interestingly, we observed very low protein levels of FoxO1 and constant levels of SMAD2 in MGS KO MEFs. Lastly, we analyzed transcriptomic signatures, and determined that senescent MGS KO MEFs are more similar to actively proliferative cells than to senescent MGS WT MEFs.

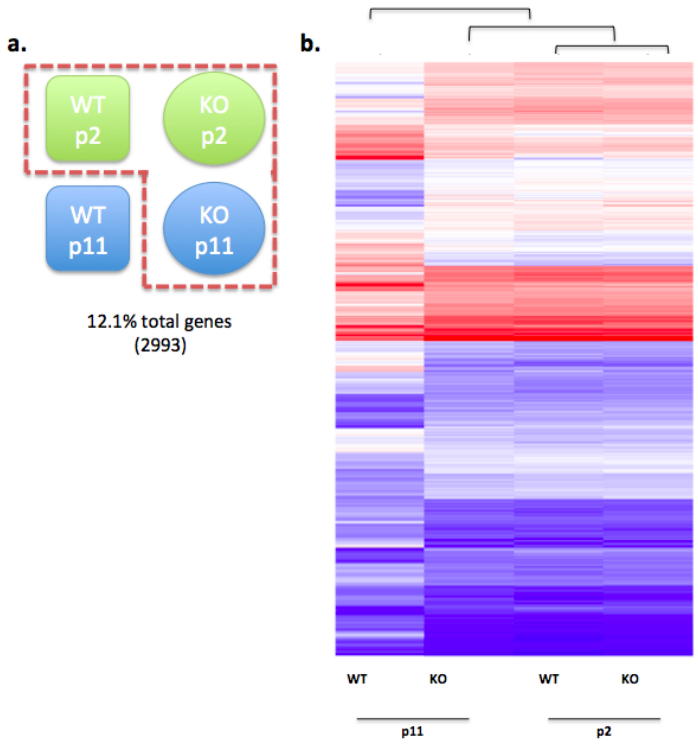

Figure 4.21: **Trancriptomic signature #5. a)** Visual representation of the comparison being made, and **b)** heatmap of pattern #5 representing the different experimental groups. Blue represents depleted genes, whereas red represents enriched genes.

Chapter 5

Metabolic phenotyping of immortalized mouse embryonic fibroblasts

5.1 Brief Introduction

In the previous chapter, we reveal two important facts: 1) when human and mouse cells enter senescence, they accumulate large quantities of glycogen, and 2) when

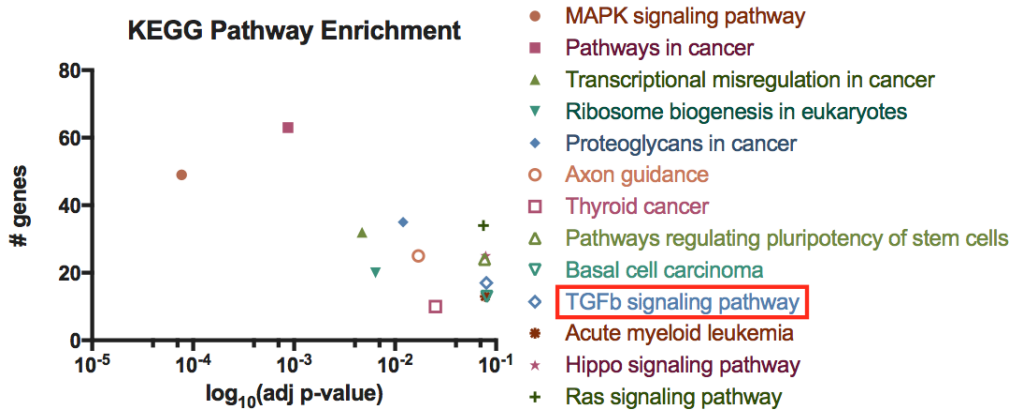

Figure 4.22: **Transcriptomic signature #5 KEGG pathway enrichment.** Graphical representation of enriched KEGG pathways that meet the criteria of highest number of genes and most significant adjusted p-value ($\log_1 0$).

glycogen is not available, primary MEFs acquire a proliferative advantage that allows them to bypass senescence and become immortalized faster than WT counterparts. Our transcriptomic analysis hints at the implication of the TGF-b pathway in addition to the glycolytic pathway, an important metabolic pathway involved in metabolic reprogramming.

Glucose metabolic reprogramming, a recently described hallmark of cancer, has received renewed attention since Otto Warburg's initial studies. Warburg was the first to observe that cancer cells prefer to convert their glucose carbon to lactate, even in the presence of oxygen [Warburg, 1956]. Normal cells, on the other hand, oxidize glucose to CO_2 in the mitochondria in order to maximize ATP production. Although, at first, this phenomenon seems irrational, one has to realize that the major issue for proliferative cells is not how to maximize ATP yield, rather how to maximize the flux of carbon into macromolecular synthetic pathways to reliably produce two daughter cells [Ward and Thompson, 2012]. In addition, mounting evidence is indicating that metabolic alterations in cancer cells are a primary function of activated oncogenes and inactivated tumor suppressors [Ward and Thompson, 2012].

Although most literature focuses on the shift in glucose metabolism during metabolic reprogramming, glycogen metabolism can also be reprogrammed in cancer. Glycogen levels vary greatly among different tumor types, but significantly high levels

have been observed in breast, kidney, uterus, ovary, skin, and brain cancer cell lines [Zois et al., 2014]. Furthermore, it has been shown that glycogen content is inversely related to proliferation rate [Rousset et al., 1981, Takahashi et al., 1999]. The tissue origin of the tumor is important in determining the glycogen content in cancer cell lines. For instance, it has been observed that in cancer cell lines originating from tissues with normally low glycogen content, transformation results in an unusual increase of glycogen storage. In cancer cell lines derived from the liver where glycogen levels are initially very high, the situation is inversed: the malignant process consistently results in a decrease in glycogen content [Rousset et al., 1981].

In this results chapter, we aim to clarify how the absence of glycogen affects cellular metabolic functions, and how these changes can translate into a proliferative advantage. Specifically, we focus our studies on stable immortalized MEF lines, as primary MEF cultures are very sensitive to passaging and culture conditions. Although immortalized cells are not malignant transformed cancer cells, they do exhibit the most fundamental cancer hallmark: **limitless replicative potential**.

5.2 Results

5.2.1 Model verification: characterization of immortalized MEFs cell lines

Immortalized cell lines were generated by subjecting primary MEFs to a replicative senescence protocol: 10^6 primary MEFs were passaged when a 10 cm plate reached confluence. Cells were genotyped by Western blot in order to verify that MGS KO MEFs were devoid of MGS protein (Figure 5.1b). In addition, glycogen was not detected in immortalized MGS KO MEFs (Figure 5.1a). It is important to note that although MGS WT MEFs did contain measurable amounts of glycogen, levels were lower than in primary proliferative WT MEFs (p2) (Figure 4.6).

5.2.2 Immortalized MGS KO MEFs maintain a proliferative advantage over wild types

In order to determine whether differences in cell proliferation were maintained after spontaneous immortalization, we performed an assay to assess the difference in proliferation capacity between genotypes. The same number of MGS WT and

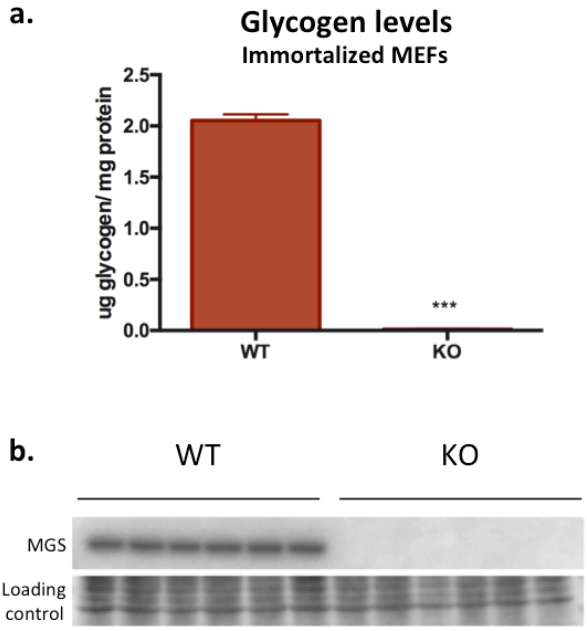

Figure 5.1: **Immortalized MGS KO MEF model verification. a)** Glycogen levels were measured in both genotypes and expressed as [ug glycogen / mg protein] (n=5). Results are presented as the mean $+/-$ s.e.m. The following p value was considered to be statistically significant: *** $p \leq 0.001$, and **b)** representative Western blot from total homogenates of cell samples obtained from both MGS WT and KO immortalized MEFs. Loading control was performed using the REVERT total protein stain (LI-COR).

KO immortalized MEFs were plated, and subsequently cell number was determined at days 1, 2, 3 and 4. MGS KO immortalized cells showed a statistically significant increase in cellular proliferation at days 3 and 4, when compared to WT counterparts (Figure 5.2).

5.2.3 Immortalized MGS KO MEFs demonstrate an enhanced migratory capacity

We assessed the migratory capacity of cells by subjecting them to the wound healing assay which consists of measuring 2D cell migration into a wound (i.e. cell free area). The visual progress of the cell front is tracked by capturing images at

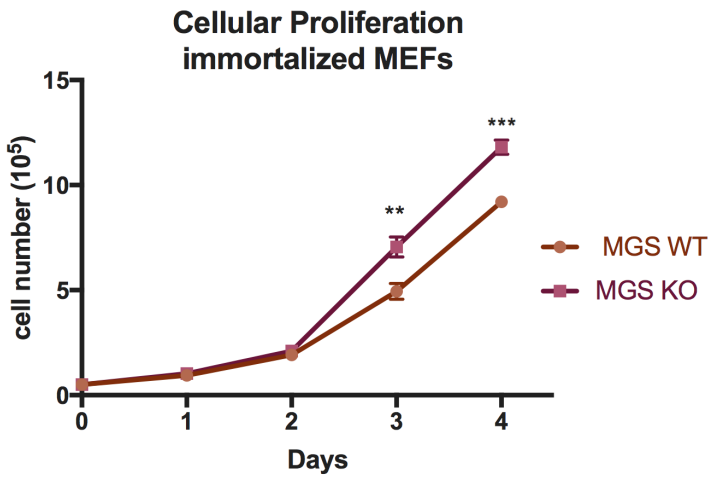

Figure 5.2: **Proliferative capacity of immortalized MEFs.** *In vitro* growth curve of immortalized MGS WT and KO MEFs. Cell number was determined by counting cells with the Scepter automatic counter. Days refers to days in culture. Results are presented as the mean $+/-$ s.e.m of 5 independent experiments. The following p values were considered to be statistically significant: ** $p \leq 0.01$, *** $p \leq 0.001$.

determined time points after the original wound is drawn. The migratory capacity is determined by performing a kinetic analysis of cell migration by generating and quantifying kymographs, which allows us to calculate cell speed (micra/hours).

We performed the wound healing assay on two independent immortalized MEF cell lines per genotype. After kymograph quantification, we observed that immortalized MGS KO MEFs cell lines consistently exhibited faster cell migration when compared to WT counterparts (Figure 5.3).

In order to discard the possibility that differences in cell speed were due to cell proliferation and not cell migration in this specific context, we performed the same experiment using a more restrictive medium (1% FBS). The decrease in essential growth factors consequently severely affected cell migration: both genotypes showed a considerable decrease in cell speed. Despite adverse culture conditions, immortalized MGS KO cells continued to display faster migration rates than wild types (Figure 5.3). Therefore, by slightly changing the medium, we confirmed that possible differences in cell migration rates actually reflected cell migration and not proliferation in this specific context. These results further confirm that by removing the cell's capacity to synthesize glycogen, we are actually bestowing an important proliferative advantage, a characteristic preserved after spontaneous

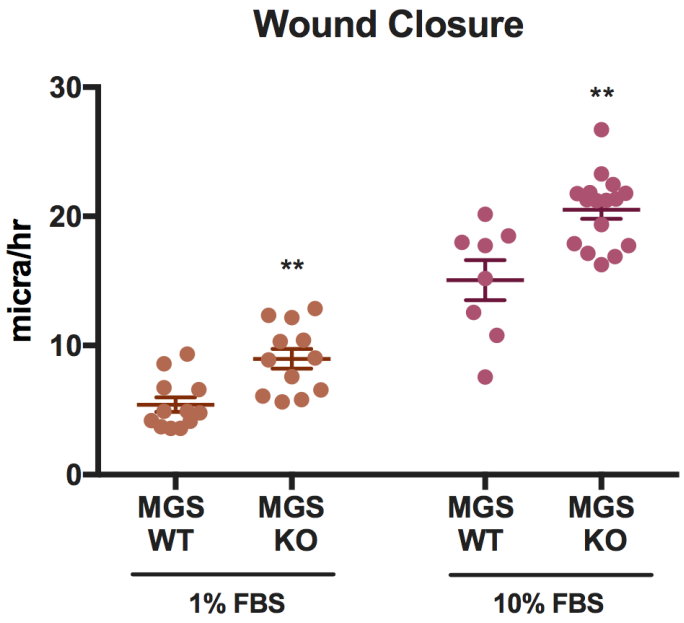

Figure 5.3: **Wound healing assay.** The progress of the cell front is assessed by quantifying kymographs, which determines cell speed in [micra/hr]. MGS WT and KO MEFs were either incubated in 1% FBS or 10% FBS medium to reduce proliferation to a minimum and therefore track cell migration. Results are presented as the mean $+/-$ s.e.m of 4 independent experiments. The following p value was considered to be statistically significant: ** $p \leq 0.01$.

immortalization.

5.2.4 Immortalized MGS KO MEFs exhibit increase capacity for colony formation

After observing that the migratory capacity of cells lacking glycogen is enhanced, we proceeded to gauge the colony formation capacity of both immortalized genotypes. The colony formation assay is an *in vitro* cell survival assay that tests the ability of a single cell to grow into a colony [Franken et al., 2006]. Fundamentally, we are testing the limitless replicative potential of single cells, an important hallmark of cancer [Hanahan and Weinberg, 2000].

We assessed the colony formation capacity of a MGS WT and a MGS KO immortalized cell line. After quantification of results, we observed that immortalized MEFs lacking glycogen formed significantly more colonies than WT counterparts

(Figure 5.4 a, b).

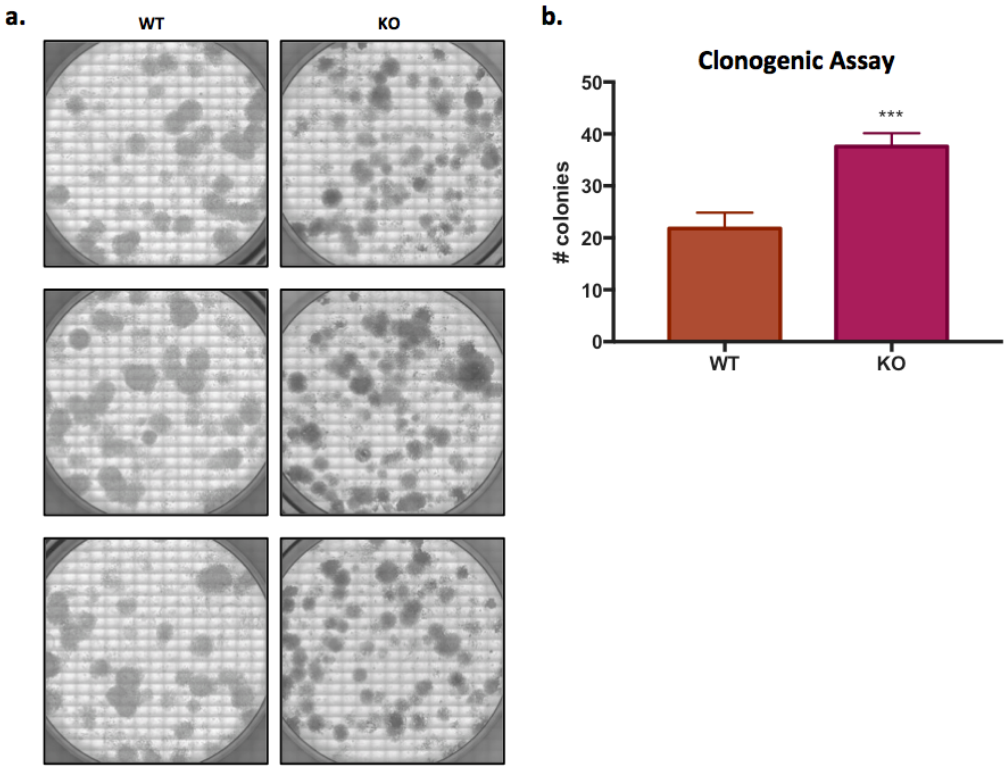

Figure 5.4: **Clonogenic assay. a)** Visual representation of colonies formed from 250 seeded cells incubated for 14 days, and **b)** quantification of colonies per well. Results are presented as the mean $+/-$ s.e.m of 3 independent experiments. The following p value was considered to be statistically significant: *** $p \leq 0.001$.

5.2.5 Immortalized MGS KO MEFs exhibit increased lactate levels

Phenol red is routinely added to cell culture medium in order to detect extracellular pH variations. Under normal neutral conditions, the medium is a pink-red color. However, 2 days after plating immortalized MGS WT and KO MEFs, we observed striking differences in medium color: the medium of immortalized MGS KO MEFs was bright yellow, whereas the medium of WT cells was more pink in color (Figure 5.5). This result suggests that culturing immortalized MGS KO

MEFs results in an increased acidification of the media. Cell number did not significantly change between wells, therefore the difference in medium color is not due to a difference in cell number.

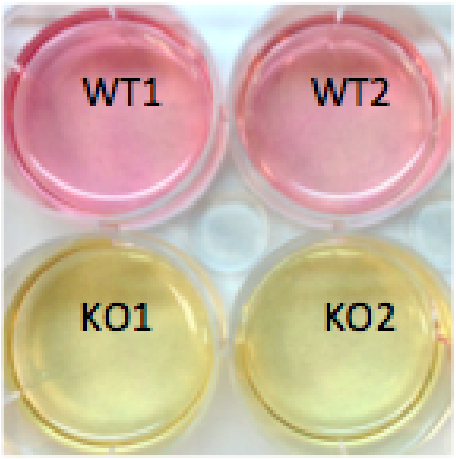

Figure 5.5: **Medium color of immortalized MEFs.**

The striking differences in medium color incited us to measure the final product of glycolysis, lactate, which can explain the medium acidification. We proceeded to measure the levels of medium lactate, which represents the lactate that was excreted to the extracellular space by the immortalized cells. We observed that extracellular lactate levels are significantly higher in immortalized MGS KO MEFs in comparison to WT counterparts (Figure 5.6 a). We also determined that intracellular lactate levels were significantly higher in immortalized MEFs lacking glycogen (Figure 5.6 b). This indicates a higher turnover of pyruvate to lactate in immortalized cells lacking glycogen.

5.2.6 Immortalized MGS KO MEFs exhibit higher levels of glycolysis than WT counterparts

Since MGS KO MEFs seemed to be more glycolytic due to the increased intra- and extracellular lactate levels, we decided to assess glycolytic function by directly measuring the extracellular acidification rate (ECAR) using the Seahorse Bioanalyzer FX24. This commercial method allows the assessment of key parameters of glycolytic flux, including glycolysis, glycolytic capacity and glycolytic reserve (Figure 5.7). The Seahorse glycolysis protocol is based on the fact that

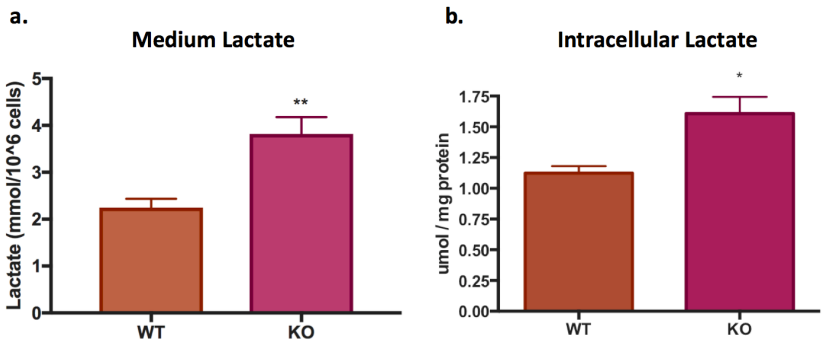

Figure 5.6: **Lactate levels in immortalized MEFs a)** Medium lactate levels measured relative to cell number expressed in [mmol lactate/10^6 cells], and **b)** intracellular lactate levels expressed in [umol lactate/mg protein]. Results are presented as the mean $+/-$ s.e.m of 3-5 independent experiments. The following p values were considered to be statistically significant: * $p \leq 0.05$, ** $p \leq 0.01$.

as pyruvate is converted to lactate, protons are generated which are then exported out of the cell, thereby resulting in the acidification of the extracellular medium.

Globally, we observed that immortalized MGS KO MEFs exhibit higher ECAR levels than WT counterparts, regardless of which glycolytic modulator has been added to the medium (Figure 5.8). This implies that immortalized cells lacking the ability to synthesize glycogen exhibit higher glycolysis levels than WT cells. In addition, we calculated a significantly higher glycolytic capacity for immortalized MGS KO MEFs. However, the derived glycolytic reserve was significantly lower for MGS KO cells, which could be due to changes in mitochondrial respiration which force the cells to operate at higher glycolytic levels (Figure 5.9).

In order to further corroborate our results concerning glycolysis, we measured glucose-6-phosphate (G6P) and ATP, which is are important cellular parameters of metabolism. In both cases, we detected significantly higher levels of G6P and ATP for immortalized MGS KO MEFs (Figure 5.10 a, b).

5.2.7 Mitochondrial function is impaired in immortalized MGS KO MEFs

In the previous section, we observed important glycolytic differences between immortalized MGS WT and KO MEFs. The logical experimental progression was to measure whether differences in oxidative phosphorylation existed between geno-

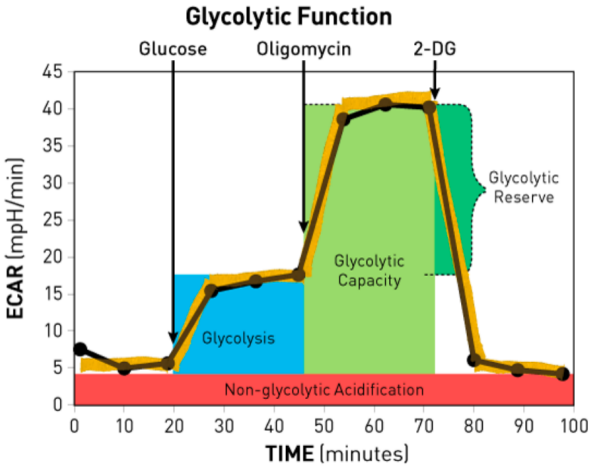

Figure 5.7: **Schematic representation of *in vitro* glycolysis stress test.** Adapted from (Agilent Techonologies)

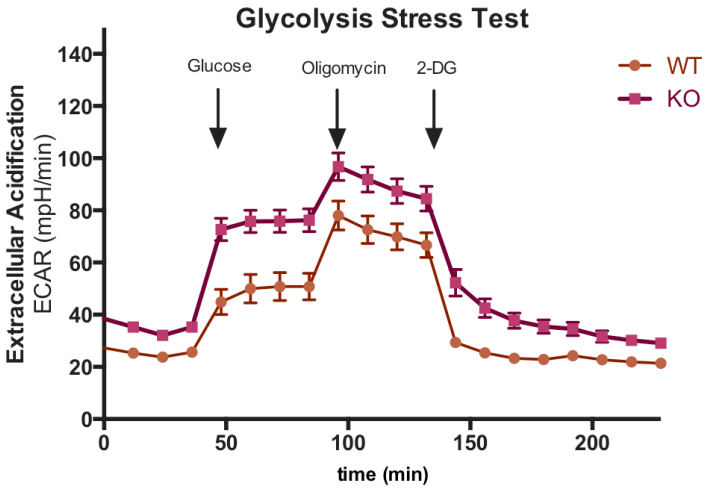

Figure 5.8: **Glycolysis Stress Test in immortalized MEFs.** Extracellular acidification rate (ECAR) traces that show the glycolytic response of MGS WT and KO MEFs in response to glucose, oligomycin and 2-DG injection where indicated. Results are presented as the mean +/− s.e.m of 3-5 independent experiments.

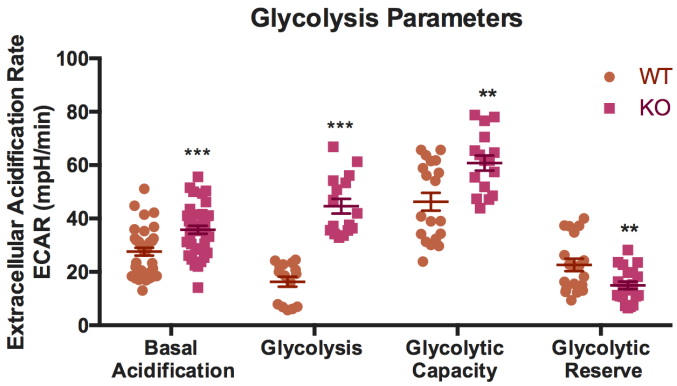

Figure 5.9: **Glycolytic parameters in immortalized MEFs.** Basal acidification, glycolysis, glycolytic capacity and glycolitic reserve were derived from the Seahorse Glycolysis Stress Test experiment (Figure 7.1). Results are expressed as [mpH/min] and normalized to cell number. Results are presented as the mean +/− s.e.m of 3-5 independent experiments. The following p values were considered to be statistically significant: ** $p \leq 0.01$, *** $p \leq 0.001$.

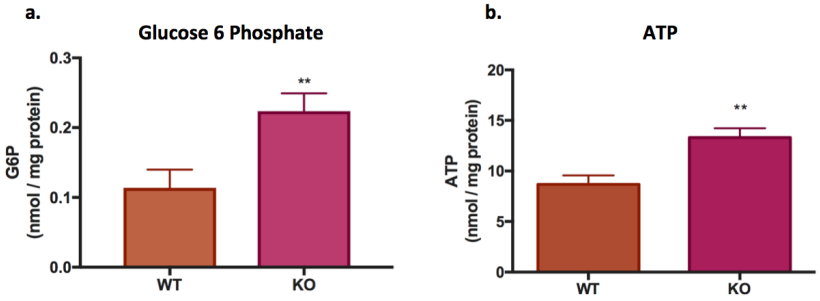

Figure 5.10: **Glucose 6 Phosphate and ATP levels in immortalized MEFs. a)** Intracellular G6P levels were measured in MGS WT and KO immortalized MEFs, results are expressed as [nmol/mg protein](n=5), and **b)** cellular ATP levels were also measured in the same samples and reported as [nmol/mg protein], (n=5). Results are presented as the mean +/− s.e.m. The following p value was considered to be statistically significant: ** $p \leq 0.01$.

types. Therefore, in this section, we proceeded to measure mitochondrial function using the Mito Stress Test Seahorse assay.

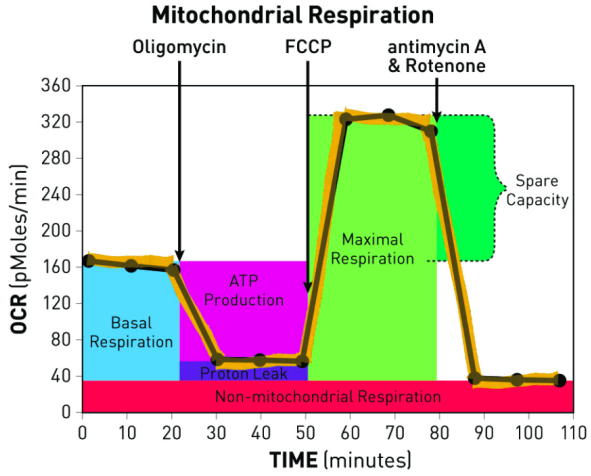

Figure 5.11: **Schematic representation of *in vitro* mitochondrial stress test.** Adapted from (Agilent Techonologies)

This assay relies on the principle that in order to completely oxidize pyruvate to generate ATP, oxygen needs to be present to act as the final electron acceptor. As follows, mitochondrial function is assessed by monitoring the oxygen consumption rate (OCR) of cells in order to measure several key parameters, including: basal respiration, ATP production, proton leak, maximal respiration, spare respiratory capacity and non-mitochondrial respiration (Figure 5.11).

We observed that MGS KO immortalized MEFs exhibit significantly lower levels of mitochondrial respiration than WT counterparts (Figure 5.12). Furthermore, all calculated mitochondrial function parameters are significantly lower in cells lacking glycogen (Figure 5.13). The lower glycolytic reserve capacity that we measured in the previous section is therefore explained by the decreased respiration, as MGS KO immortalized MEFs are operating as a higher glycolytic level.

5.2.8 Mitochondrial parameters: mitochondrial mass and reactive oxygen species (ROS)

Mitochondrial Mass

Besides the oxygen consumption rate, other mitochondrial parameters can be as-

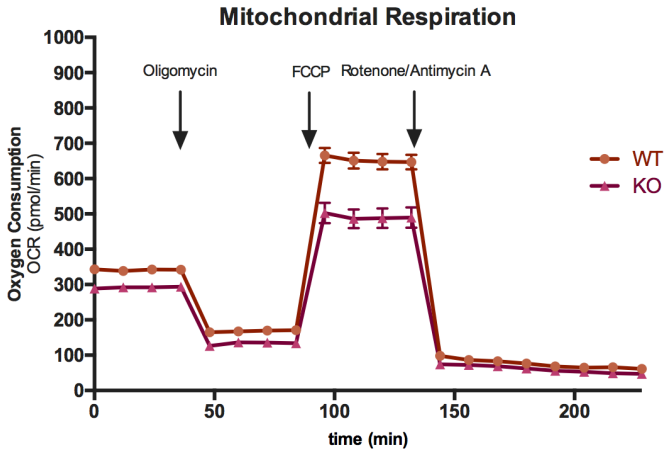

Figure 5.12: **Mito Stress Test in immortalized MEFs.** Oxygen consumption rate (OCR) traces that show the respiratory response of MGS WT and KO MEFs in response to oligomycin, FCCP and rotenone/antimycin A injection where indicated. Results are presented as the mean +/− s.e.m of 3-5 independent experiments.

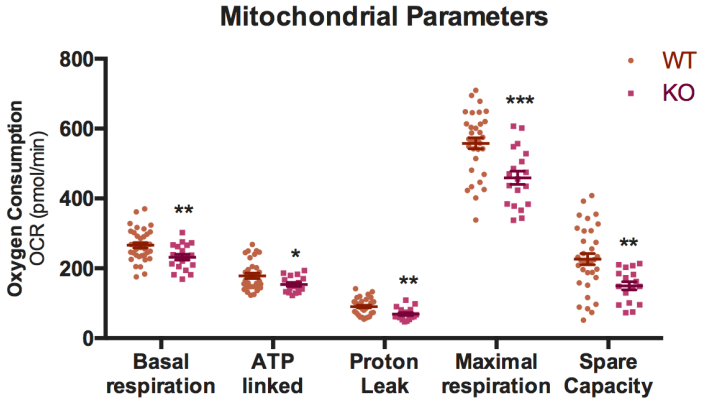

Figure 5.13: **Mitochondrial parameters in immortalized MEFs.** Basal respiration, ATP linked respiration, proton leak, maximal respiration and spare capacity were derived from the Seahorse Mito Stress experiment (Figure 5.12). Results are expressed as [pmol/min] and normalized to cell number. Results are presented as the mean +/− s.e.m of 3-5 independent experiments. The following p values were considered to be statistically significant: * $p \leq 0.05$, ** $p \leq 0.01$, *** $p \leq 0.001$.

sessed in order to further clarify changes in mitochondrial function. The first important parameter to analyze is the mitochondrial mass contained in cells. It has previously been described that a reduction in mitochondrial mass will shift energy dependence onto glycolysis [van der Windt et al., 2012]. We proceeded to measure whether the mitochondrial mass was affected through (1) Western blotting, (2) cytometric detection of fluorescent probes in live cells, and (3) assessment of the mtDNA copy number.

Porin (VDAC1), a voltage-dependent anion-selective channel present in the outer mitochondrial membrane, is often used as a loading control for mitochondrial proteins as it is expressed at steady-state levels and is unrelated to OXPHOS [Okada et al., 2004]. Therefore it can be used as a mitochondrial mass readout, ammenable to comparisons between different cell types or gentoypes. Through Western blotting and densitometric quantification (Figure 5.14 **a**, **b**), we detected significantly lower protein levels of VDAC1 in MGS KO immortalized MEFs relative to WT counterparts, suggesting a decreased mitochondrial mass.

To further corroborate these results, we incubated live cells of both genotypes with the Mitotracker Green fluorescent probe, which stains mitochondria irrespective of mitochondrial membrane potential. The ability to probe mitochondria *in situ* without resorting to tissue disruption is essential as mitochondria removed from their cellular environment might behave differently than in normal conditions. Moreover, tissue disruption can cause damage to mitochondrial networks [Agnello et al., 2008], possibly affecting results. Immortalized MEFs of both genotypes were incubated with Mitotracker green and cellular fluorescence was detected by cytometry. We determined fluorescence levels to be significantly higher in WT cells, suggesting a larger mitochondrial load (Figure 5.14 **c**), as did VDAC1 protein level results.

Lastly, we assessed mitochondrial DNA copy number which is a critical readout of overall mitochondrial health. The mitochondrial genome is separate from the nuclear genome, and in humans, encodes 13 proteins which are components of the electron transport chain [Rooney et al., 2015]. In order to determine mitochondrial DNA copy number, we isolated DNA from the immortalized MEF cell lines, and measured mtDNA copy number relative to nuclear DNA copy number through real time PCR. Again, we determined the mtDNA copy number to be significantly lower in immortalized MGS KO MEFs (Figure 5.14 **d**). This result agrees with our previous quantifications of mitochondrial mass.

Reactive Oxygen Species (ROS)
It is widely accepted that mitochondria are the main source of reactive oxygen

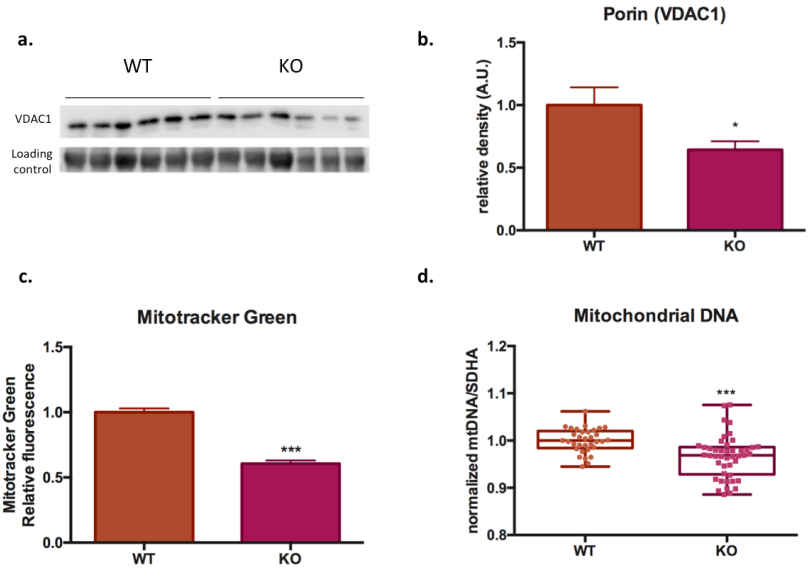

Figure 5.14: **Assessing mitochondrial mass in immortalized MEFs. a)** Western blot of porin (VDAC1) from total homogenates of cell samples obtained from both MGS and KO immortalized MEFs, loading control was performed using the REVERT total protein strain (LI-COR), **b)** densitometric quantification of Porin Western blot, normalized to immortalized WT and expressed as arbitrary units (A.U.), **c)** cells were labeled with Mitotracker Green and analyzed by flow cytometry, data shown as normalized mean of fluorescence intensity values (MFI) against immortalized WT MEFs, 4 independent experiments, and **d)** mitochondrial content for both genotypes assessed by mtDNA copy number (RT-PCR), results are normalized to SDHA, a nuclear gene. Results are presented as the mean $+/-$ s.e.m. The following p values were considered to be statistically significant: * $p \leq 0.05$, *** $p \leq 0.001$.

species in the cell, a byproduct of normal metabolism which, in high concentrations, can contribute to oxidative stress and aging. At low levels, however, ROS have been shown to be beneficial and to participate in physiological cell signaling [Thannickal and Fanburg, 2000]. Mitochondrial-specfic ROS, also known as superoxide (O_2^-), are produced during oxidative phosphorylation in the ETC when protons leak through mitochondrial complexes I and III. Superoxides can further react to generate other ROS in the form of hydrogen peroxide (H_2O_2) and hydroxyl radicals. These ROS, in turn, damage mitochondria and decrease the efficiency of the ETC, which results in a positive feedback loop of mitochondrial oxidative damage [Balaban et al., 2005]. Considering the important overlap between aging, senescence and oxidative damage, we assessed ROS levels in immortalized cells through cytometric quantification.

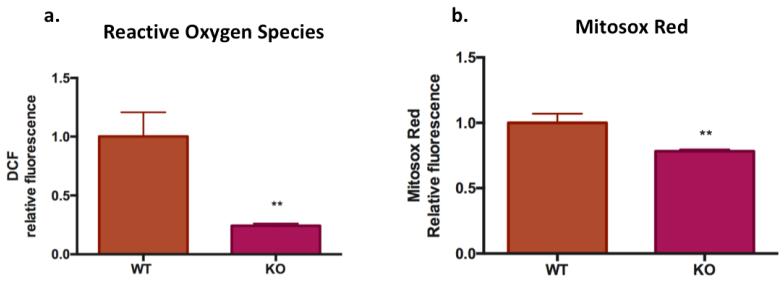

Live Cell Probe	Detects
DCF	General cellular ROS indicator
Mitosox Red	Mitochondrial superoxide indicator

Figure 5.15: **Reactive oxygen species (ROS) levels in immortalized MEFs.** MGS WT and KO immortalized MEFs were either labeled with **a)** H_2DCFDA (DCF), or with **b)** Mitosox Red and analyzed by flow cytometry. Data is shown as normalized mean of fluorescence intensity values (MFI) against immortalized WT MEFs. Results are presented as mean $+/-$ s.e.m of 5 independent experiments. The following p value was considered to be statistically significant: ** p-value $\leq$ 0.01.

For this, we assayed two fluorescent live cell probes: (1) DCF which detects the general ROS levels in the cell, and (2) MitoSox Red, which is a superoxide-specific readout of ROS levels. For both probes, we detected significantly lower fluorescence levels in MGS KO immortalized MEFs after subjecting the cells to the same protocol (Figure 5.15 **a**, **b**).

5.3 Conclusions

For the first time, we showed that immortalized MEFs lacking glycogen proliferated and migrated faster than WT counterparts. Furthermore, we demonstrated that MGS KO MEFs had an increased capacity to form colonies from single cells. Proliferative alterations were also accompanied by a significant increase of intra- and extracellular lactate levels.

We proceeded to measure real time bioenergetic changes in immortalized MEFs of both genotypes in order to determine differences in metabolic preferences. Through these experiments, we established that, in the absence of glycogen, immortalized cells exhibited a metabolic shift towards glycolysis, with a corresponding loss of mitochondrial function. Subsequently, we showed that immortalized MGS KO MEFs exhibited significantly lower mitochondrial content, as well as significant decreases in ROS levels.

Chapter 6

Hepatic glycogen and proliferative challenges

6.1 Brief Introduction

Glycogen was originally though to only serve as a glucose depot, however, recent discoveries are starting to change age-old preconceptions [Greenberg et al., 2006]. In the previous two results chapters, we demonstrate the important role of glycogen in several proliferative contexts. Considering the interesting *in vitro* results we obtained regarding glycogen metabolism and cellular proliferation, we dedicate our last results chapter to test whether our original observations are maintained *in vivo*.

As previously mentioned, MGS KO mice are not a feasible model for our *in vivo* experiments mainly due to the fact that about 90% of MGS KO mice die shortly after birth due to cardiac defects [Pederson et al., 2004]. Therefore, we use liver glycogen synthase (LGS) KO mice, which lack the ability to synthesize glycogen exclusively in the liver. Consequently, we perform assays that allow us to challenge the proliferative capacity of hepatocytes in the liver in both a physiological and pathological context.

In order to understand the role of glycogen in a physiological context, we subject LGS KO mice to a partial hepatectomy (Phx) protocol which involves the removal of two-thirds of the liver [Mitchell and Willenbring, 2008]. As a consequence of hepatic insufficiency and intricate signaling pathways, hepatocytes participate in one or two rounds of the cell cycle and then become quiescent once again [Mohammed and Khokha, 2005]. This well-established *in vivo* protocol is therefore an appropriate model for determining how the lack of hepatic glycogen affects hepatocyte proliferation.

To test the role of glycogen in a pathological context, on the other hand, we subject mice to a long term treatment with a hepatotoxic agent in order to induce hepatocellular carcinoma (HCC) [Heindryckx et al., 2009]. This specific protocol

allows us to assess whether the lack of hepatic glycogen leads to a more or less severe induction of HCC *in vivo*.

Before we can begin to analyze the proliferative capacity of the hepatocytes in the livers of LGS KO mice in both physiological and pathological situations, we first have to characterize these mice in an unchallenged context.

6.2 Characterization of LGS KO mice in an unchallenged setting

LGS KO mice are incapable of storing hepatic glycogen due to the lack of the main synthesizing enzyme, liver glycogen synthase. LGS is the hepatic isoform of glycogen synthase, and synthesizes glycogen by the same mechanism MGS does in other tissues.

In normal conditions, hepatic glycogen serves to maintain blood glucose homeostasis between meals. Once glycogen stores are exhausted, however, the liver relies on gluconeogenesis, an important hepatic pathway that generates glucose from non-carbohydrate carbon substrates (i.e. lactate). Correspondingly, LGS KO mice are hypoglycemic due to the unavailability of hepatic glycogen to maintain normal glucose levels. In addition, the gluconeogenic pathway is upregulated in LGS KO mice, as the liver battles chronic hypoglycemia [Irimia et al., 2010].

We started the characterization of these animals by confirming the absence of LGS through Western blot in liver homogenates (Figure 6.1). Subsequently, we showed that Periodic Acid-Schiff (PAS) staining, a carbohydrate-specific histological stain, was undetectable in LGS KO hepatocytes (Figure 6.2a). Some epithelial cells, especially those lining hepatic blood vessels, stained positive for PAS. This could be due to a reliance on MGS rather than LGS, in this case.

In addition, we measured no significant differences in either body weight (Figure 6.2b) or body fat (Figure 6.2c). It is worth noting that the liver to body weight (L:BW) ratio also reflected the lack of glycogen in the livers of LGS KO mice: LGS KO mice presented a statistically significant decrease in the L:BW ratio compared to WT counterparts, as shown in Figure 6.2d. Lastly, we corroborated a hypoglycemic state in fed LGS KO mice (Figure 6.2e).

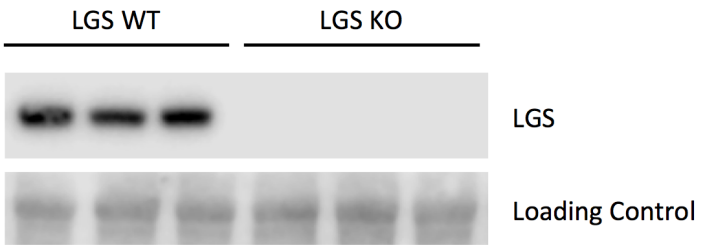

Figure 6.1: **Western blot of LGS protein in LGS WT and KO livers.** Representative Western blot from liver homogenate obtained from LGS WT and KO mice. Loading control was performed using the REVERT total protein stain (LI-COR).

6.3 Physiological proliferative hepatic challenge: regenerative proliferation in LGS KO mice

6.3.1 Brief Introduction

Hepatic regeneration is a recognized phenomenon since ancient Greek times when Prometheus, in eternal punishment, had an eagle eat his liver every day, only to have it regenerate overnight (Figure 6.3). Although this phenomenon plays a central role in a Greek myth, this is actually a true physiological occurrence, and it is referred to as liver regeneration.

The liver plays an important role in maintaining metabolic homeostasis and protecting the organism from ingested toxins. After acute chemical (ie.CCl_4) or physical injury causing direct liver damage, normally quiescent hepatocytes will reenter the cell cycle in order to undergo several rounds of cell division to make up for missing functional liver mass [Taub, 2004].

In a clinical context, physicians use the peculiar characteristic of liver regeneration to their advantage. For example, in the event of a hepatic tumors, an oncological surgeon can remove tumor masses from the liver of a relatively healthy patient (i.e. no cirrhosis, good enough liver function, etc.) and expect hepatic regeneration back to the original size. However, if the tumors affect multiple lobes, are too close to blood vessels, or make up a significant portion of the hepatic tissue, liver resection surgery may not be the best treatment course [Parks and Garden, 2001].

The two thirds partial hepatectomy (Phx) mouse model, a highly-controlled model of hepatic regeneration, involves the surgical resection of two-thirds of the hepatic

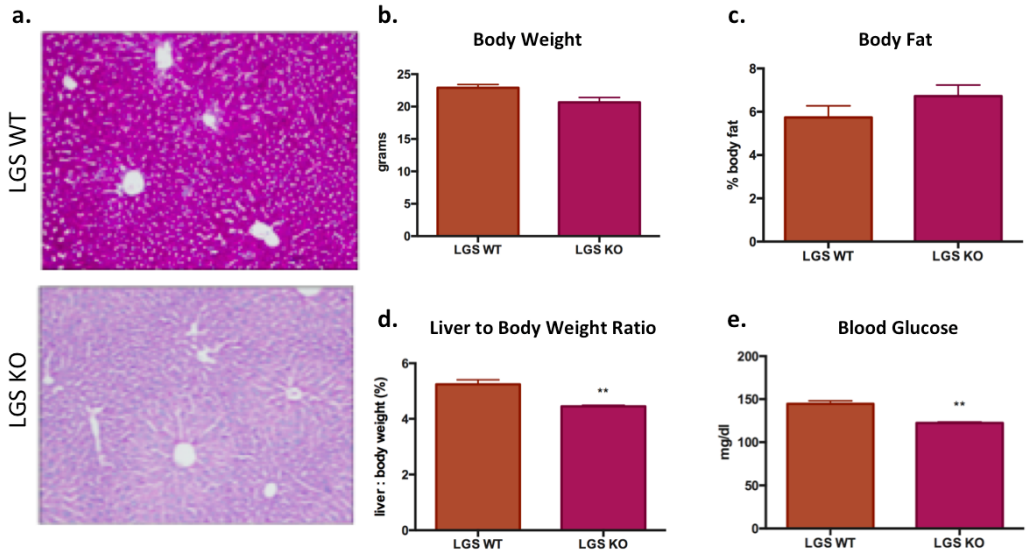

Figure 6.2: **Physiological parameters of LGS WT and KO mice.** Mice of both genotypes were assessed for various physiological parameters in order to determine differences due to the lack of hepatic glycogen: **a.** PAS staining of WT and KO LGS liver samples (20x magnification), **b.** body weight [g], **c.** body fat content [%], **d.** liver to body weight ratio [%], and **e.** fed blood glucose levels [mg/dl]. Results are presented as the mean $+/-$ s.e.m of n≥5 individuals. The following p value was considered to be statistically significant: ** $p \leq 0.01$.

mass by removing the left lateral and median lobes [Mitchell and Willenbring, 2008]. The remaining lobes will grow in size until metabolic homeostasis and hepatic function have been completely recovered (Figure 6.4) [Hata et al., 2007]. It is important to clarify that the resected lobes will not 'regenerate' and grow back. Rather, the hepatocytes present in the remaining lobes undergo a highly-controlled and short-lived hyperplastic response [Zou et al., 2012]. This proliferative response does not rely on the action of liver stem or progenitor cells, it is solely based on the capacity of hepatocytes to complete several rounds of the cell cycle [Thorgeirsson, 1996].

The regenerative response due to partial hepatectomy consists of three separate phases: 1) priming and cell cycle entry of normally quiescent hepatocytes, 2) cell cycle progression, and 3) termination of regeneration (Figure 6.5) [Mohammed and Khokha, 2005]. In mice, the maximal hepatocytic proliferative phase happens 36 hours after the Phx, where the highest percentage of hepatocytes in S

Figure 6.3: **Prometheus in eternal punishment.** The ancient Greeks were already aware of the regenerative capability of the liver. (Adapted from ancient.eu)

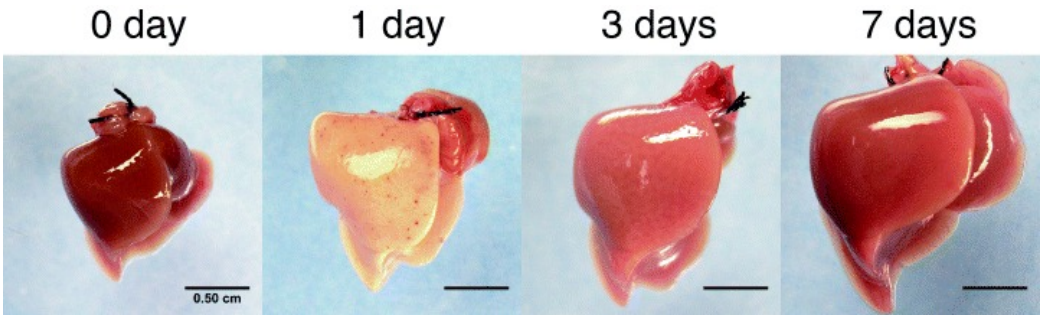

Figure 6.4: **Hepatic regeneration in mice following two-thirds partial hepatectomy.** The picture series represents a time course evolution of the liver after a two-thirds partial hepatectomy. As can be appreciated from the images, the volume of the hepatic tissue is gradually restored over the course of a week. In addition, 24h after the operative procedure, there is a peak in hepatic steatosis, which resolves as the liver grows in size. Adapted from [Hata et al., 2007].

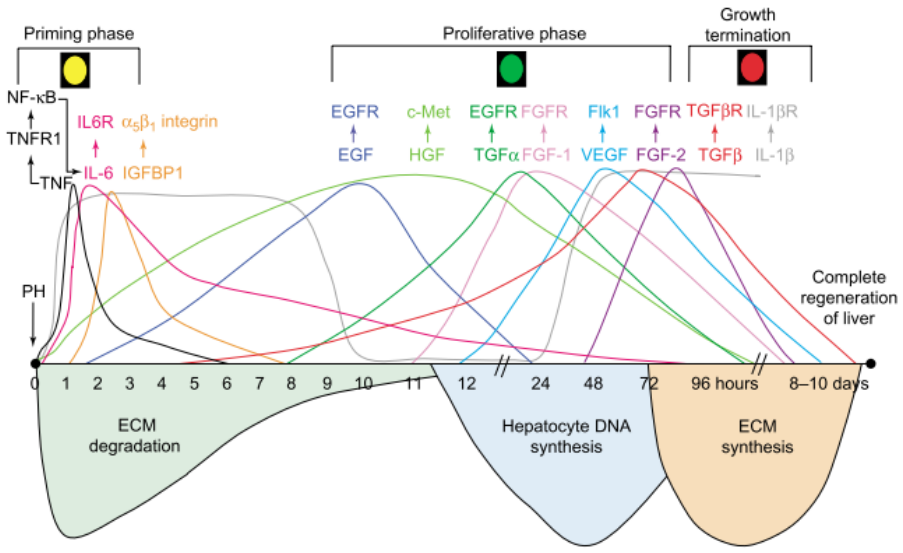

Figure 6.5: **Schematic representation of molecular signaling during hepatic regeneration.** Adapted from [Mohammed and Khokha, 2005].

phase are detected. Eventually, the liver is fully regenerated one week after the original resection of liver tissue [Mitchell and Willenbring, 2008]. Additionally, it is important to mention that Phx models a clean regenerative response, in the sense that no necrosis or inflammation is involved during the regenerative process [Michalopoulos, 2007].

The role of glycogen during the regenerative response of the Phx model has not been fully elucidated. It has been demonstrated that rats undergoing Phx have the lowest glycogen levels around 24 hours post-Phx, which coincides with a peak in hepatic steatosis (Figure 6.4) [Lea et al., 1972, Hata et al., 2007]. We decided to use this well-established hepatocytic proliferative model in LGS KO mice, in order to determine whether the lack of glycogen affects *in vivo* hepatic regeneration.

6.3.2 Results

Experimental groups

In order to test the effect of glycogen on hepatic regeneration after Phx, we subjected WT and LGS KO mice to Phx at various time points: 24h, 36h, 48h, and 72h postoperative (n≥5 per genotype). These time points were specifically chosen in order to make sure we covered the proliferative and terminal phase of the partial

hepatectomy regenerative response.

Metabolic parameters postoperative

We did not measure any differences in body weight between LGS WT and KO mice anytime post-Phx (Figure 6.6a). However, we did observe that LGS KO mice maintained low blood glucose levels, whereas WT mice presented more glycemic fluctuations (Figure 6.6b). Additionally, we measured liver triglyceride levels 24h post-Phx, as this time point is described as the peak in hepatic steatosis [Hata et al., 2007]. We did see a statistically significant increase in triglyceride levels at 24h, however, there where no differences detected between genotypes (Figure 6.6c). Additionally, we visually assessed glycogen levels in LGS WT liver samples through PAS staining, were we observed a sharp decrease 24h post-Phx (Figure 6.7). Lastly, through closer inspection, we determined that hepatocytes were indeed cycling in response to Phx as we detected mitotic hepatocytes (Figure 6.8).

Initial differences in liver to body weight ratio are resolved post-Phx.

In the context of Phx, the L:BW ratio is an indirect measure of liver regeneration postoperative. As previously mentioned, before Phx, LGS WT mice show significantly higher L:BW ratios as their livers weigh more due to the presence of glycogen. However, 24h post-Phx, the difference in L:BW ratio between WT and LGS KO animals is no longer significant. At 36h post-Phx, LGS KO mice show significantly higher L:BW ratios, and this time point coincides with the peak in hepatocytic proliferation. At 48h postoperative and on, the original difference between genotypes is no longer detected. Hence, the initial differences in the L:BW ratio are resolved post-Phx (Figure 6.9 a, b).

A significantly higher proportion of LGS KO hepatocytes are in S phase 36h and 48h postoperative.

Besides measuring the L:BW ratio as an index of liver regeneration, there is a more direct way of quantifying liver regeneration. We can specifically measure hepatocyte proliferation by injecting mice with 5-bromo-2'-deoxyuridine (BrdU) 2 hours before sacrifice. BrdU is a synthetic analog of thymidine that incorporates into newly synthesized DNA. Thus, we can assess hepatocyte proliferation through the immunohistochemical detection of BrdU positive cells [Mokrỳ and

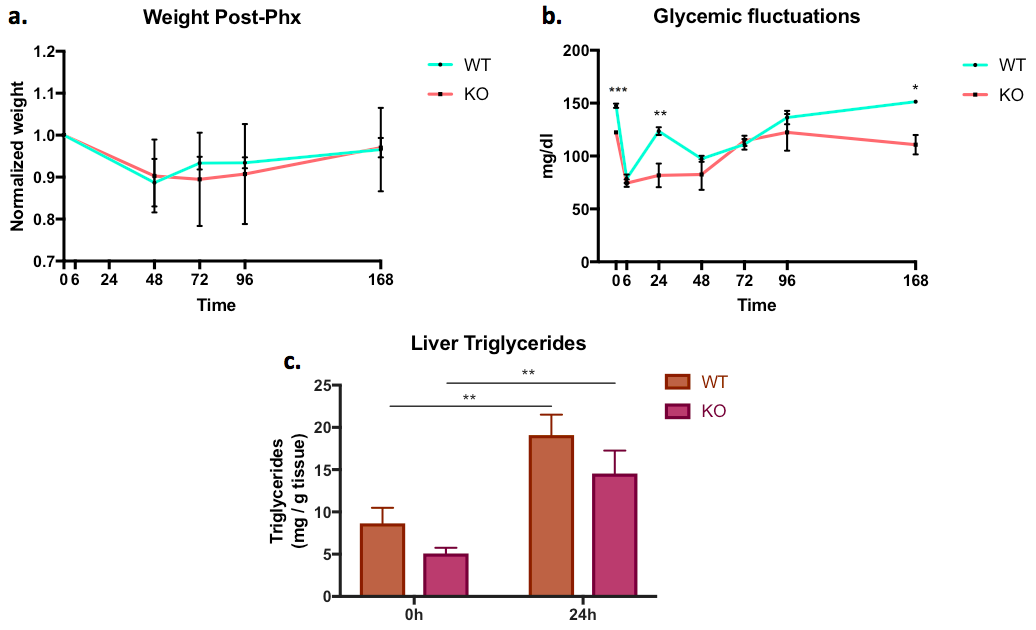

Figure 6.6: **Physiological parameters of LGS WT and KO mice post-Phx.** Mice of both genotypes were assessed for various physiological parameters post-Phx in order to determine physiological differences due to the lack of hepatic glycogen: specifically, we measured **a)** body weight [g] **b)** blood glucose determination [mg/dl], and **c)** liver triglyceride levels expressed in [mg/g tissue]. Results are presented as the mean $+/-$ s.e.m of n≥5 individuals. The following p values were considered to be statistically significant: * $p \leq 0.05$, ** $p \leq 0.01$, *** $p \leq 0.001$.

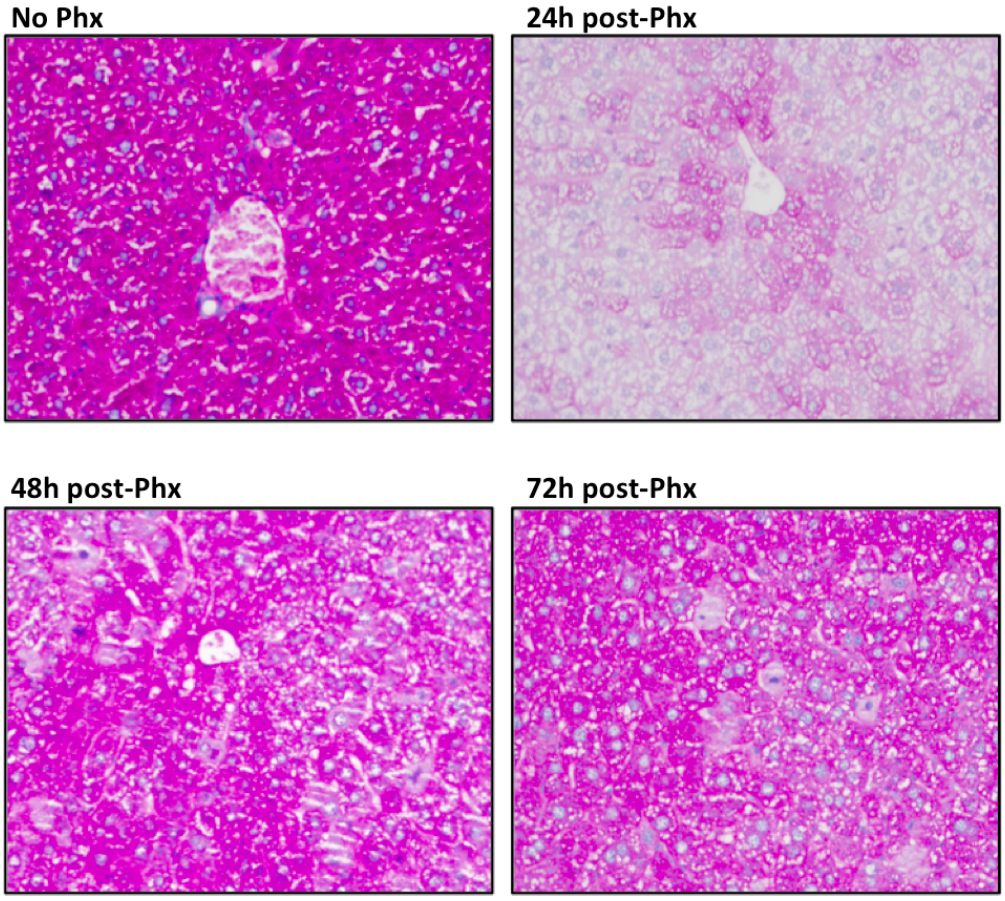

Figure 6.7: **PAS staining of LGS WT livers following partial hepatectomy.** Visual representation of glycogen content in LGS WT mice before Phx, 24h post-Phx, 48h post-Phx and 72h post-Phx. Note the presence of vesicles in the hepatocytes at time point 24h: these are accumulated lipids (steatosis). Images were taken with a 20x objective lens.

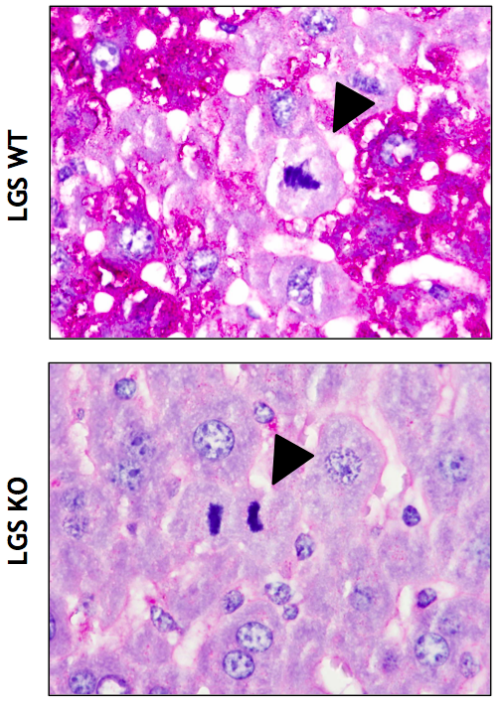

Figure 6.8: **Representative images of hepatocytes undergoing mitosis 36h post-Phx.** PAS staining of liver samples 36 post-Phx. Arrowheads indicate hepatocytes undergoing mitosis, the condensed chromatin is clearly visible in both LGS WT and KO liver samples. Images were taken with a 100x objective lens using oil immersion.

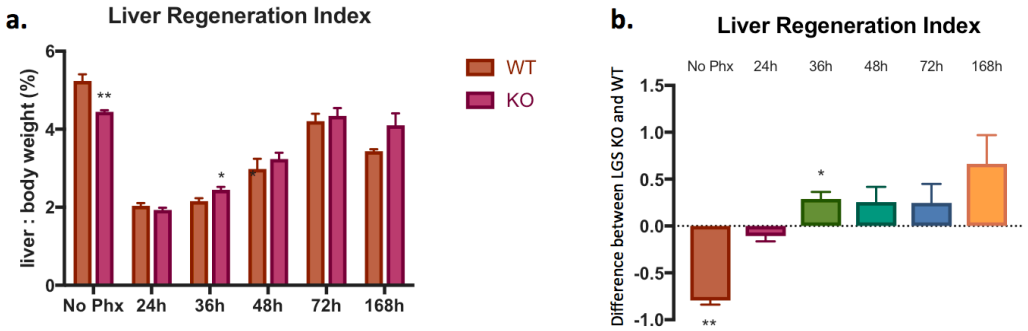

Figure 6.9: **Liver regeneration index following partial hepatectomy. a)** The liver to body weight ratio expressed as a percentage of total body weight at the indicated time points. **b)** The difference between the liver to body weight ratio of LGS WT and KO mice, expressed as a percentage. Results are presented as the mean +/− s.e.m of n≥5 individuals. The following p values were considered to be statistically significant: * $p \leq 0.05$, ** $p \leq 0.01$.

Němecek, 1995].

We quantified the BrdU-positive hepatocytes as a percentage of total cells and performed this analysis for all animals that underwent Phx at each time point. We measured the highest levels of BrdU incorporation at 36h post-Phx for both WT and LGS KO animals (Figures 6.10, and 6.11), which agrees with previous studies [Lea et al., 1972]. In addition, we measured significant differences between genotypes at time points 36h and 48h post-Phx: LGS KO mice showed higher levels of hepatocytic BrdU incorporation than WT counterparts (Figure6.11). This allows us to confirm that LGS KO mice show faster hepatocytic proliferation in response to hepatic resection.

LGS KO mice show increased levels of cell cycle-related proteins 36h post-Phx

In order to gain a deeper understanding as to why LGS KO mice showed improved rates of hepatic regeneration, we performed a mechanistic study at time point 36h post-Phx. First, we determined that the original genotypes were maintained: LGS KO animals remain devoid of MGS protein 36h postoperative (Figure 6.12). Next, we probed proteins known to be involved in cell cycle regulation following a partial hepatectomy, namely: cyclin D1, pRB, p53 and p21 (Figure 6.13).

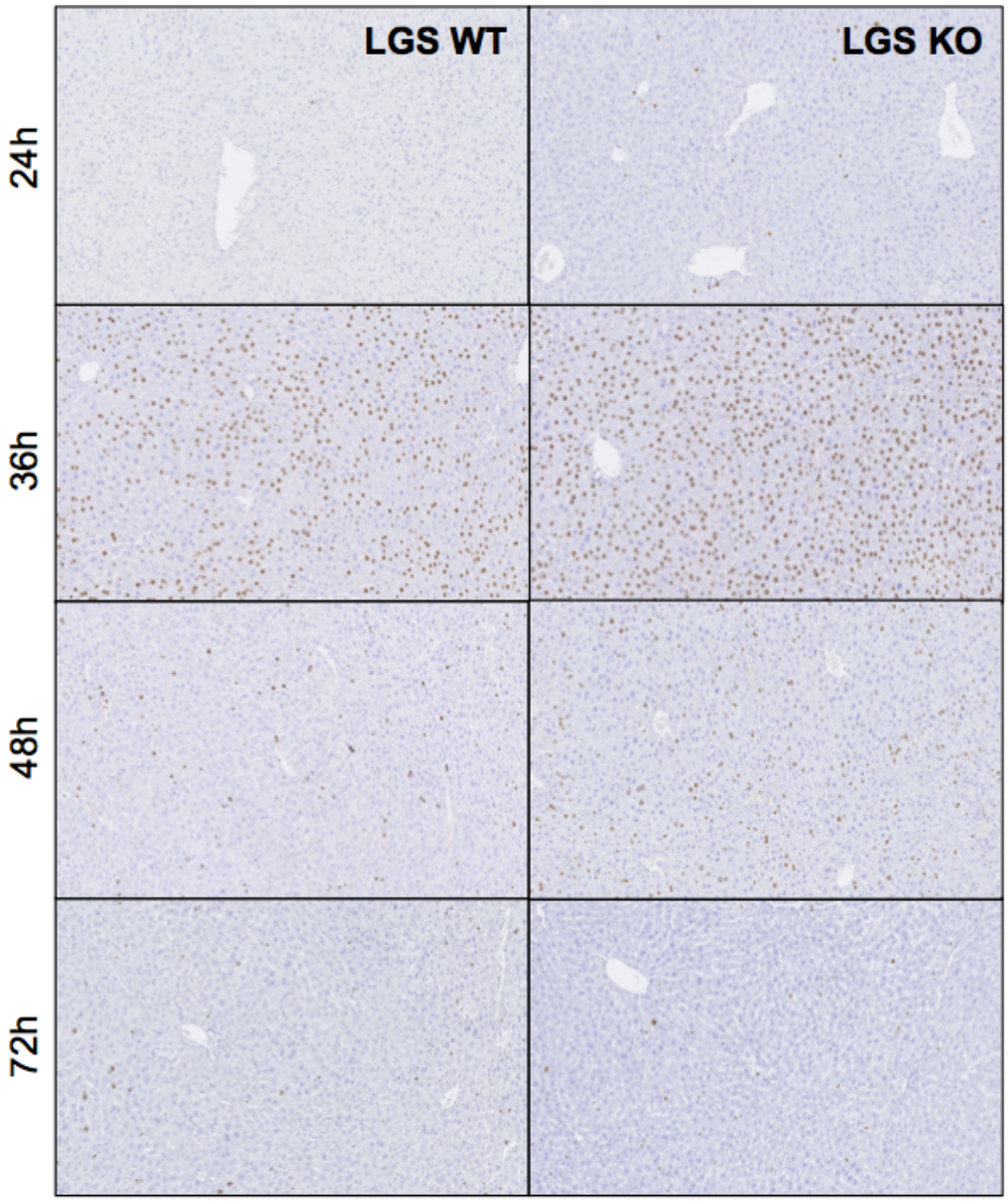

Figure 6.10: **Representative images of BrdU incorporation at different time points post-operative.** Mice were injected with BrdU 2h before sacrifice in order to allow hepatocytic incorporation. Hepatic tissue was harvested, fixed and embedded in paraffin. Immunohistochemistry was performed on 4um liver slices using a primary antibody against BrdU. Images were taken with a 10x objective lens and 10 fields per sample were quantified, (n≥5).

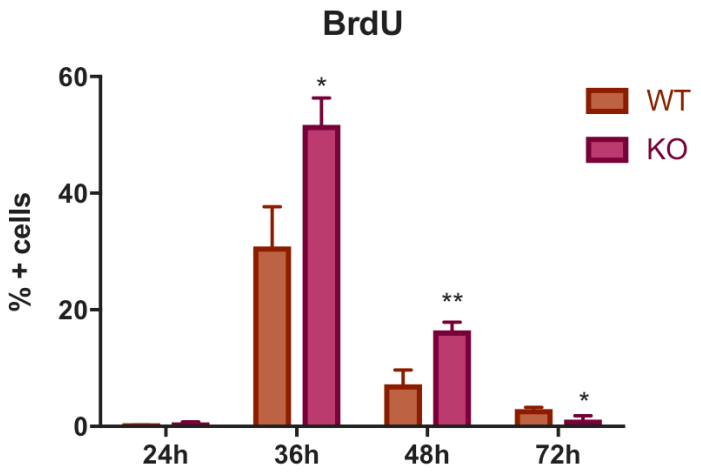

Figure 6.11: **Quantification of BrdU positive hepatocytes after partial hepatectomy.** Hepatocytes positive for BrdU incorporation were quantified as a percentage of total hepatocytes in 10x microscopic fields. 10 fields per sample were quantified. Non-hepatocytic cells positive for BrdU were not taken into account. Results are presented as the mean $+/-$ s.e.m of n≥5 individuals. The following p values were considered to be statistically significant: * $p \leq 0.05$, ** $p \leq 0.01$.

Cyclin D1 is an important protein that cycles during the cell cycle. More specifically, it regulates cyclin-dependent kinase (CDK) 4 and CDK 6, whose activity is critical for the transition between the G1 and S phases of the cell cycle. In the context of liver regeneration, cyclin D1 protein levels have been shown to increase in both mice and humans. Furthermore, in primary rat hepatocytes stimulated with insulin, the expression cyclin D1 coincides with DNA synthesis, thereby confirming the role of cyclin D1 in hepatocyte cell cycle proliferation [Núñez et al., 2017]. In our samples, we observed that cyclin D1 levels are significantly increased in the liver homogenates of LGS KO mice 36h postoperative. (Figures 6.13, and 6.14 a).

Under non-proliferative conditions, Retinoblastoma (RB) protein is bound to the E2F transcription factor. However, once cyclin D1 is bound with CDK4, the cyclin D1 - CDK4 complex phosphorylates RB forcing the release of E2F [Giacinti and Giordano, 2006]. In essence, RB controls progression through the restriction point within the G1-phase of the cell cycle. Therefore, the cellular levels of pRB provide an indication of cell cycle progression past the G1 checkpoint. In our samples, we observed that pRB levels were significantly increased in the liver homogenates of LGS KO mice 36h postoperative (Figures 6.13, and 6.14 b). Cyclin D1 and pRB protein levels in our samples 36h post-Phx suggest that more hepa-

tocytes are undergoing a G1 to S phase transition in LGS KO mice.

p53 is another important player in the regulation of the cell cycle, and functions as a tumor suppressor. DNA damage and other stress signals increase the levels of p53 and can lead to growth arrest, DNA repair and apoptosis [Charni et al., 2017]. We observed low p53 protein levels and no significant differences between genotypes. (Figures 6.13, and 6.14 c). On the contrary, for p21, an important cyclin-dependent inhibitor (CKI), we detected significantly lower levels in LGS KO mice having undergone Phx 36h prior (Figures 6.13, and 6.14 d). These results suggests a higher proportion of hepatocytes in LGS KO mice subjected to Phx undergo a G1-S phase transition 36h postoperative.

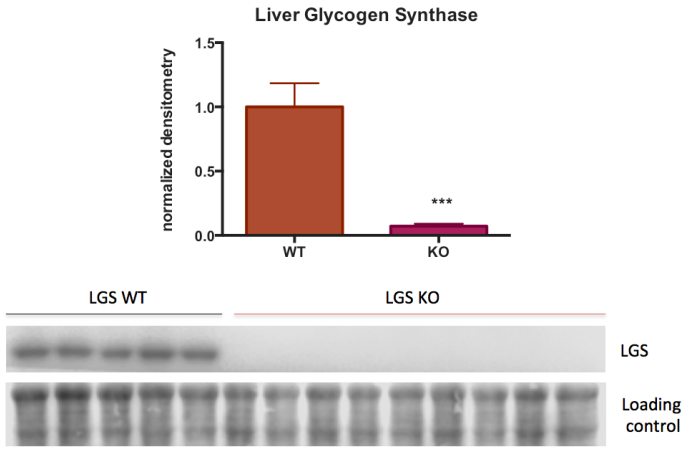

Figure 6.12: **Western blot of LGS 36h after partial hepatectomy.** Western blot of LGS protein in LGS WT and KO liver homogenates at time point 36h. Loading control was performed using the REVERT total protein stain (LI-COR). Graph represents densitometric quantification of LGS Western blot, normalized to LGS WT and expressed as arbitrary units (A.U.). Results are presented as the mean $+/-$ s.e.m. The following p value was considered to be statistically significant: *** $p \leq 0.001$.

6.3.3 Conclusions

For the first time, we show that the absence of hepatic glycogen affects the regenerative capacity of livers subjected to a two-thirds partial hepatectomy.

Specifically, we show that the initial differences observed in liver to body weight

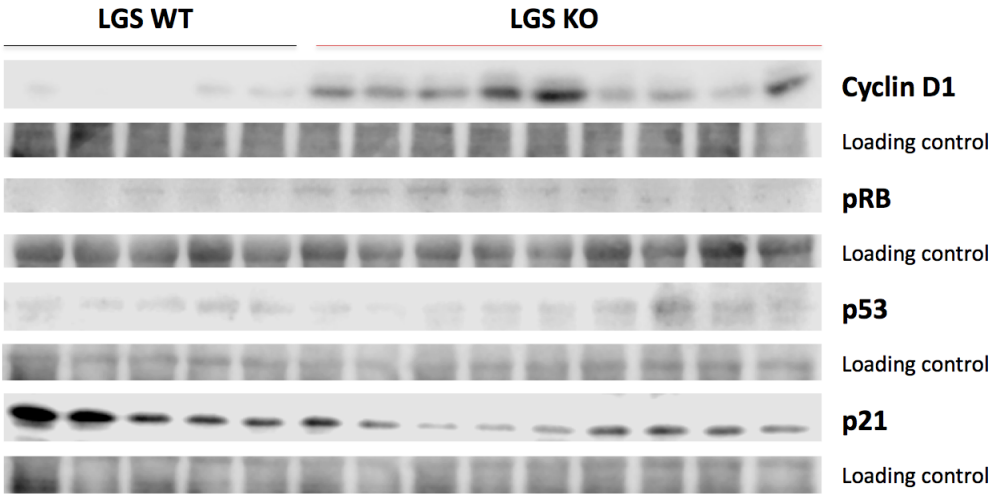

Figure 6.13: **Western blots of cell cycle-related proteins 36h after partial hepatectomy.** Cyclin D1, pRB, p53 and p21 were probed by Western blot in order to determine whether levels were altered 36h post-Phx. Loading control was performed using the REVERT total protein stain (LI-COR).

ratio are resolved after hepatic resection. Moreover, we show that a significantly higher proportion of LGS KO hepatocytes are in the S phase at 36h and 48h post-Phx. We further support this observation by revealing that by 36h, LGS KO liver homogenates demonstrate higher protein levels of cyclin D1 and pRB, but significantly lower p21 levels.

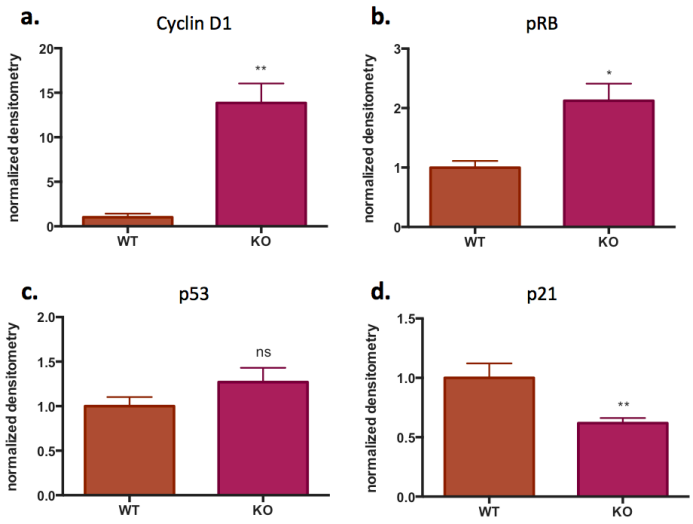

Figure 6.14: **Densitometric quantification of Western blots of cell cycle-related proteins 36h after partial hepatectomy.** Western blots of Cyclin D1, pRB, p53 and p21 were quantified by densitometry and normalized to LGS WT. Results are expressed as arbitrary units (A.U.). Results are presented as the mean $+/-$ s.e.m. The following p values were considered to be statistically significant: * $p \leq 0.05$, ** $p \leq 0.01$.

6.4 Hepatocellular carcinoma induction in LGS KO mice: long term N-nitrosodiethylamine (DEN)

6.4.1 Brief Introduction

Hepatocellular carcinoma (HCC) is the most common type of primary malignancy in the liver, and around 500,000 new patients are diagnosed annually [Heindryckx et al., 2009]. Generally, HCC stems from prior chronic liver damage such as cirrhosis or hepatitis infections [Tsukuma et al., 1993]. During the early stages of HCC, the tumor can be treated either by liver transplantation or, as we have previously seen, by partial hepatectomy.

Several animal protocols exist to mimic HCC progression and include either chemically-induced HCC (DEN, CCl_4, among others), xenograft models or genetic mouse models. For our purposes, the chemically-induced HCC model was most suitable to test the effect of glycogen on hepatic malignancies.

N-nitrosodiethylamine (DEN) is a hepatotoxic chemical commonly used in experimental settings to provoke hepatic injury. DEN works by alkylating DNA, thereby inducing DNA damage and oxidative stress specifically in the liver. Long term DEN treatment in mice exposed to the toxin will induce hepatocellular carcinomas (HCC), with the injury-fibrosis-malignancy cycle seen in humans [Heindryckx et al., 2009].

Several factors are critical for the long term DEN treatment to work, and include: administered dose, sex, age, and strain. Male mice have been shown to exhibit higher rates of HCC after DEN treatment. This is explained by the fact that androgens have a stimulating effect on HCC, whereas estrogens have an inhibitory effect [Nakatani et al., 2001]. Besides gender, the age at the time of exposure is critical as hepatocytes in the livers of newborn mouse pups are more sensitive to mitotic signals than are hepatocytes in adult livers [Fausto, 2000].

Glycogen metabolism is known to be reprogrammed during tumorigenesis, as many observational studies have concluded [Rousset et al., 1981, Lea et al., 1972, Nigam and Cantero, 1973, Hammond et al., 1978]. However, it is not yet clear what effect glycogen has on the course of tumorigenesis, principally due to the fact that glycogen levels are differentially modulated in different tumor types. In general, it has been postulated that the malignant process is associated with an increase of glycogen storage in tumors proceeding from tissues of low glycogen content. In contrast, the malignant process in tumors originating from the liver re-

sults in a decrease in glycogen storage [Rousset et al., 1981]. However, the exact role of glycogen still remains unclear and contradictory.

Therefore, our aim in this results section is to determine how glycogen affects pathological HCC progression *in vivo*. For this, we subjected both LGS Het (Ctrl) and KO mice to a long term DEN protocol (Figure 6.15). Importantly, LGS Het mice have the same hepatic glycogen levels than LGS WT mice (results not shown).

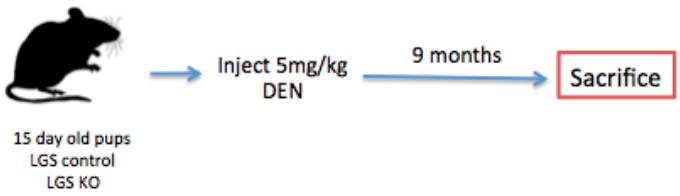

Figure 6.15: **Schematic representation of the hepatocellular carcinomal animal model induced by DEN injection.**

6.4.2 Results

Control mice present better survival rates than LGS KOs

We observed a difference in the survival rates between genotypes. LGS KO mice were less resistant to the low dose DEN injections, whereas all control mice survived the course of treatment (Figure 6.16). Unfortunately, we were not able to recover the cadavers of the LGS KO mice to perform a post-mortem study to determine cause of death.

Physiological parameters

We measured no significant differences in body weight between genotypes at the end of the DEN protocol (Figure 6.17a). Furthermore, we did not detect any differences in L:BW ratio (Figure 6.17b). This is significant as LGS KO mice start from a lower L:BW ratio, likely due to the lack of hepatic glycogen. Therefore, the difference in L:BW resolved after DEN treatment.

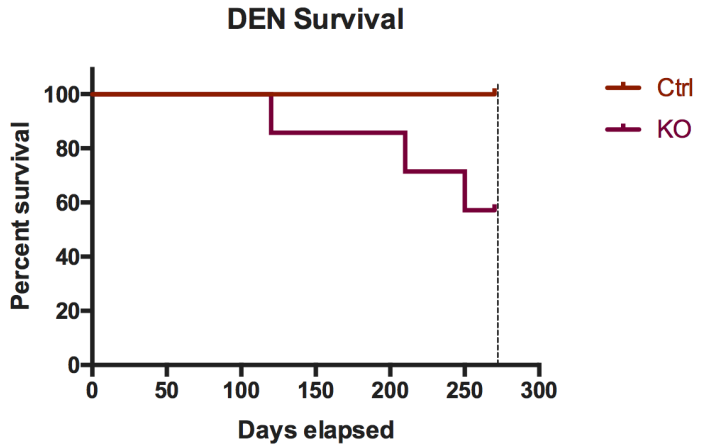

Figure 6.16: **Control animals present better survival rates than LGS KO mice after DEN treatment.** We calculated the Kaplan Meier statistics to determine survival in this experimental context. The dashed line represents the end of the DEN treatment (270 days). (n≥7).

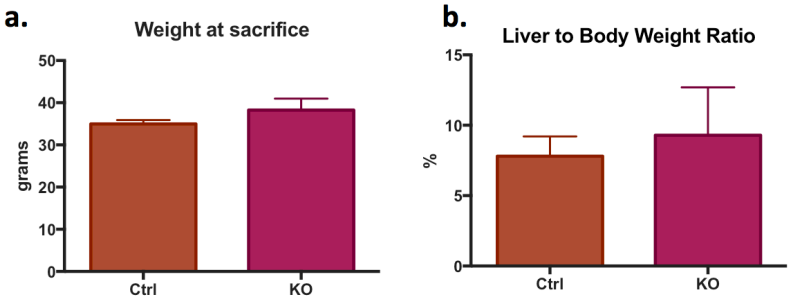

Figure 6.17: **Physiological parameters of mice at the end of the DEN protocol.** We calculated both **a)** body weight [grams], and **b)** liver to body weight ratio [%] at sacrifice. Results are presented as the mean $+/-$ s.e.m of n≥4 individuals.

LGS KO mice develop a higher tumor burden

For both genotypes, we visually detected macroscopic hepatic lesions upon sacrifice (Figure 6.18). Next, we proceeded to quantify hepatic lesions in two ways: first, we counted the number of visible tumors, and secondly, we measured the corresponding surface area of each tumor. From surface area data, we calculated the tumor burden in each DEN-treated mouse.

We observed a tendency for LGS KO to present more tumors than control mice, however this did not reach statistically significant levels (Figure 6.19a). Interestingly, we demonstrated that LGS KO mice presented a significantly higher tumor burden than control mice (Figure 6.19b).

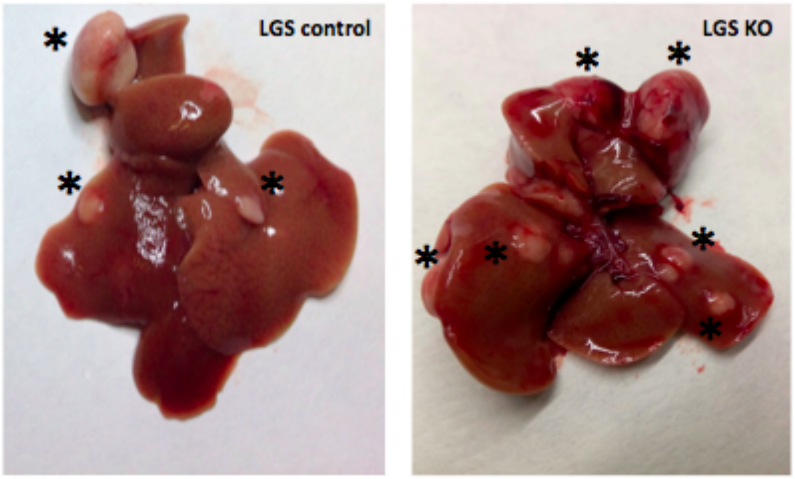

Figure 6.18: **Macroscopic lesions due to long term DEN treatment.** Macroscopic view of representative livers from littermate mice 9 months after initiation of the DEN protocol. Asterisks denote tumor masses.

Histopathological study of hepatic DEN liver

In order to clarify the types of hepatic lesions the animals developed during the protocol, we performed a histopathological study of the harvested hepatic samples (n=4 for each genotype).

The majority of the lesions described in the liver samples were benign hepatocellular proliferations, nodular hyperplasia and/or hepatocellular adenomas (Figure

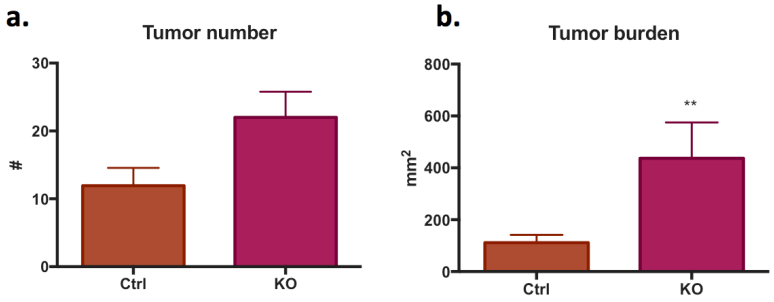

Figure 6.19: **Quantification of macroscopic lesions at sacrifice.** We quantified lesions by visual inspection. Specifically, we measured a) tumor number, and b) tumor burden [mm^2]. Results are presented as the mean $+/-$ s.e.m of n≥4 individuals. The following p value was considered to be statistically significant: ** $p \leq 0.01$.

Hepatic lesion	LGS Ctrl (%)	LGS KO (%)
Hepatocellular carcinoma (HCC)	0	25
Hepatocellular adenoma/nodular hyperplasia	100	100
Clear hepatocyte foci	25	50
Eosinophilic hepatocyte, cytoplasmic inclusions	75	100
Dilated vessels and/or bile ducts	0	25
Mononuclear inflammatory cells in portal area	50	50
Nuclear pleomorphism and anaplasia	0	25
Basophilic foci	100	75
Hepatocyte steatosis	50	50
Eosinophilic foci	0	25
Centrilobular vacuolization	0	25
Focal area of hepatocyte necrosis	0	25
Centrilobular vacuolation	0	50

Table 6.1: **Hepatic lesions observed in the livers of LGS Ctrl and KO mice after DEN treatment**

6.20). Due to the fact that the histological distinction between both lesions sometimes is not clear, we considered hepatic adenoma when there was clear compression of the adjacent liver parenchyma/hepatocytes, absence of lobular architecture - central veins, portal triads- and/or liver plates impinging obliquely on the surrounding parenchyma.

The eosinophilic inclusions observed in the lesions described are a normal finding in pre-neoplastic and neoplastic lesions (Figure 6.21). Specifically, these lesions

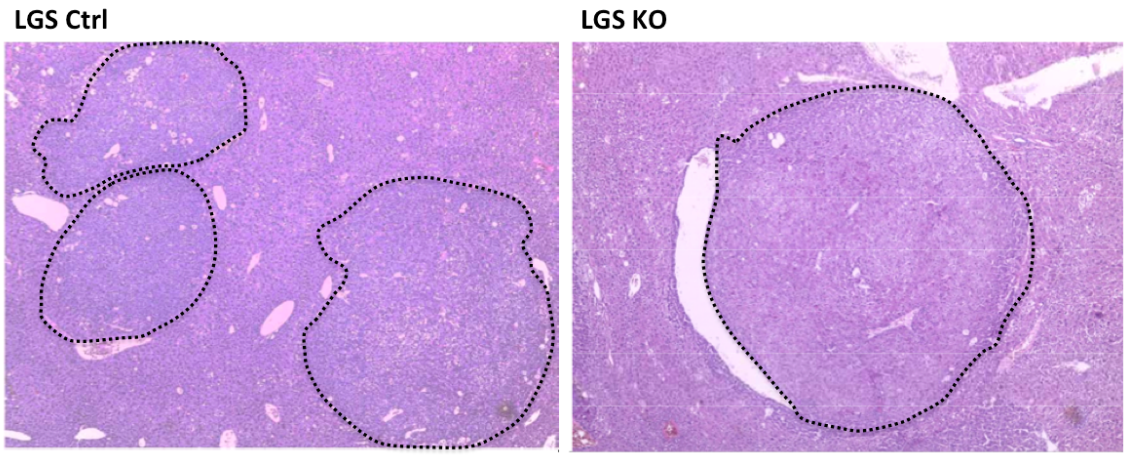

Figure 6.20: **Hepatocellular nodular hyperplasia** Representative hematoxylin and eosin (H&E) stain of hepatocellular nodular hyperplasias in both LGS Ctrl and KO mice. Images were taken with a 4x objective lens.

have also been described in the present model of carcinogenesis in C57BL/6 mice. This mouse strain is relatively less susceptible than other strains to hepatocarcinogens, but they are more vulnerable to develop early focal lesions containing a large number of these type of cytoplasmic inclusions. The origin of these inclusions could be dilated cisternae of rough endoplasmic reticulum, among others [Helyer and Petrell, 1978]. Other frequently observed lesions were focal foci of altered hepatocytes: clear, eosinophil and/or basophilic (Figure 6.22).

Importantly, the only malignant hepatocellular carcinoma, was detected in a LGS KO liver sample (Figure 6.23). The HCC was of epithelial origin with a glandular appearance, multiple focal areas of necrosis, and was infiltrative to the adjacent hepatic tissue. Furthermore, we detected moderate cellular and nuclear pleomorphism and anaplasia.

Lastly, we noted an interesting correlation between glycogen and proliferation in nodular hyperplasias in LGS control animals: glycogen levels were nearly absent from nodular hyperplasias that stained positive for Ki67, a marker of proliferation (Figure 6.24).

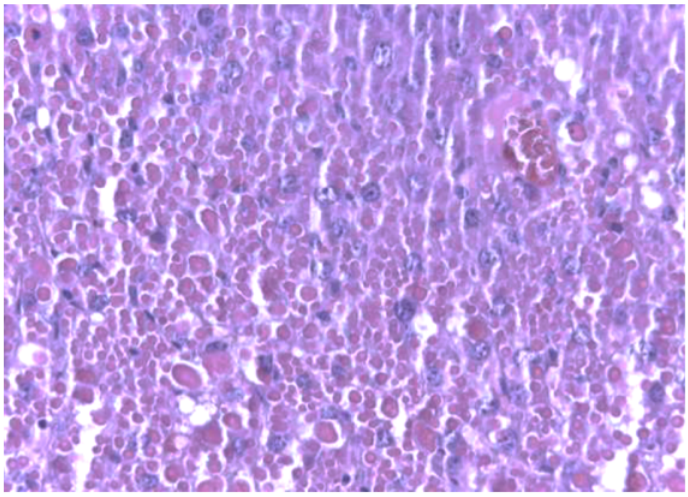

Figure 6.21: **Eosinophilic intracytoplasmic bodies** Representative H&E stain of eosinophilic intracytoplasmic bodies in LGS KO. Image was taken with a 20x objective lens.

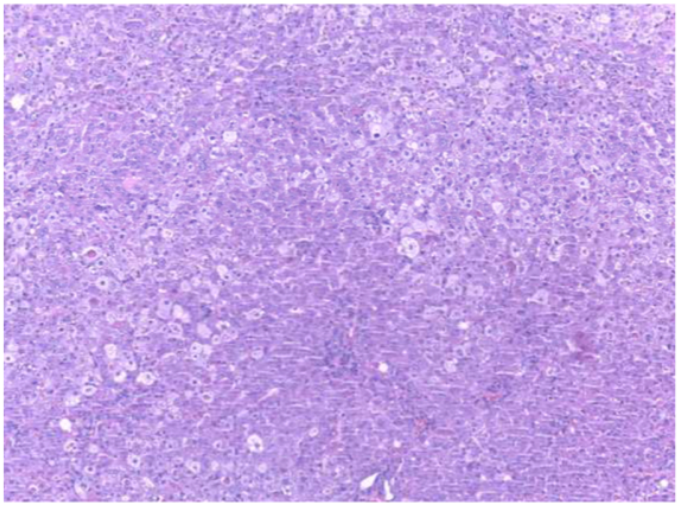

Figure 6.22: **Clear hepatocyte foci** Representative H&E stain of clear hepatocyte foci in LGS KO. Image was taken with a 10x objective lens.

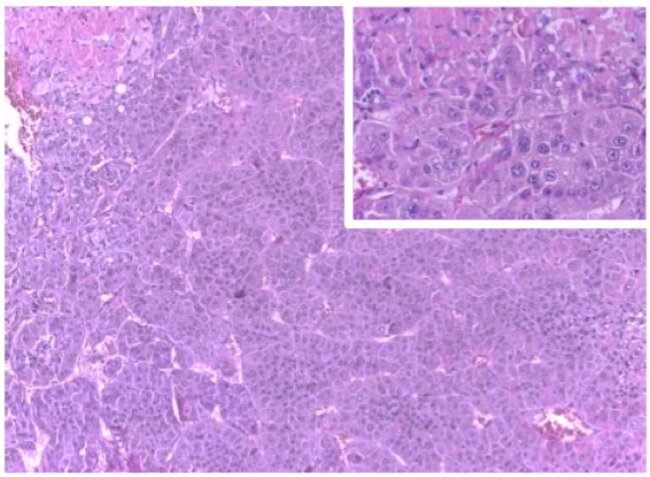

Figure 6.23: **Hepatocellular carcinoma (HCC)** H&E stain of a HCC in a LGS KO animal. Large image was taken with a 4x objective lens, while inset is at 20x magnification.

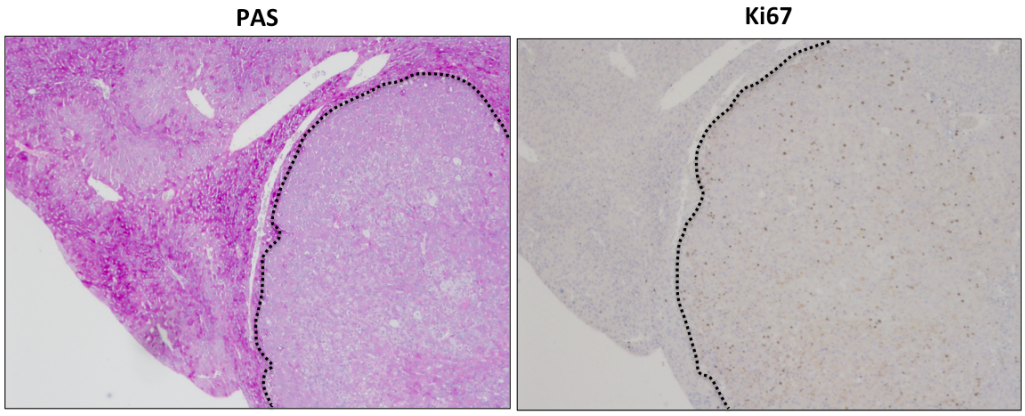

Figure 6.24: **PAS and Ki67 stainings of hepatocellular nodular hyperplasia/adenoma.** PAS and Ki67 stainings were performed on liver sections of a LGS control animal subjected to the DEN protocol. Images were taken at 4x magnification.

6.4.3 Conclusions

Mice lacking hepatic glycogen were more sensitive to DEN treatment than LGS control mice, exhibiting decreased survival rates and significantly higher tumor burden.

Part V

Global Discussion

The general consensus is that glycogen is an intracellular store of glucose that can be mobilized either during high energetic demand or to maintain homeostasis. However, it is becoming increasingly clear that glycogen is an important regulator of cellular proliferation. Here, we aim to elucidate the role of glycogen in proliferation, specifically in the context of aging, tumorigenesis, and hepatic regeneration.

First, we focus on the role of glycogen in senescence, an irreversible condition where the cell cycle is stalled at the G1 phase. We unequivocally show that glycogen accumulates during senescence in both mouse and human cells. This specific metabolic characteristic of senescence is evolutionarily conserved as there is further evidence that glycogen accumulates in chronologically aged *S.cerevisiae* [Lin et al., 2001].

The accumulation of glycogen during cellular senescence has already been reported [Seo et al., 2008, Favaro et al., 2012]. We further establish that muscle glycogen synthase (MGS) is induced during senescence which leads to a massive increase of glycogen levels. It would be interesting to determine how exactly MGS is regulated during senescence. Glycogen synthase kinase 3 (GSK3), a negative regulator of MGS, has been shown to be inactivated in a variety of senescence models [Seo et al., 2008]. Since GSK3 is a promiscuous protein that participates as a regulatory switch for a variety of pathways, its upstream regulation in senescence remains to be clarified.

Interestingly, it has been demonstrated that completely abolishing glycogen mobilization by glycogen phosphorylase (GP), induces glycogen accumulation, and leads to premature senescence and a shortened lifespan in *S. cerevisiae*, *C. elegans* and human cancer cells [Favre et al., 2008, Gusarov et al., 2017, Favaro et al., 2012]. Nonetheless, it remains unclear whether the glycogen molecule it-

self or the mobilization of glycogen is contributing to senescence.

In order to test whether the presence of glycogen affects the senescent response, we resort to a glycogen-free cell model: mouse embryonic fibroblasts (MEFs) isolated from MGS KO embryos. Since most MGS KO mice are neonatal lethal, isolating MEFs from embryos is a way to detour the lethality while still exploiting the utility of the model. We discarded using MGS knockdowns of cancer cell lines due to the heterogeneity of cancer cell lines with regards to glycogen metabolism [Takahashi et al., 1999]. Furthermore, MEFs offer a straight-forward model to solely assess the contribution of glycogen to senescence in a non-tumoral context, whereas cancer cells have already bypassed senescence.

We can divide results from this section into the study of three different proliferative phases: 1) actively proliferative primary MEFs at low passages, 2) senescent MEFs, and 3) immortalized MEF cell lines. In the early passages of primary MEFs, we do not observe significant differences between genotypes, as is evident from the population doubling levels (PDL) and transcriptomic signature analysis (Figures 4.10, 4.19).

When primary MEFs are subjected to replicative senescence, however, they display several senescence-related markers, including proliferative plateau (PDL), flattened cell morphology, positive SA-B-Gal staining, and an increased protein expression of senescence markers (Figures 4.10, 4.11, 4.12, 4.13). Nonetheless, we also observe striking differences: MEFs lacking glycogen reach plate confluence and immortalize faster than WT cells. This proliferative phenotype is further conserved after immortalization (Figure 5.2). These results suggest that glycogen may be modulating the senescent response.

To further assess the effect of glycogen absence during senescence, we perform a transcriptomic analysis of MGS WT and KO senescent cells. Gene set enrichment analysis (GSEA) reveals a growth arrest phenotype for both genotypes: genes in charge of DNA replication and controlling the cell cycle are depleted during senescence. Remarkably, WT cells show an enrichment of genes in the TGF-b pathway while MGS KO cells are counter-enriched for the same pathway (Figure 4.17). This suggests that glycogen modulates the TGF-b pathway during senescence. TGF-b is known to participate in some aspects of senescence [Campisi, 2013, Munoz-Espin et al., 2013, Kuilman and Peeper, 2009, Acosta et al., 2013]. Specifically, Tremain et al were the first to demonstrate that in keratinocytes overexpressing a ras oncogene, the inactivation of TGF-b secretion or the TGF-b response can accelerate malignant transformation by bypassing senescence [Tremain et al., 2000]. In addition, TGF-b ligands have been shown to

mediate paracrine senescence through the senescence-associated secretory phenotype (SASP) [Acosta et al., 2013]. To date, however, there are no described associations between glycogen and the TGF-b pathway. This renders our results an interesting starting point to further explore the connection between glycogen metabolism and cytostatic cellular responses, and to establish whether glycogen is directly modulating TGF-b or through other intermediaries.

In order to validate the results regarding TGF-b in senescent MEFs, we turn our attention to FoxO1, a transcription factor that has been shown to play an important role in metabolic and cell cycle regulation [Kousteni, 2012, Schmidt et al., 2002]. Importantly, FoxO1 acts as a nodal point for the integration of the TGF-b and PI3K pathways, the latter which encompasses the insulin-dependent regulation of GSK3 and MGS [Seoane et al., 2004, Gomis et al., 2006, Van Der Vos and Coffer, 2008].

FoxO1 complexes with the canonical effectors of the TGF-b pathway, SMADs, and together localize to the nucleus where they bind and regulate target genes [Seoane et al., 2004]. We show that MEFs lacking glycogen are incapable of regulating both FoxO1 and SMAD levels, resulting in lower protein levels than wild types in senescence (Figure 4.18). Interestingly, both SMAD2 and FoxO1 are considered critical tumor suppressors, and their loss results in apoptosis evasion and uncontrolled cell growth, respectively [Yang et al., 2009, Samanta and Datta, 2012, Coomans de Brachène and Demoulin, 2016]. These results suggest that the lack of glycogen during senescence modulates TGF-b signaling through the deregulation of both FoxO1 and SMAD2.

Through further analysis of microarray results, we also determine that MGS KO senescent MEFs are transcriptionally more similar to actively proliferating cells than to senescent WT cells (Figures 4.21, 4.22). The genes shared between MGS KO senescent cells and actively proliferating cells are enriched in many important pathways involved in cancer (Figure 4.22). Among the enriched phenotypes, we highlight aberrant transciptional regulation, ribosome biogenesis, and proteoglycan effectors which are all known to participate in tumorigenesis [Lee and Young, 2013, Pelletier et al., 2018, Iozzo and Sanderson, 2011]. Furthermore, the enrichment identified MAPK, RAS and TGF-b pathways, all of which are crucial for malignancy [Burotto et al., 2014, Fernández-Medarde and Santos, 2011, Massagué, 2008].

From our analysis, we determine that glycogen modulates senescence, and in its absence, cells enter a pseudo-senescent state which allows for faster immortalization. Interestingly, once MGS KO MEFs are immortalized, they continue to

manifest faster proliferation rates (Figure 5.2). We also note that immortalized glycogen-free cells exhibit cancer-like properties. Specifically, MGS KO MEFs have an increased migratory capacity *in vitro* (Figure 5.3) and a higher replicative potential demonstrated through an improved clonogenic capacity (Figure 5.4).

Ergo, we test the metabolic consequences of removing glycogen by performing live cell analysis, which reveals a metabolic shift towards glycolysis, in addition to a decrease in mitochondrial mass (Figures 5.8, 5.12, 5.13, 5.14). These results bring the Warburg effect to mind, suggesting that glycogen-free cells reprogram their energetic needs.

Interestingly, glycogen-free immortalized MEFs exhibit lower reactive oxygen species (ROS) levels than wildtype counterparts. Possible contributing factors include a lower mitochondrial respiration rate and decreased mitochondrial mass (Figures 7.2, 5.14). TGF-b has also been shown to control ROS production, while ROS influences TGF-b signaling [Krstic et al., 2015]. Specifically, TGF-b increases ROS production while at the same time suppressing antioxidant enzymes, leading to a redox imbalance [Liu and Desai, 2015]. Thus, it would be interesting to assess whether lower ROS levels are a direct result of glycogen modulating TGF-b, or whether other mechanisms are at play.

In the last part of this thesis, and taking into account our previous results, we question whether glycogen is important in *in vivo* proliferative contexts. We discard MGS KO as model for our *in vivo* experimentation due to the high neonatal lethality, which makes *in vivo* experimentation unpractical and tedious. Thus, we take advantage of another glycogen-free model: mice lacking hepatic glycogen, LGS KO. The advantage to using this model is that protocols assaying *in vivo* hepatocytic proliferation are relatively simple and straightforward. Consequently, we test the proliferative capacity of glycogen-free hepatocytes through two proliferative challenges: hepatic regeneration and hepatocellular carcinoma (HCC) induction.

Partial hepatectomy offers a 'clean' proliferative hepatic challenge, which allows us to focus only on the proliferative aspect of cycling hepatocytes. Importantly, we show that there is a higher proportion of LGS KO hepatocytes in the S phase of the cell cycle 36h and 48h after the Phx. We also show higher protein levels of cyclin D1 and pRB, and lower levels of p21 in LGS KO liver homogenates at 36h. These results suggest that glycogen is an important regulator of hepatocytic proliferation, independently of the enzyme that regulates its synthesis.

We further test the proliferative capacity of LGS KO hepatocytes in a pathological

HCC context. Although both LGS control and KO mice develop tumors after N-nitrosodiethylamine (DEN) treatment, LGS KO mice show higher mortality and tumor burden (Figures 6.16, 6.19). Therefore, our results suggest that glycogen plays a protective role in animals exposed to DEN.

Although our *in vivo* results are promising, further experimentation is necessary to clarify the tissue-specific details regarding the relevance of glycogen and proliferation in the context of cancer. Specifically, the malignant transformation of liver cells has been associated with a significant decrease of glycogen levels. On the other hand, cancer cell lines originating from tissues with low glycogen content (i.e. brain, lung, and breast), have been shown to accumulate glycogen during malignancy [Rousset et al., 1981]. A possible explanation for this phenomenon may lie in the microenvironment of the malignant cells. For instance, if a hepatocyte becomes malignant, it can depend on the glycogen present in the healthy hepatocytes in its immediate surroundings rather than store its own energy. On the other hand, malignant cells originating from environments where glycogen levels are low have to secure their proper energy store. Therefore, our results concerning the link between liver cancer and the lack of hepatic glycogen should be taken within experimental context, until further clarification.

Another factor that would be informative to test is how cells lacking glycogen fare in conditions of nutrient stress. It has been demonstrated that glycogen plays a protective role in cells during times of nutrient stress: wild type *S.cerevisiae* survive much longer in nutrient stress conditions than mutants lacking glycogen and trehalose (another storage carbohydrate present in yeast) [Silljé et al., 1999]. This is due to the glucose buffering capacity of glycogen and trehalose during times of nutrient stress. Therefore, it is conceivable that in conditions of low glucose, our experimental cell model could demonstrate higher sensitivity to extracellular conditions.

In summary, we show that glycogen accumulates in senescent cells. When glycogen is not available, however, cells acquire a proliferative advantage which allows for a modified senescent state, in addition to faster immortalization. Once immortalized, glycogen-free cells exhibit higher proliferation and migratory rates, and an increased clonogenic capacity. Also, these same cells experience a metabolic shift towards glycolysis. Our *in vivo* results show that the lack of hepatic glycogen contributes to increased hepatocytic proliferation during liver regeneration. Lastly, in the pathological context of hepatocellular carcinoma induction, our results suggest that glycogen plays a protective role.

The results of the present study may have a great impact on our understanding of

the role of glycogen in aging and proliferation. In turn, this positions glycogen as a novel target for therapeutic intervention to combat aging. Presently, several pharmacological glycogen modulators are being tested for their effectiveness in metabolic diseases, such as diabetes [Zois et al., 2014, Zois and Harris, 2016]. Consequently, we should take advantage of this plethora of pharmaceutical information involving the modulation of glycogen metabolism and apply it to the context of senolytic agents, which are small molecules designed to induce the death of senescent cells. In conclusion, our promising results regarding glycogen and proliferative responses pave the way for further experimental clarification and possible therapeutic answers.

Barcelona,
March 2018.

Part VI

Conclusions

1. Glycogen accumulation is a conserved feature of replicative senescence in both human and mouse cells.

2. Glycogen levels are closely associated to the proliferative state of cells.

3. When glycogen is absent, mouse embryonic fibroblasts (MEF) acquire a proliferative advantage inducing a pseudo-senescent state, leading to faster immortalization.

4. The TGF-b pathway is counter-enriched in senescent MEFs lacking glycogen, resulting in the modulation of members of the TGF-b and Fox01 pathways.

5. In the absence of glycogen, immortalized MEFs exhibit a *metabolic shift* towards glycolysis, favoring lower reactive oxygen species (ROS) levels and increased proliferation rates.

6. Mice lacking liver glycogen demonstrate faster rates of hepatic regeneration.

7. Glycogen plays a protective role in the context of DEN-induced hepatocellular carcinoma.

Part VII

Methods

Chapter 7

Methods

7.1 Cell culture and cell-based assays

7.1.1 Cell culture

MGS WT and KO mouse embryonic fibroblasts were isolated from mouse embryos at d.p.c 14.5. Human embryonic lung fibroblasts (HLF-1) were acquired from ATCC (Reference: CCL-153). Cells were cultured in complete medium which consisted of DMEM (high glucose) supplemented with 10% FBS, 2 mM L-glutamine, 100 U/ml penicillin, and 100 U/ml streptomycin. Cells were incubated at 37°C with 5% CO_2 in normoxic conditions.

7.1.2 Mouse embryonic fibroblast (MEFs) generation

Timed crosses between progenitors of interest were set up, and at 14.5 d.p.c, pregnant females were sacrificed to harvest embryos. Isolated embryos in maternal tissues were placed in petri dishes filled with PBS 1x for further processing. Methodically, each embryo was removed from the placental tissues, the tail tip and head were cut and saved for genotyping, and all innards were removed. The

cleaned and emptied bodies were placed in 15 ml falcon tubes containing 2 ml 0.25% trypsin, and incubated for 30 minutes at 37°C. Trypsin was inactivated by the addition of 4 ml complete MEF medium to the falcon tube, and embryonic tissues were manually dissociated by aspirating the solution up and down. Tissues were allowed to settle to the bottom of the tube, and the supernatant was gently removed and replaced by complete MEF medium. Resuspended cells and debris were transfered to three 10 cm plates and allowed to attach overnight in normal incubation conditions: 37°C with 5% CO_2 . The next day cells were washed twice with PBS 1x and were either subjected directly to experimental protocols or cryopreserved for future use.

7.1.3 Replicative senescence assay

In order to induce replicative senescence, recently isolated MEFs for both genotypes (MGS WT and KO) were cultured in complete MEF medium. 1,000,000 cells were passaged in 10 cm plates each time confluence was reached. Around passage 11, cells demonstrated a clear decrease in proliferative capacity.

The population doubling level (PDL) represents the total number of times the cell population has doubled since isolation *in vitro*, and gives an estimate as to when primary cells reach senescence. The PDL calculation goes as follows:

$$\mathbf{n} = 3.32\ (\log \mathbf{UCY} - \log \mathbf{l}) + \mathbf{X}$$

where **n** = the final PDL number at end of a given subculture, **UCY** = the cell yield at that point, **l** = the cell number used as inoculum to begin that subculture, and **X** = the doubling level of the inoculum used to initiate the subculture being quantitated.

7.1.4 3T3 immortalization protocol

3T3 refers to 3-day transfer, and is a technique to generate immortalized cell lines from primary cell cultures. Primary mouse embryonic fibroblasts were transferred every three days, and plated at a density of 1,000,000 cells in 10 cm plates. After about 15 generations in culture, MEFs spontaneously immortalized with a stable growth rate. Population doubling level was measured the same way as in the replicative senescence protocol.

7.1.5 Stress-induced premature senescence (SIPS) protocol

200,000 cells were plated in triplicate in 10 cm plates and cultured in complete MEF medium. 24h later, they were treated with 5nM epoxomicin or an equal amount of the solvent (DMSO) in the presence of complete medium continuously for 14 days. Fresh inhibitor was added every day to exclude the possibility of its inactivation at 37°C. Cells were then washed and snap-frozen to determine glycogen content.

7.1.6 Cytochemical detection of SA-B-Gal

Cells were fixed and stained for SA-B-Gal as described in [Dimri et al., 1995]. Briefly, cells were washed in PBS 1x and fixed in 2% formaldehyde / 0.2% glutaraldehyde for 5 minutes. Next, cells were washed and incubated at 37°C (no CO_2) with fresh SA-B-Gal staining solution for 12 hours. SA-B-Gal solution consists of: 1 mg/ml 5-bromo-4-chloro-3-indolyl B-D-galactoside (X-Gal), 40 mM citric acid, sodium phosphate (pH 6.0), 5 mM potassium ferrocyanide, 5 mM potassium ferricyanide, 150 mM NaCl, and 2 mM $MgCl_2$. Blue-stained senescent cells are viewed by light microscopy.

7.1.7 Cell proliferation assay

50,000 cells were plated in triplicate in 6-well plates and cultured in complete MEF medium. At the indicated time points, cells were gently trypsinized with 0.25% trypsin and counted using the Scepter automatic counter.

7.1.8 Wound healing assay

200,000 cells were plated in triplicate in 6-well plates and cultured in complete MEF medium. The next day, a 20 ul tip was used to scratch the confluent cell monolayer. The medium was then aspirated and replaced in order to remove any floating debris. Next, the 6-well plate was placed in the incubator of the ScanR automated microscope, which maintains the temperature at 37°C and CO_2 concentration at 5%. 4 regions per well were marked, verifying that the scratch was centered in the objective field and that both edges of the wound were visible. During the next 24h, images were taken of each region every 10 minutes. Image J was used to compile images of every marked location into videos. Kinetic analysis of cell speed was performed in Image J using the Kymograph macros.

7.1.9 Clonogenic assay

Single cell suspensions were prepared by trypsinization. Cells were washed with PBS 1x and incubated with a 0.05% trypsin/EDTA solution for 5 minutes. When cells started becoming rounded, we added 3 volumes of complete MEF medium to neutralize the trypsin. Cells were detached by gently pipetting up and down, until forming a homogenous cell suspension. Cells were carefully counted using a hemocytometer and diluted in order to seed the appropriate number of cells. For this experiment, we plated 250 cells in triplicate in 6-well plates and cultured in complete MEF medium. Plates were incubated in a 5% CO_2 environment at 37˚C for a period of 14 days. At the end of the experiment, we carefully removed the medium and washed each plate with PBS 1x thrice. We proceeded to fix the colonies with 2ml 10% neutral buffered formalin solution for 25 minutes. Next, we stained colonies with 5ml 0.01% (w/v) crystal violet in distilled H_2O for 20 minutes. Once dyed, we washed the excess crystal violet with distilled H_2O, and allowed plates to air dry. Plates were scanned using the ScanR automated microscope, and colonies were counted using Image J.

7.2 Metabolite determinations

7.2.1 Glycogen quantification: Amyloglucosidase-based assay

Glycogen content in hepatic tissues and cells was determined by an amyloglucosidase-based assay described in [García-Rocha et al., 2001]. Briefly, cells were scraped with 30% KOH (w/v), and frozen tissue samples were homogenized with a Polytron in a relation 1:4 (w/v) with 30% KOH. The resulting extract was heated to 100˚C for 15 min, and then spotted on chromatography paper 31ET (Whatman, Maidstone). The glycogen was precipitated from the chromatography paper by immersion in ice-cold 66% ethanol (v/v). After two ethanol washes, the papers were air dried and incubated with amyloglucosidase, as previously described [Chan and Exton, 1976]. The resulting glucose was measured by reaction with hexokinase-G-6-P dehydrogenase (Glucose HK CP, ABX Pentra) and adapted to the Cobas Bio auto-analyzer (ABX Diagnostics). Results are expressed in ug glycogen /mg protein or ug glycogen/mg tissue.

7.2.2 Glycogen quantification: Fluorescence assay

In order to measure low glycogen levels in cells, we determine glycogen content through fluorescence detection, instead of absorbance, which allows for an assay

that is 50 times more sensitive. Cells were harvested by adding 150 ul 30% KOH to a 6 cm plate, and each sample was then homogenized with a 25G insulin needle. The solution is then heated to 100°C for 15 minutes. Glycogen precipitation is performed in solution by adding 100% cold ethanol directly to extracts, in order to achieve a final ethanol concentration of 66%. The mixture is allowed to precipitate at -20°C during two days. Next, samples are centrifuged at 15,000 rpm at 4°C, and washed twice with 66% ethanol at room temperature. The pellet is dried during 2 hours at 37°C and is resuspended in 300 ul amyloglucosidase solution at 37°C with agitation. The resulting glucose concentration is determined using a protocol described in [Zhu et al., 2009].

7.2.3 Intracellular ATP, lactate, and G6P measurements

To measure intracellular ATP, lactate and G6P in cell samples, culture medium was aspirated from 10 cm dishes and directly frozen in liquid nitrogen for later use. For processing, 200 ul of 10% perchloric acid was added to each dish and cells were scratched and harvested. Next, samples were centrifuged at 13,000g at 4°C for 15 minutes. The pellet was resuspended in 100 ul KOH 30% in order to determine protein concentration. The pH of the supernatant was monitored on ice using 15 ul of a universal pH indicator. In order to keep the pH of the samples neutral, potassium carbonate was slowly added to samples until samples reached a yellow-green tint, indicative of a neutral pH. Once samples were all neutralized, they were again subjected to centrifugation at 13,000g at 4°C for 15 minutes. The supernatant was kept at -20°C until ATP, lactate or G6P measurement.

The neutralized extract was analyzed spectrophotometrically for ATP, lactate and G6P by standard enzymatic methods, described in [Goodman et al., 1974].

7.2.4 Extracellular Lactate

Cellular medium was collected and frozen at -20°C until analysis. Medium lactate concentration was determined by the Lactate Assay kit (Sigma).

7.2.5 Liver triglycerides

Hepatic triglyceride samples were prepared in 3 mol/L KOH based on the method described by Salmon and Flatt [Salmon and Flatt, 1985], and quantified using the TAG assay (Sigma).

7.3 Electrophoresis and immunoblotting

7.3.1 Western Blot analysis

For protein detection in primary and immortalized MEFs, cells were lysed and scraped with a buffer containing 25 mM Tris-HCl (pH 7.4), 25 mM NaCl, 1% Triton X-100, 0.1% SDS, 10 mM NaF, 10 mM PPi, 1 mM sodium orthovanadate, 0.5 mM EGTA, and 25 nM oxadaic acid supplemented with protease inhibitor mixture tablet (Roche). After scraping, samples were homogenized with a 25G insulin needle, and left on ice for 10 minutes. Next, samples were centrifuged at 15,000g at 4°C for 15 minutes, the supernatant was collected, and protein concentration was determined using the Bradford assay.

For protein detection in the liver, frozen pulverized hepatic tissue was homogenized at 4°C using a Mini-Beadbeater in 10 volumes of the homogenization buffer containing 50 mM Tris-HCL (pH 7.4), 150 nM NaCl, 1 mM EDTA, 5 mM sodium pyrophosphate, 1 mM sodium orthovanadate, 50 mM NaF, 1% NP-40, 1 mM PMSF and a protease inhibitor mixture tablet (Roche). Homogenates were rotated for 30 minutes at 4°C in an orbital shakers and centrifuged at 16,000 x g for 15 minutes at 4°C. The supernatant was kept and protein concentration was determined using the Bradford assay.

For both cell and liver protein extracts, equal amounts of protein per sample were separated by standard SDS-polyacrylamide gel electrophoresis and transferred to immobilon membranes (Millipore). Next, membranes were incubated at 4°C overnight with the appropriate antibody. Antibody dilutions, blocking solution and secondary antibodies are detailed in Table 8.1. Where otherwise specified, loading control of the Western blot membrane was performed using the REVERT total protein stain (LI-COR).

7.4 Live-cell metabolic assays

For all metabolic experiments, 40,000 cells were seeded in a XF24 cell culture microplate (Agilent techologies) the day before measurement, and left in an incubator at 37°C, 5% CO_2 overnight.

Once drugs and reagents were added, the flux plate containing the injection ports was allowed to calibrate for 30 minutes in the Seahorse XF Analyzer. During probe calibration, cells plated in the cell culture microplate were carefully washed

with PBS 1x and then, Seahorse XF medium was added to each well. For the mitochondrial function test, the Seahorse medium was supplemented with glutamine and glucose, as previously mentioned. The cell culture microplate was placed at 37°C without CO_2, which can alter media pH and disrupt extracellular acidification rate readings.

Seahorse XF Glycolysis Stress Test: This commercial test kit assesses glycolytic function in cells. For this, 10x concentrations of glycolysis reagents were prepared in seahorse medium which did not contain either glutamine or glucose. Next, each reagent was manually added to the correct injection port (4 maximum): 100 mM glucose (port A), 100 uM oligomycin (port B) and 500 mM 2-deoxy-glucose (2-DG).

In order to gauge glycolytic parameters, the ECAR is measured in real time while different glycolytic modulators are sequentially injected into the medium (Table 7.1). First, the baseline ECAR is measured in the basal assay medium, which lacks pyruvate and glucose. Next, a saturating concentration of glucose is injected into the individual wells, which results in an increase in ECAR as cells use the injected glucose to catabolize it through the glycolytic pathway to pyruvate. This second ECAR measurement represents glycolysis under saturating glucose concentrations.

Injection Number	Glycolytic Modulator	Target	Effect on ECAR
1	Glucose	Glycolysis	Increase
2	Oligomycin	ATP Synthase Complex V	Increase
3	2-DG	Glycolysis	Decrease

Table 7.1: **Seahorse XF Glycolysis Stress Test modulators.** List of glycolytic modulators, in order of injection, target and effect on extracellular acidification rate (ECAR). Adapted from Agilent Seahorse.

The second injection is oligomycin, a mitochondrial drug which inhibits ATP synthase (Complex V), an integral player of the electron transport chain. By inhibiting the ETC, this forces energy production to shift solely to glycolysis, thereby inducing an increase in ECAR. This represents the maximal glycolytic capacity of the cells.

The last glyolytic modulator is 2-deoxy-glucose (2-DG), which is a glucose analog that competitively binds to glucose hexokinase, thereby inhibiting glycolysis. The ECAR measured after 2-DG addition represents medium acidification due to

other cellular processes besides glycolysis (non-glycolytic acidfication).

Seahorse XF Cell Mito Stress Test: This commercial test kit assesses mitochondrial function in cells. For this, 10x concentrations of mitochondrial drugs were prepared in seahorse medium supplemented with 2 mM glutamine and 10 mM glucose. Next, each drug was manually added to the correct injection port (4 maximum): 1 uM Oligomycin A (port A), 0.5 uM FCCP (port B), 0.5 uM Rotenone and 0.5 uM Antimycin A (port C).

Injection Number	Mitochondrial Modulator	Target	Effect on OCR
1	Oligomycin	ATP Synthase Complex V	Decrease
2	FCCP	inner mitochondrial membrane	Increase
3	Rotenone/ antimycin A	Complex I and III (respectively)	Decrease

Table 7.2: **Seahorse XF Mito Stress Test modulators.** List of mitochondrial respiration modulators, in order of injection, target and effect on oxygen consumption rate (OCR). Adapted from Agilent Seahorse user guide.

Similarly to ECAR, OCR is measured in real time while different mitochondrial modulators are sequentially injected into individual wells (Table 7.2). First, the baseline OCR is measured in the basal assay medium, which is supplemented with glucose and pyruvate. This value indicates the basal respiration rate of the cells. Next, oligomycin is added, and results in a sharp decrease in OCR as mitochondria are negatively affected by the inhibition of ATP synthase (complex V).

The second injection contains carbonyl cyanide-4-(trifluoromethoxy) phenylhydrazone (FCCP), which readily uncouples oxygen consumption from ATP production, thereby maximally increasing oxygen consumption. The last injection is a mixture of antimycin A and rotenone which act to inhibit complexes I and III of the ETC, respectively. These modulators essentially shutdown mitochondrial respiration, and the resulting OCR represents non-mitochondrial respiration due to other cellular processes not related to the mitochondria.

7.5 Flow cytometry

7.5.1 Mitotracker Green

To determine mitochondrial mass, 120,000 cells were plated in 6 cm plates. Cells were incubated overnight to allow for attachment. The next day, cells were washed

once with PBS 1x, and then were incubated with 10 nM Mitotracker Green probe for 30 minutes at 37°C with 5%CO_2. The negative control consisted of cells incubated only with PBS. After incubation, cells were gently washed with PBS and trypsinized. Next, cells were harvested with ice cold PBS at 4°C and kept on ice until analysis. The negative control was used to set the flow cytometer compensation and gate parameters for negative and positive Mitotracker green events. Mitotracker Green fluorescence was detected using the FL-1 channel with a Gallios Flow Cytometer research system (Beckman Coulter), until 10,000 events were analyzed. Results are expressed as mean fluorescence intensity (MFI) normalized against WT.

7.5.2 H_2DCFDA detection

To determine general reactive oxidative species levels, 120,000 cells were plated in 6 cm plates. Cell were incubated overnight to allow for attachment. The next day, cells were washed once with PBS, and then were incubated with 5 uM H_2DCFDA fluorescent probe for 1 hour at 37°C with 5%CO_2. The negative control consisted of cells incubated only with PBS. After incubation, cells were gently washed with PBS and trypsinized. Next, cells were harvested with ice cold PBS at 4°C and kept on ice until analysis. The negative control was used to set the flow cytometer compensation and gate parameters for negative and positive H_2DCFDA events. H_2DCFDA fluorescence was detected using the FL-1 channel with a Gallios Flow Cytometer research system (Beckman Coulter), until 10,000 events were analyzed. Results are expressed as mean fluorescence intensity (MFI) normalized against WT.

7.5.3 Mitosox Red

To determine mitochondrial superoxide levels in immortalized cells, 120,000 cells were plated in 6cm plates. Cells were incubated overnight to allow for attachment. The next day, cells were washed once with PBS, and were incubated with 5 uM Mitosox Red for 30 minutes at 37°C with 5%CO_2. The negative control consisted of cells incubated only with PBS. After incubation, cells were gently washed with PBS and trypsinized. Next, cells were harvested with ice cold PBS at 4°C and kept on ice until analysis. The negative control was used to set the flow cytometer compensation and gate parameters for negative and positive Mitosox Red events. Mitosox Red fluorescence was detected by the FL-3 channel with a Gallios Flow Cytometer research system (Beckman Coulter), until 10,000

events were analyzed. Results are expressed as mean fluorescence intensity (MFI) normalized against WT.

7.6 Molecular Biology techniques

7.6.1 Quantitative RT-PCR

RNA
Frozen tissues and cells were homogenized by Polytron or 25G insulin syringe, respectively, in Trizol (Invitrogen). Next, mRNA was isolated using the RNeasy Mini kit (Qiagen), according to manufacturer's instructions. 1 ug mRNA was reverse transcripted to cDNA using the Superscript One-Step RT-PCR System (Invitrogen). To assess changes in gene expression, qRT-PCR was performed using the comparative CT method using SYBR Green I Master (Roche) on the QuantStudio 6 Flex Real-Time PCR system (ThermoFisher Scientific). 18s and UBC housekeeping genes were used as endogenous controls for gene normalization. Primer sequences are listed in Table 7.3.

DNA
Total DNA from cell samples was extracted with the DNeasy Blood and Tissue Kit (Qiagen), according to manufacturer's instructions. We quantified mitochondrial DNA by RT-PCR using the QuantStudio 6 Flex Real-Time PCR system (ThermoFisher Scientific). Total DNA was used as a template and was amplified with specific oligodeoxynucleotides for mitochondrial DNA (mND-1) or nuclear DNA (SDHA). We calculated the mitochondrial DNA copy number by using SDHA amplification as a reference for nuclear DNA content. The primers used for qPCR are indicated in Table 7.3.

Gene	Name	Sequence
Gys1	mMGS FW	5'-GAACGCAGTGCTTTTCGAGG-3'
Gys1	mMGS RV	5'-CCAGATAGTAGTTGTCACCCCAT-3'
SDHA	mSDHA FW	5'-GGAACACTCCAAAAACAGACCT-3'
SDHA	mSDHA RV	5'-CCACCACTGGGTATTGAGTAGAA-3'
mND-1	mMND1 FW	5'-GGCTACATACAATTACGCAAAG-3'
mND-1	mMND1 RV	5'-TAGAATGGAGTAGACCGAAAGG-3'

Table 7.3: **RT-PCR primers**

7.6.2 Microarray

RNA sample collection and generation of biotinylated complementary RNA (cRNA) probe were carried out essentially as described in the standard Affymetrix Genechip protocol. 10 ug of total RNA was used to prepare cRNA probe using a custom superscript kit (Invitrogen). For expression profiling, 25 ng of RNA per sample was processed using isothermal amplification SPIA Biotin system (NuGen technologies). Each sample was hybridized with an Affymetrix Mouse Gene 1.0 ST microarray at the IRB Barcelona Functional Genomics Laboratory.

Preprocessing and quality control
We used Bioconductor to perform RMA background correction, quantile normalization and RMA summarization using the RMA function from the oligo package to obtain probeset expression estimates [Gentleman et al., 2004, Carvalho and Irizarry, 2010].

Differential expression analysis
We used the limma package from Bioconductor to fit a linear model with a factorial design at two levels (group and time), and taking into account paired replicated. Differentially expressed genes were detected using Bayes, setting the BH adjusted p-value at 0.05 and FC greater than 1.5. Additionally, we used the GaGa package [Rossell, 2009] to identify patterns of expression across the four groups, setting the FDR at 0.05

7.7 Histology and Immunohistochemistry

7.7.1 Sample preparation

To prepare tissue samples for staining, harvested livers were fixed in 4% paraformaldehyde at 4°C overnight. Next, fixed samples were embedded in paraffin and sectioned at 4 um for staining.

7.7.2 Histological staining

To prepare liver sections for staining, they were first deparaffinized and then hydrated by passing through decreasing concentrations of alcohol. Once stained, samples were dehydrated once again in increasing concentration of alcohol and in xylene. Samples were mounted in mounting media and observed using the Nikon Olympus E600 microscope.

Hematoxylin and eosin (H&E) staining: H&E staining is the gold standard when it comes to studying biopsies. Specifically, hematoxylin stains nuclei blue, while eosin stains the cytoplasm pink. 4 um sections were stained in hematoxylin for 3-5 min, then differentiated in 1% acidic alcohol (1% HCl in 70% alcohol), and lastly stained with 1% Eosin Y for 10 min. Samples were then mounted and analyzed. The histopathological study in DEN treated mice was performed by Dr.Neus Prats of the IRB Barcelona Histopathology Facility.

Period Acid-Schiff (PAS) staining: To detect glycogen, liver tissue was oxidized with 5% periodic acid for 10 min, stained with Schiff reagent for 30 min, counter-stained with hematoxylin, dehydrated and mounted. To confirm glycogen staining specificity, liver tissue was also treated with diastase, an enzyme that degrades glycogen (PAS-D). This allowed us to confirm positive glycogen staining: PAS-D staining reveals a light pink stain where the normal strong magenta stain of glycogen is present on serial sections. PAS and PAS-D stains were performed using the Artisanlink Pro machine (DAKO AR165 kit), according to the manufacturer's instructions.

7.7.3 Immunohistochemistry (IHC)

Immunohistochemistry is a technique which allows the visualization of cellular components (i.e. proteins) in tissue samples. Furthermore, IHC reveals the existence and localization of the target protein in the tissue.

IHC involves the staining of a tissue using a primary antibody directed towards a specific protein target. After washing, tissues are incubated with a secondary antibody that carries a molecule with horseradish peroxidase (HRP) enzymes. Once the secondary antibody is given some time to detect the primary antibodies, the excess is washed away. Next, 3,3' Diaminobenzidine (DAB) is added. The HRP enzyme transforms the DAB substrate into a brown precipitate that is deposited in the tissue where the reaction took place. This gives us a visual indication of where the original epitope was located within the tissue. Furthermore, we perform a counterstain with hematoxylin in order to locate the nuclei.

To prepare liver sections for staining, they were first deparaffinized and then hydrated by passing through decreasing concentrations of alcohol. Once stained, samples were dehydrated once again in increasing concentration of alcohol and in xylene. Samples were mounted in mounting media and observed using the Nikon Olympus E600 microscope.

5-bromo-2-deoxyuridine (BrdU)
BrdU is a synthetic analog of thymidine and is used to identify cells in the S phase. *In vivo* BrdU labeling was performed by injecting mice with 100 mg/kg BrdU 2 hours before sacrifice. Liver samples were then fixed and processed as previously described. Deparaffinized tissue sections were subjected to heat-induced epitope retrieval in order to denature the DNA and facilitate BrdU antibody binding. Sections were stained for BrdU overnight at 4°C (1:200 dilution, Cell Signaling). Samples were counterstained with hematoxylin for nuclei visualization.

Ki67
Ki67 is a marker of cellular proliferation and it is present during the active phases of the cell cycle (G1, S, G2, and mitosis), and absent from quiescent G0 cells. Liver samples were fixed and processed as previously described. Deparaffinized tissues sections were incubated with the Ki67 antibody overnight at 4°C (1:400, Cell Signaling). Samples were counterstained with hematoxylin for nuclei visualization.

7.8 Animal studies and procedures

All procedures were approved by the Barcelona Science Park's Animal Experimentation Committee and were carried out in accordance with the European Community Council Directive and National guidelines for the care and use of laboratory animals. All comparisons were among littermates. Mice were allowed free access to a standard chow diet and water and maintained on a 12h/12h light/dark cycle under specific pathogen-free conditions in the Animal Research Center at the Barcelona Science Park. Mice were weaned at 3 weeks of age, and tail clipping were taken for genotyping.

MGS KO mice were generated as reported in [Sinadinos et al., 2014]: the *Gys1* gene was disrupted by the insertion of a cassette containing LacZ and NeoR genes between exons 5 and 6. **LGS KO mice** [Gys2tm1a(KOMP)Wtsi], were generated by the Sanger Institute Mouse Genetics Project and were backcrossed to the C57BL/6J stain for more than eight generations.

For timed matings, breeding pairs or trios were set up by introducing female mice into cages with one male in the late afternoon. The next morning, female mice were checked for vaginal plugs which are indicative of mating. This corresponds to embryonic day 0.5. For MEF preparation, females were sacrificed at d.p.c. 14.5.

7.8.1 Physiological Parameters

Glycemia: Blood glucose levels were measured using a glucometer (Ascensia Breeze 2, Bayer Healthcare).
Body fat and lean mass: Total body fat and lean mass were monitored by EchoMRI-100 (EchoMRI, Houston, Texas, USA).
Liver to body weight: Liver to body weight ratio was calculated by weighing the whole liver with a precision scale at sacrifice and dividing by body weight.

7.8.2 Partial hepatectomy (Phx)

Surgical procedure
Partial hepatectomy refers to the removal of two-thirds of the liver, by specifically removing the median and left lateral lobes. The procedure was performed on 5-10 week old mice. The mice were weighed before and after the procedure.

First, the animal was placed in a plexiglass chamber to induce anesthesia with 2% isofluorane, and once completely anesthetized, the animal was transferred to a heating pad and the anesthesia was maintained for the duration of the operation through a size-appropriate mouthpiece. The abdominal fur was first removed, and then the area was disinfected with 70% ethanol. The abdominal skin was incised horizontally, and then the muscular layer was cut to a size of about 3 cm, in order to expose the xiphoid process.

Once the liver was located, the falciform ligament was cut in order to further expose the liver. First, the median lobe was identified, and then 4-0 silk suture was tied, making sure to maintain a distance from the suprahepatic vena cava to avoid venous obstruction. Next, the median lobe was carefully excised. The same procedure was performed for the left lateral lobe, however the suture was tied as close as possible to the stump since, in this case, there was no risk of venous obstruction. The median lobe was fixed in 4% formaldehyde at 4°C overnight, and then embedded in paraffin blocks for future processing. The left lateral lobe was snap frozen in liquid nitrogen for Western blotting. The samples harvested during the procedure correspond to time 0 for analysis, a starting point comparison.

The muscular layer of the peritoneum was stitched using 5-0 suture, and then the skin was closed with wound clips. Animals were administered an analgesic, Brupex (0.1 mg/kg), and were closely monitored during the hours and days following

the operation.

Sacrifice
Two hours before sacrifice, animals were injected with bromodeoxyuridine (BrdU), 125 mg/kg, in order to track S phase hepatocytes (actively replicating the DNA) during the two hour window. Animals were weighed and then sacrificed by cervical dislocation at specific time points (24h, 36h, 48h, 72h). Once harvested, livers were weight for calculating the liver to body weight ratio. Next, half of the liver was fixed in 4% formaldehyde at 4°C overnight, and then embedded in paraffin, while the other half was snap-frozen in liquid nitrogen.

7.8.3 N-nitrosodiethylamine (DEN) treatment

DEN administration
15 day old male mice were injected intraperitoneally with a single dose of DEN (5 mg/kg, diluted in PBS 1x) and were monitored daily during the following week. After the initial week, mice were monitored once weekly until sacrifice at 9 months of age.

Sacrifice
At sacrifice, mice were weighed and the harvested liver was weighed and visually inspected for macroscopic hepatic lesions. The harvested liver was fixed in 4% paraformaldehyde at 4°C overnight, and then embedded in paraffin blocks for future processing.

7.9 Statistical Analysis

Results are presented as the mean $+/-$ s.e.m. Unless otherwise indicated, significance between two variables was analyzed using an unpaired Student's t test, performed with the GraphPad Prism software (La Jolla, Ca, USA). The following p values were considered to be statistically significant: * $p \leq 0.05$, ** $p \leq 0.01$, *** $p \leq 0.001$.

Part VIII

Supplementary Information

Chapter 8

Supplementary Tables

Antibody	Reference	Dilution	Usage	Secondary Antibody	Buffer
BrdU	Cell Signaling	1:200	IHC	Mouse	3% BSA PBS-tween
CHK1	Cell Signaling	1:1000	Western Blot	Mouse	5% BSA TBS-tween
cyclin D1	Cell signaling	1:1000	Western Blot	Rabbit	5% BSA TBS-tween
FoxO1	Cell signaling	1:1000	Western Blot	Rabbit	5% BSA TBS-tween
GADPH	Thermo Fisher Scientific	1:10,000	Western Blot	Mouse	3% BSA PBS-tween
Ki67	Cell Signaling	1:400	IHC	Rabbit	3% BSA PBS-tween
LGS	in house	1:30,000	Western Blot	Rabbit	3% BSA PBS-tween
MGS	Cell Signaling	1:1000	Western Blot	Rabbit	3% BSA PBS-tween
p-MGS (Ser641)	Cell Signaling	1:1000	Western Blot	Rabbit	3% BSA PBS-tween
p16	Santa Cruz	1:200	Western Blot	Mouse	5% BSA TBS-tween
p21	Santa Cruz	1:200	Western Blot	Rabbit	3% BSA PBS-tween
p38	Cell signaling	1:1000	Western Blot	Rabbit	5% BSA TBS-tween
p-p38 (Thr180/Tyr182)	Cell signaling	1:1000	Western Blot	Rabbit	5% BSA TBS-tween
p53	Cell signaling	1:1000	Western Blot	Mouse	5% BSA TBS-tween
p-p53 (Ser15)	Cell signaling	1:1000	Western Blot	Rabbit	5% BSA TBS-tween
Porin	Abcam	1:1000	Western Blot	Rabbit	3% BSA PBS-tween
SMAD2	Cell signaling	1:1000	Western Blot	Rabbit	5% BSA TBS-tween

Table 8.1: **Antibodies**

Num	Entrez ID	Gene Symbol	Gene Name	Fold Change	p-value adjusted
1	14936	Gys1	glycogen synthase 1, muscle	-6,604	0,022

Table 8.2: **Top downregulated gene(s) in MGS KO versus WT MEFs at passage 2**

Num	Entrez ID	Gene Symbol	Gene Name	Fold Change	p-value adjusted
1	654795	Sdr39u1	short chain dehydrogenase/reductase family 39U, member 1	-33,415	0,001
2	271786	Galnt13	UDP-N-acetyl-alpha-D-galactosamine:polypeptide N-acetylgalactosaminyltransferase 13	-32,403	0,010
3	12845	Comp	cartilage oligomeric matrix protein	-27,761	0,005
4	319909	Ism1	isthmin 1 homolog (zebrafish)	-24,661	0,012
5	216028	Lrrtm3	leucine rich repeat transmembrane neuronal 3	-22,614	0,004
6	15446	Hpgd	hydroxyprostaglandin dehydrogenase 15 (NAD)	-21,800	0,013
7	56188	Fxyd1	FXYD domain-containing ion transport regulator 1	-21,194	0,032
8	666048	Gm12824	predicted gene 12824	-20,929	0,001
9	21828	Thbs4	thrombospondin 4	-18,222	0,020
10	230099	Car9	carbonic anhydrase 9	-18,128	0,002
11	15430	Hoxd10	homeobox D10	-17,826	0,006
12	208777	Sned1	sushi, nidogen and EGF-like domains 1	-17,099	0,013
13	11607	Agtr1a	angiotensin II receptor, type 1a	-16,033	0,005
14	14184	Fgfr3	fibroblast growth factor receptor 3	-14,053	0,012
15	14366	Fzd4	frizzled homolog 4 (Drosophila)	-13,920	0,011
16	12587	Mia1	melanoma inhibitory activity 1	-13,156	0,013
17	20309	Cxcl15	chemokine (C-X-C motif) ligand 15	-12,474	0,033
18	14176	Fgf5	fibroblast growth factor 5	-11,455	0,005
19	66425	Pcp4l1	Purkinje cell protein 4-like 1	-11,393	0,010
20	320712	Abi3bp	ABI gene family, member 3 (NESH) binding protein	-11,240	0,001

Table 8.3: **Top 20 differentially down regulated genes in MGS KO versus WT MEFs at passage 11**

Num	Entrez ID	Gene Symbol	Gene Name	Fold Change	p-value adjusted
1	231507	Plac8	placenta-specific 8	33,677	0,009
2	80976	Syt13	synaptotagmin XIII	19,727	0,015
3	13024	Ctla2a	cytotoxic T lymphocyte-associated protein 2 alpha	17,144	0,074
4	20706	Serpinb9b	serine (or cysteine) peptidase inhibitor, clade B, member 9b	13,599	0,037
5	15413	Hoxb5	homeobox B5	12,445	0,005
6	54613	St3gal6	ST3 beta-galactoside alpha-2,3-sialyltransferase 6	11,634	0,015
7	218461	Pde8b	phosphodiesterase 8B	11,535	0,004
8	15424	Hoxc5	homeobox C5	10,801	0,005
9	216616	Efemp1	epidermal growth factor-containing fibulin-like extracellular matrix protein 1	10,442	0,039
10	100102	Pcsk9	proprotein convertase subtilisin/kexin type 9	10,360	0,059
11	27226	Pla2g7	phospholipase A2, group VII (platelet-activating factor acetylhydrolase, plasma)	10,081	0,033
12	97848	Serpinb6c	serine (or cysteine) peptidase inhibitor, clade B, member 6c	9,703	0,024
13	15228	Foxg1	forkhead box G1	9,473	0,025
14	75395	0610040B09Rik	RIKEN cDNA 0610040B09 gene	9,374	0,066
15	229357	Gpr149	G protein-coupled receptor 149	9,226	0,069
16	19224	Ptgs1	prostaglandin-endoperoxide synthase 1	9,095	0,020
17	12642	Ch25h	cholesterol 25-hydroxylase	8,724	0,030
18	15410	Hoxb3	homeobox B3	8,557	0,017
19	68545	Ecscr	endothelial cell surface expressed chemotaxis and apoptosis regulator	8,454	0,017
20	80976	Syt13	synaptotagmin XIII	8,446	0,001

Table 8.4: **Top 20 differentially upregulated genes in MGS KO versus WT MEFs at passage 11**

Num	Entrez ID	Gene Symbol	Gene Name	Fold Change	p-value adjusted
1	74488	Lrrc15	leucine rich repeat containing 15	-26,249	0,002
2	231507	Plac8	placenta-specific 8	-20,869	0,001
3	100102	Pcsk9	proprotein convertase subtilisin/kexin type 9	-20,557	0,002
4	13024	Ctla2a	cytotoxic T lymphocyte-associated protein 2 alpha	-18,231	0,006
5	14619	Gjb2	gap junction protein, beta 2	-16,390	0,009
6	22771	Zic1	zinc finger protein of the cerebellum 1	-13,236	0,001
7	80976	Syt13	synaptotagmin XIII	-13,089	0,002
8	22042	Tfrc	transferrin receptor	-11,525	0,005
9	20715	Serpina3g	serine (or cysteine) peptidase inhibitor, clade A, member 3G	-10,893	0,001
10	73884	Zdbf2	zinc finger, DBF-type containing 2	-10,540	0,000
11	12903	Crabp1	cellular retinoic acid binding protein I	-10,167	0,001
12	407831	Tmem204	transmembrane protein 204	-9,965	0,008
13	68545	Ecscr	endothelial cell surface expressed chemotaxis and apoptosis regulator	-9,856	0,001
14	16012	Igfbp6	insulin-like growth factor binding protein 6	-9,040	0,001
15	68498	Tspan11	tetraspanin 11	-9,017	0,007
16	13032	Ctsc	cathepsin C	-8,863	0,002
17	229357	Gpr149	G protein-coupled receptor 149	-8,397	0,006
18	13025	Ctla2b	cytotoxic T lymphocyte-associated protein 2 beta	-8,232	0,002
19	70417	Megf10	multiple EGF-like-domains 10	-7,926	0,007

Table 8.5: **Top 20 differentially down regulated genes in p11 MGS WT versus p2 MGS WT MEFs**

Num	Entrez ID	Gene Symbol	Gene Name	Fold Change	p-value adjusted
1	20309	Cxcl15	chemokine (C-X-C motif) ligand 15	46,821	0,001
2	26968	Islr	immunoglobulin superfamily containing leucine-rich repeat	43,742	0,001
3	271786	Galnt13	UDP-N-acetyl-alpha-D-galactosamine:polypeptide N-acetylgalactosaminyltransferase 13	40,548	0,001
4	319909	Ism1	isthmin 1 homolog (zebrafish)	37,993	0,001
5	18162	Npr3	natriuretic peptide receptor 3	28,126	0,000
6	56188	Fxyd1	FXYD domain-containing ion transport regulator 1	26,657	0,002
7	654795	Sdr39u1	short chain dehydrogenase/reductase family 39U, member 1	24,428	0,000
8	11607	Agtr1a	angiotensin II receptor, type 1a	23,496	0,000
9	78896	1500015O10Rik	RIKEN cDNA 1500015O10 gene	23,441	0,008
10	12824	Col2a1	collagen, type II, alpha 1	23,029	0,010
11	12759	Clu	clusterin	21,158	0,016
12	387314	Tmtc1	transmembrane and tetratricopeptide repeat containing 1	18,847	0,001
13	320712	Abi3bp	ABI gene family, member 3 (NESH) binding protein	18,526	0,004
14	208777	Sned1	sushi, nidogen and EGF-like domains 1	17,402	0,001
15	70370	Fbln7	fibulin 7	16,593	0,001
16	12587	Mia1	melanoma inhibitory activity 1	16,242	0,001
17	12845	Comp	cartilage oligomeric matrix protein	14,952	0,001
18	14560	Gdf10	growth differentiation factor 10	14,895	0,002
19	103511	Fam26e	family with sequence similarity 26, member E	13,989	0,001

Table 8.6: **Top 20 differentially upregulated genes in p11 MGS WT versus p2 MGS WT MEFs**

Num	Entrez ID	Gene Symbol	Gene Name	Fold Change	p-value adjusted
1	13040	Ctss	cathepsin S	-10,451	0,082
2	17242	Mdk	midkine	-8,542	0,014
3	14619	Gjb2	gap junction protein, beta 2	-7,345	0,077
4	66214	1190002H23Rik	RIKEN cDNA 1190002H23 gene	-6,446	0,008
5	100647	Upk3b	uroplakin 3B	-6,334	0,042
6	59095	Fxyd6	FXYD domain-containing ion transport regulator 6	-6,195	0,053
7	80891	Fcrls	Fc receptor-like S, scavenger receptor	-5,519	0,074
8	22771	Zic1	zinc finger protein of the cerebellum 1	-5,263	0,022
9	16565	Kif21b	kinesin family member 21B	-4,856	0,008
10	14585	Gfra1	glial cell line derived neurotrophic factor family receptor alpha 1	-4,551	0,057
11	16002	Igf2	insulin-like growth factor 2	-4,490	0,029
12	16164	Il13ra1	interleukin 13 receptor, alpha 1	-4,265	0,016
13	12260	C1qb	complement component 1, q subcomponent, beta polypeptide	-4,243	0,083
14	72042	Cotl1	coactosin-like 1 (Dictyostelium)	-4,134	0,025
15	100102	Pcsk9	proprotein convertase subtilisin/kexin type 9	-3,862	0,075
16	54712	Plxnc1	plexin C1	-3,730	0,085
17	109225	Ms4a7	membrane-spanning 4-domains, subfamily A, member 7	-3,626	0,046
18	329278	Tnn	tenascin N	-3,594	0,022
19	80879	Slc16a3	solute carrier family 16 (monocarboxylic acid transporters), member 3	-3,563	0,093

Table 8.7: **Top 20 differentially down regulated genes in p11 MGS KO versus p2 MGS KO MEFs**

Num	Entrez ID	Gene Symbol	Gene Name	Fold Change	p-value adjusted
1	15228	Foxg1	forkhead box G1	16,079	0,011
2	64058	Perp	PERP, TP53 apoptosis effector	12,391	0,014
3	97848	Serpinb6c	serine (or cysteine) peptidase inhibitor, clade B, member 6c	11,481	0,014
4	109620	Dsp	desmoplakin	10,633	0,012
5	26358	Aldh1a7	aldehyde dehydrogenase family 1, subfamily A7	9,315	0,020
6	12813	Col10a1	collagen, type X, alpha 1	8,181	0,025
7	234214	Sorbs2	sorbin and SH3 domain containing 2	7,604	0,048
8	93970	Klra18	killer cell lectin-like receptor, subfamily A, member 18	7,541	0,006
9	20706	Serpinb9b	serine (or cysteine) peptidase inhibitor, clade B, member 9b	7,268	0,028
10	58237	Nkain4	Na+/K+ transporting ATPase interacting 4	7,201	0,014
11	20309	Cxcl15	chemokine (C-X-C motif) ligand 15	6,465	0,028
12	239405	Rspo2	R-spondin 2 homolog (Xenopus laevis)	6,006	0,043
13	18162	Npr3	natriuretic peptide receptor 3	5,957	0,014
14	18619	Penk	preproenkephalin	5,922	0,072
15	319586	Celf5	CUGBP, Elav-like family member 5	5,330	0,063
16	13638	Efna3	ephrin A3	5,236	0,008
17	16508	Kcnd2	potassium voltage-gated channel, Shal-related family, member 2	5,194	0,024
18	235674	Acaa1b	acetyl-Coenzyme A acyltransferase 1B	5,098	0,035
19	12578	Cdkn2a	cyclin-dependent kinase inhibitor 2A	4,939	0,011

Table 8.8: **Top 20 differentially upregulated genes in p11 MGS KO versus p2 MGS KO MEFs**

Bibliography

[Acosta et al., 2013] Acosta, J. C., Banito, A., Wuestefeld, T., Georgilis, A., Janich, P., Morton, J. P., Athineos, D., Kang, T. W., Lasitschka, F., Andrulis, M., Pascual, G., Morris, K. J., Khan, S., Jin, H., Dharmalingam, G., Snijders, A. P., Carroll, T., Capper, D., Pritchard, C., Inman, G. J., Longerich, T., Sansom, O. J., Benitah, S. A., Zender, L., and Gil, J. (2013). A complex secretory program orchestrated by the inflammasome controls paracrine senescence. *Nature Cell Biology*, 15(8):978–990.

[Adams and Turnbull, 1996] Adams, P. L. and Turnbull, D. M. (1996). Disorders of the electron transport chain. *J. lnher. Metab. Dis*, 19:463–469.

[Agnello et al., 2008] Agnello, M., Morici, G., and Rinaldi, A. M. (2008). A method for measuring mitochondrial mass and activity. *Cytotechnology*, 56(3):145–149.

[Aird and Zhang, 2013] Aird, K. M. and Zhang, R. (2013). Detection of senescence-associated heterochromatin foci (sahf). In *Cell Senescence*, pages 185–196. Springer.

[Alberts et al., 2002] Alberts, B., Johnson, A., Lewis, J., Raff, M., Roberts, K., and Walter, P. (2002). Cancer as a microevolutionary process.

[Anand et al., 2008] Anand, P., Kunnumakara, A. B., Sundaram, C., Harikumar, K. B., Tharakan, S. T., Lai, O. S., Sung, B., and Aggarwal, B. B. (2008). Expert Review Cancer is a Preventable Disease that Requires Major Lifestyle Changes. 25(9).

[Balaban et al., 2005] Balaban, R. S., Nemoto, S., and Finkel, T. (2005). Mitochondria, Oxidants, and Aging. *Cell*, 120:483–495.

[Baqué et al., 1997] Baqué, S., Guinovart, J. J., and Ferrer, J. C. (1997). Glycogenin, the primer of glycogen synthesis, binds to actin. *FEBS letters*, 417(3):355–359.

[Bataller and Brenner, 2005] Bataller, R. and Brenner, D. (2005). Liver fibrosis. *The journal of clinical investigation*, 115(2):209–218.

[Berg et al., 2002] Berg, J., Tymoczko, J., and Stryer, L. (2002). Glycogen metabolism. *Biochemistry*, page 338.

[Bittles and Harper, 1984] Bittles, A. and Harper, N. (1984). Increased glycolysis in ageing cultured human diploid fibroblasts. *Bioscience Reports*, 4(1984):751–756.

[Bouskila et al., 2008] Bouskila, M., Hirshman, M. F., Jensen, J., Goodyear, L. J., and Sakamoto, K. (2008). Insulin promotes glycogen synthesis in the absence of GSK3 phosphorylation in skeletal muscle. *American journal of physiology. Endocrinology and metabolism*, 294:E28–E35.

[Bouskila et al., 2010] Bouskila, M., Hunter, R. W., Ibrahim, A. F., Delattre, L., Peggie, M., Van Diepen, J. A., Voshol, P. J., Jensen, J., and Sakamoto, K. (2010). Allosteric regulation of glycogen synthase controls glycogen synthesis in muscle. *Cell metabolism*, 12(5):456–466.

[Brown, 2004] Brown, A. M. (2004). Brain glycogen re-awakened. *Journal of neurochemistry*, 89(3):537–552.

[Burotto et al., 2014] Burotto, M., Chiou, V. L., Lee, J. M., and Kohn, E. C. (2014). The MAPK pathway across different malignancies: A new perspective. *Cancer*, 120(22):3446–3456.

[Campisi, 2013] Campisi, J. (2013). Aging , Cellular Senescence , and Cancer. *Annu. Rev. Physiol.*, 75:685–705.

[Carmeliet, 2003] Carmeliet, P. (2003). Angiogenesis in health and disease. *Nature medicine*, 9(6):653.

[Carvalho and Irizarry, 2010] Carvalho, B. S. and Irizarry, R. A. (2010). A framework for oligonucleotide microarray preprocessing. *Bioinformatics*, 26(19):2363–2367.

[Champe and Harvey, 1994] Champe, P. C. and Harvey, R. A. (1994). Metabolic effects of insulin and glucagon. *Biochemistry. 2nd ed. Philadelphia: Lippincott-Raven*, pages 269–80.

[Chan and Exton, 1976] Chan, T. M. and Exton, J. H. (1976). A rapid method for the determination of glycogen content and radioactivity in small quantities of tissue or isolated hepatocytes. *Analytical Biochemistry*, 71(1):96–105.

[Charni et al., 2017] Charni, M., Aloni-Grinstein, R., Molchadsky, A., and Rotter, V. (2017). P53 on the crossroad between regeneration and cancer. *Cell Death and Differentiation*, 24(1):8–14.

[Chen and Weinstein, 2016] Chen, M. A. and Weinstein, D. A. (2016). Glycogen storage diseases : Diagnosis , treatment and outcome. 1:45–72.

[Childs et al., 2014] Childs, B. G., Baker, D. J., Kirkland, J. L., Campisi, J., and Deursen, J. M. V. (2014). Senescence and apoptosis : dueling or complementary cell fates ? *EMBO reports*, 15(11):1139–1153.

[Chondrogianni et al., 2015] Chondrogianni, N., Georgila, K., Kourtis, N., Tavernarakis, N., and Gonos, E. S. (2015). 20S proteasome activation promotes life span extension and resistance to proteotoxicity in Caenorhabditis elegans. *FASEB Journal*.

[Chondrogianni et al., 2008] Chondrogianni, N., Trougakos, I. P., Kletsas, D., Chen, Q. M., and Gonos, E. S. (2008). Partial proteasome inhibition in human fibroblasts triggers accelerated M1 senescence or M2 crisis depending on p53 and Rb status. *Aging Cell*, 7(5):717–732.

[Christofk et al., 2008] Christofk, H. R., Vander Heiden, M. G., Harris, M. H., Ramanathan, A., Gerszten, R. E., Wei, R., Fleming, M. D., Schreiber, S. L., and Cantley, L. C. (2008). The M2 splice isoform of pyruvate kinase is important for cancer metabolism and tumour growth. *Nature*, 452(7184):230–233.

[Collado and Serrano, 2010] Collado, M. and Serrano, M. (2010). Senescence in tumours: evidence from mice and humans. *Nature Reviews Cancer*, 10(1):51–57.

[Coomans de Brachène and Demoulin, 2016] Coomans de Brachène, A. and Demoulin, J.-B. (2016). FOXO transcription factors in cancer development and therapy. *Cellular and Molecular Life Sciences*, 73(6):1159–1172.

[Coppé et al., 2010] Coppé, J.-P., Desprez, P.-Y., Krtolica, A., and Campisi, J. (2010). The Senescence-Associated Secretory Phenotype: The Dark Side of Tumor Suppression. *Annual Review of Pathology: Mechanisms of Disease*.

[Correia-Melo et al., 2014] Correia-Melo, C., Hewitt, G., and Passos, J. F. (2014). Telomeres, oxidative stress and inflammatory factors: partners in cellular senescence? *Longevity & healthspan*, 3(1):1.

[de Souza et al., 2011] de Souza, A. C. S., Justo, G. Z., de Araújo, D. R., and Cavagis, A. D. M. (2011). Defining the molecular basis of tumor metabolism: a continuing challenge since warburgs discovery. *Cellular Physiology and Biochemistry*, 28(5):771–792.

[Dimri et al., 1995] Dimri, G. P., Leet, X., Basile, G., Acosta, M., Scorrt, G., Roskelley, C., Medrano, E. E., Linskensi, M., Rubeljii, I., Pereira-smithii, O., Peacocket, M., and Campisi, J. (1995). A biomarker that identifies senescent human cells in culture and in aging skin in vivo. 92(September):9363–9367.

[Dolivo et al., 2016] Dolivo, D., Hernandez, S., and Dominko, T. (2016). Cellular lifespan and senescence: a complex balance between multiple cellular pathways. *BioEssays*, 38:S33–S44.

[Duran et al., 2013] Duran, J., Saez, I., Gruart, A., Guinovart, J. J., and Delgado-García, J. M. (2013). Impairment in long-term memory formation and learning-dependent synaptic plasticity in mice lacking glycogen synthase in the brain. 5(December 2012):550–556.

[Fausto, 2000] Fausto, N. (2000). Liver regeneration. *Journal of hepatology*, 32:19–31.

[Favaro et al., 2012] Favaro, E., Bensaad, K., Chong, M. G., Tennant, D. A., Ferguson, D. J. P., Snell, C., Steers, G., Turley, H., Li, J. L., Günther, U. L., Buffa, F. M., McIntyre, A., and Harris, A. L. (2012). Glucose utilization via glycogen phosphorylase sustains proliferation and prevents premature senescence in cancer cells. *Cell Metabolism*, 16(6):751–764.

[Favre et al., 2008] Favre, C., Aguilar, P. S., and Carrillo, M. C. (2008). Oxidative stress and chronological aging in glycogen-phosphorylase-deleted yeast. *Free Radical Biology and Medicine*, 45(10):1446–1456.

[Fernández-Medarde and Santos, 2011] Fernández-Medarde, A. and Santos, E. (2011). Ras in cancer and developmental diseases. *Genes and Cancer*, 2(3):344–358.

[Ferrer et al., 1997] Ferrer, J. C., Baqué, S., and Guinovart, J. J. (1997). Muscle glycogen synthase translocates from the cell nucleus to the cytosol in response to glucose. *FEBS Letters*, 415(3):249–252.

[Fidler, 2003] Fidler, I. J. (2003). The pathogenesis of cancer metastasis: the'seed and soil'hypothesis revisited. *Nature Reviews Cancer*, 3(6):453.

[Fidler et al., 2010] Fidler, I. J., Balasubramanian, K., Lin, Q., Kim, S. W., and Kim, S.-J. (2010). The brain microenvironment and cancer metastasis. *Molecules and cells*, 30(2):93–98.

[Fontana et al., 2010] Fontana, L., Partridge, L., and Longo, V. D. (2010). Extending healthy life spanfrom yeast to humans. *science*, 328(5976):321–326.

[Franken et al., 2006] Franken, N. a. P., Rodermond, H. M., Stap, J., Haveman, J., and van Bree, C. (2006). Clonogenic assay of cells in vitro. *Nature protocols*, 1(5):2315–9.

[Friedman and Nunnari, 2014] Friedman, J. R. and Nunnari, J. (2014). Mitochondrial form and function. *Nature*, 505(7483):335.

[García-Rocha et al., 2001] García-Rocha, M., Roca, A., De La Iglesia, N., Baba, O., Fernández-Novell, J. M., Ferrer, J. C., and Guinovart, J. J. (2001). Intracellular distribution of glycogen synthase and glycogen in primary cultured rat hepatocytes. *Biochem. J.*, 357(1):17–24.

[Gentleman et al., 2004] Gentleman, R. C., Carey, V. J., Bates, D. M., and Others (2004). Bioconductor: Open software development for computational biology and bioinformatics. *Genome Biol*, 5(10):R80.

[Giacinti and Giordano, 2006] Giacinti, C. and Giordano, A. (2006). RB and cell cycle progression. *Oncogene*, 25(38):5220–5227.

[Gibbs et al., 2006] Gibbs, M. E., Anderson, D. G., and Hertz, L. (2006). Inhibition of glycogenolysis in astrocytes interrupts memory consolidation in young chickens. *Glia*, 54(3):214–222.

[Gitenay et al., 2014] Gitenay, D., Wiel, C., Lallet-Daher, H., Vindrieux, D., Aubert, S., Payen, L., Simonnet, H., and Bernard, D. (2014). Glucose metabolism and hexosamine pathway regulate oncogene-induced senescence. *Cell death & disease*, 5(2):e1089.

[Gomis et al., 2006] Gomis, R. R., Alarcon, C., He, W., Wang, Q., Seoane, J., Lash, A., and Massague, J. (2006). A FoxO-Smad synexpression group in human keratinocytes. *Proceedings of the National Academy of Sciences*, 103(34):12747–12752.

[Goodman et al., 1974] Goodman, M. N., Berger, N. M., and Ruderman, N. B. (1974). Glucose metabolism in rat skeletal muscle at rest: effect of starvation, diabetes, ketone bodies, and free fatty acids. *Diabetes*, 23:881–888.

[Gray et al., 2001] Gray, M. W., Burger, G., and Lang, B. F. (2001). The origin and early evolution of mitochondria. *Genome biology*, 2(6):REVIEWS1018.

[Greenberg et al., 2006] Greenberg, C., Jurczak, M., Danos, A., and Brady, M. (2006). Glycogen branches out : new perspectives on the role of glycogen metabolism in the integration of metabolic pathways. *Am J Physiol Endocrinol Metab*, 291(62):1–8.

[Gusarov et al., 2017] Gusarov, I., Pani, B., Gautier, L., Smolentseva, O., Eremina, S., Shamovsky, I., Katkova-zhukotskaya, O., Mironov, A., and Nudler, E. (2017). Glycogen controls Caenorhabditis elegans lifespan and resistance to oxidative stress. *Nature Communications*, 8(May 2016):1–12.

[Hammond et al., 1978] Hammond, K. D., Balinsky, D., Livers, H., and Cultures, H. C. (1978). Activities of Key Gluconeogenic Enzymes and Glycogen Synthase in Rat and Human Livers , Hepatomas , and Hepatoma Cell Cultures Activities of Key Gluconeogenic Enzymes and Glycogen Synthase in Rat. 1(MAY):1317–1322.

[Hanahan and Weinberg, 2000] Hanahan, D. and Weinberg, R. A. (2000). The Hallmarks of Cancer. *Cell*, 100:57–70.

[Hanahan and Weinberg, 2011] Hanahan, D. and Weinberg, R. A. (2011). Hallmarks of Cancer : The Next Generation. *Cell*, 144(5):646–674.

[Harley et al., 1990] Harley, C. B., Futcher, B., and Greider, C. W. (1990). Telomeres shorten during ageing of human fibroblasts. *Nature*, 345:458–460.

[Harman, 1972] Harman, D. (1972). The biologic clock: the mitochondria? *Journal of the American Geriatrics Society*, 20(4):145–147.

[Harper, 2014] Harper, S. (2014). Economic and social implications of aging societies. *Science*, 346(6209):587–591.

[Hata et al., 2007] Hata, S., Namae, M., and Nishina, H. (2007). Liver development and regeneration: From laboratory study to clinical therapy. *Development, Growth & Differentiation*, 49(2):163–170.

[Hayflick, 1965] Hayflick, L. (1965). The limited in vitro lifetime of human diploid cell strains. *Experimental cell research*, 37(3):614–636.

[Hayflick and Moorhead, 1961] Hayflick, L. and Moorhead, P. (1961). The serial cultivation of human diploid cell strains. *Experimental Cell Research*, 25(3):585–621.

[Heindryckx et al., 2009] Heindryckx, F., Colle, I., and Vlierberghe, H. V. (2009). Experimental mouse models for hepatocellular carcinoma research. *Int. J. Exp. Path*, 90:367–386.

[Helyer and Petrell, 1978] Helyer, B. J. and Petrell, M. (1978). Cytoplasmic inclusions in spontaneous hepatomas of cba/h-t6t6 mice. histochemistry and electron microscopy. *Journal of the National Cancer Institute*, 60(4):861–869.

[Houtkooper et al., 2011] Houtkooper, R. H., Argmann, C., Houten, S. M., Cantó, C., Jeninga, E. H., Andreux, P. A., Thomas, C., Doenlen, R., Schoonjans, K., and Auwerx, J. (2011). The metabolic footprint of aging in mice. *Scientific Reports*, 1(1):134.

[Hsu and Sabatini, 2008] Hsu, P. P. and Sabatini, D. M. (2008). Cancer cell metabolism: Warburg and beyond. *Cell*, 134(5):703–707.

[Iozzo and Sanderson, 2011] Iozzo, R. V. and Sanderson, R. D. (2011). Proteoglycans in cancer biology, tumour microenvironment and angiogenesis. *Journal of Cellular and Molecular Medicine*, 15(5):1013–1031.

[Irimia et al., 2010] Irimia, J. M., Meyer, C. M., Peper, C. L., Zhai, L., Bock, C. B., Previs, S. F., McGuinness, O. P., DePaoli-Roach, A., and Roach, P. J. (2010). Impaired glucose tolerance and predisposition to the fasted state in liver glycogen synthase knock-out mice. *Journal of Biological Chemistry*, 285(17):12851–12861.

[Jeon et al., 2012] Jeon, S.-M., Chandel, N. S., and Hay, N. (2012). AMPK regulates NADPH homeostasis to promote tumour cell survival during energy stress. *Nature*, 485(7400):661–5.

[Jones et al., 2005] Jones, R. G., Plas, D. R., Kubek, S., Buzzai, M., Mu, J., Xu, Y., Birnbaum, M. J., and Thompson, C. B. (2005). AMP-activated protein kinase induces a p53-dependent metabolic checkpoint. *Molecular Cell*, 18(3):283–293.

[Jurk et al., 2012] Jurk, D., Wang, C., Miwa, S., Maddick, M., Korolchuk, V., Tsolou, A., Gonos, E. S., Thrasivoulou, C., Jill Saffrey, M., Cameron, K., and von Zglinicki, T. (2012). Postmitotic neurons develop a p21-dependent senescence-like phenotype driven by a DNA damage response. *Aging Cell*, 11(6):996–1004.

[Kapeta et al., 2010] Kapeta, S., Chondrogianni, N., and Gonos, E. S. (2010). Nuclear Erythroid Factor 2-mediated Proteasome Activation Delays Senescence in Human Fibroblasts * . 285(11):8171–8184.

[Kaplon et al., 2013] Kaplon, J., Zheng, L., Meissl, K., Chaneton, B., Selivanov, V. A., Mackay, G., and Der, S. H. V. (2013). A key role for mitochondrial gatekeeper pyruvate dehydrogenase in oncogene-induced senescence. *Nature*, pages 2–7.

[Kaul et al., 2012] Kaul, Z., Cesare, A. J., Huschtscha, L. I., Neumann, A. A., and Reddel, R. R. (2012). Five dysfunctional telomeres predict onset of senescence in human cells. *EMBO reports*, 13(1):52–59.

[Kong et al., 2012] Kong, X., Feng, D., Wang, H., Hong, F., Bertola, A., Wang, F. S., and Gao, B. (2012). Interleukin-22 induces hepatic stellate cell senescence and restricts liver fibrosis in mice. *Hepatology*, 56(3):1150–1159.

[Kousteni, 2012] Kousteni, S. (2012). FoxO1, the transcriptional chief of staff of energy metabolism. *Bone*, 50(2):437–443.

[Krstic et al., 2015] Krstic, J., Trivanovi, T., Mojsilovic, S., and Santibanez, J. F. (2015). Transforming Growth Factor-Beta and Oxidative Stress Interplay : Implications in Tumorigenesis and Cancer Progression. *Oxidative Medicine and Cellular Longevity*, 2015.

[Kuilman and Peeper, 2009] Kuilman, T. and Peeper, D. S. (2009). Senescence-messaging secretome: SMS-ing cellular stress. *Nature Reviews Cancer*, 9(2):81–94.

[Land et al., 1983] Land, H., Parada, L. F., and Weinberg, R. a. (1983). Tumorigenic conversion of primary embryo fibroblasts requires at least two cooperating oncogenes. *Nature*, 53(9):1689–1699.

[Lea et al., 1972] Lea, M. A., Murphy, P., and Morris, H. P. (1972). Glycogen Metabolism in Regenerating Liver and Liver Neoplasms. *Cancer Research*, 32(1):61–66.

[Lee and Young, 2013] Lee, T. I. and Young, R. A. (2013). Transcriptional regulation and its misregulation in disease. *Cell*, 152(6):1237–1251.

[Lin et al., 2001] Lin, S. S., Manchester, J. K., and Gordon, J. I. (2001). Enhanced Gluconeogenesis and Increased Energy Storage as Hallmarks of Aging in Saccharomyces cerevisiae * . 276(38):36000–36007.

[Liu and Desai, 2015] Liu, R. M. and Desai, L. P. (2015). Reciprocal regulation of TGF-β and reactive oxygen species: A perverse cycle for fibrosis. *Redox Biology*, 6:565–577.

[López-otín et al., 2013] López-otín, C., Blasco, M. A., Partridge, L., and Serrano, M. (2013). Europe PMC Funders Group The Hallmarks of Aging. 153(6):1194–1217.

[Massagué, 2008] Massagué, J. (2008). TGFβ in Cancer. *Cell*, 134(2):215–230.

[Mayevsky, 2009] Mayevsky, A. (2009). Mitochondrial function and energy metabolism in cancer cells: Past overview and future perspectives.

[Meléndez et al., 1998] Meléndez, R., Meléndez-Hevia, E., Mas, F., Mach, J., and Cascante, M. (1998). Physical constraints in the synthesis of glycogen that influence its structural homogeneity: a two-dimensional approach. *Biophysical journal*, 75(1):106–114.

[Michalopoulos, 2007] Michalopoulos, G. K. (2007). Liver Regeneration. *Journal of Cell Physiology*, 213(2):286–300.

[Mitchell and Willenbring, 2008] Mitchell, C. and Willenbring, H. (2008). A reproducible and well-tolerated method for 2/3 partial hepatectomy in mice. *Nature Protocols*, 3(7):1167–1170.

[Mohammed and Khokha, 2005] Mohammed, F. F. and Khokha, R. (2005). Thinking outside the cell: Proteases regulate hepatocyte division. *Trends in Cell Biology*, 15(10):555–563.

[Mokrỳ and Němecek, 1995] Mokrỳ, J. and Němecek, S. (1995). Immunohistochemical detection of proliferative cells. *Sbornik vedeckych praci Lekarske fakulty Karlovy university v Hradci Kralove*, 38(3):107–113.

[Munoz-Espin et al., 2013] Munoz-Espin, D., Canamero, M., Maraver, A., Gomez-Lopez, G., Contreras, J., Murillo-Cuesta, S., Rodriguez-Baeza, A., Varela-Nieto, I., Ruberte, J., Collado, M., and Serrano, M. (2013). Programmed cell senescence during mammalian embryonic development. *Cell*, 155(5).

[Munoz-Espin and Serrano, 2014] Munoz-Espin, D. and Serrano, M. (2014). Cellular senescence: from physiology to pathology. *Nature reviews. Molecular cell biology*, 15(7):482–496.

[Nakatani et al., 2001] Nakatani, T., Roy, G., Fujimoto, N., Asahara, T., and Ito, A. (2001). Sex hormone dependency of diethylnitrosamine-induced liver tumors in mice and chemoprevention by leuprorelin. *Cancer Science*, 92(3):249–256.

[Newgard et al., 1989] Newgard, C. B., Hwang, P. K., and Fletterick, R. J. (1989). The family of glycogen phosphorylases: structure and functio. *Critical reviews in biochemistry and molecular biology*, 24(1):69–99.

[Nigam and Cantero, 1973] Nigam, V. N. and Cantero, A. (1973). Polysaccharides in cancer. In *Advances in cancer research*, volume 16, pages 1–96. Elsevier.

[Nita and Grzybowski, 2016] Nita, M. and Grzybowski, A. (2016). The role of the reactive oxygen species and oxidative stress in the pathomechanism of the age-related ocular diseases and other pathologies of the anterior and posterior eye segments in adults. *Oxidative Medicine and Cellular Longevity*, 2016.

[Northridge, 2012] Northridge, M. E. (2012). The strengths of an aging society.

[Núñez et al., 2017] Núñez, K. G., Gonzalez-Rosario, J., Thevenot, P. T., and Cohen, A. J. (2017). Cyclin d1 in the liver: Role of noncanonical signaling in liver steatosis and hormone regulation. *The Ochsner Journal*, 17(1):56–65.

[Obel et al., 2012] Obel, L. F., Müller, M. S., Walls, A. B., Sickmann, H. M., Bak, L. K., Waagepetersen, H. S., and Schousboe, A. (2012). Brain glycogen - new perspectives on its metabolic function and regulation at the subcellular level. *Frontiers in Neuroenergetics*, 4(MAR):1–15.

[Ogryzko et al., 1996] Ogryzko, V. V., Hirai, T. H., Russanova, V. R., and Barbie, D. A. (1996). Human fibroblast commitment to a senescence-like state in response to histone deacetylase inhibitors is cell cycle dependent . Human Fibroblast Commitment to a Senescence-Like State in Response to Histone Deacetylase Inhibitors Is Cell Cycle Dependent. 16(9):5210–5218.

[Okada et al., 2004] Okada, S. F., O'Neal, W. K., Huang, P., Nicholas, R. A., Ostrowski, L. E., Craigen, W. J., Lazarowski, E. R., and Boucher, R. C. (2004). Voltage-dependent anion channel-1 (vdac-1) contributes to atp release and cell volume regulation in murine cells. *The Journal of general physiology*, 124(5):513–526.

[Pal and Tyler, 2016] Pal, S. and Tyler, J. K. (2016). Epigenetics and aging. *Science advances*, 2(7):e1600584.

[Palmer et al., 2015] Palmer, A. K., Tchkonia, T., LeBrasseur, N. K., Chini, E. N., Xu, M., and Kirkland, J. L. (2015). Cellular senescence in type 2 diabetes: A therapeutic opportunity. *Diabetes*, 64(7):2289–2298.

[Parks and Garden, 2001] Parks, R. W. and Garden, O. J. (2001). Liver resection for cancer. *World Journal of Gastroenterology*, 7(6):766–771.

[Patil et al., 2014] Patil, M., Pabla, N., and Dong, Z. (2014). Checkpoint kinase 1 in DNA damage response and cell cycle regulation. 70(21):4009–4021.

[Patra and Hay, 2014] Patra, K. C. and Hay, N. (2014). The pentose phosphate pathway and cancer. *Trends in Biochemical Sciences*, 39(8):347–354.

[Pavlides et al., 2009] Pavlides, S., Whitaker-Menezes, D., Castello-Cros, R., Flomenberg, N., Witkiewicz, A. K., Frank, P. G., Casimiro, M. C., Wang, C., Fortina, P., Addya, S., Pestell, R. G., Martinez-Outschoorn, U. E., Sotgia, F., and Lisanti, M. P. (2009). The reverse Warburg effect: Aerobic glycolysis in cancer associated fibroblasts and the tumor stroma. *Cell Cycle*, 8(23):3984–4001.

[Pederson et al., 2004] Pederson, B. A., Chen, H., Schroeder, J. M., Shou, W., DePaoli-Roach, A. A., and Roach, P. J. (2004). Abnormal cardiac development in the absence of heart glycogen. *Molecular and cellular biology*, 24(16):7179–87.

[Pelletier et al., 2018] Pelletier, J., Thomas, G., and Volarević, S. (2018). Ribosome biogenesis in cancer: new players and therapeutic avenues. *Nature Reviews Cancer*, 18(1):51.

[Pescador et al., 2010] Pescador, N., Villar, D., Cifuentes, D., Garcia-rocha, M., Ortiz-barahona, A., Cuevas, Y., Saez-morales, D., Garcia, M. L., Vazquez, S., and Ordon, A. (2010). Hypoxia Promotes Glycogen Accumulation through Hypoxia Inducible Factor (HIF) -Mediated Induction of Glycogen Synthase 1. *PLoS ONE*, 5(3).

[Printen, 1997] Printen, J. A. (1997). PTG, a Protein Phosphatase 1-Binding Protein with a Role in Glycogen Metabolism. *Science*, 275(5305):1475–1478.

[Rath et al., 2000] Rath, V. L., Ammirati, M., Danley, D. E., Ekstrom, J. L., Gibbs, E. M., Hynes, T. R., Mathiowetz, A. M., McPherson, R. K., Olson, T. V., Treadway, J. L., et al. (2000). Human liver glycogen phosphorylase inhibitors bind at a new allosteric site. *Chemistry & biology*, 7(9):677–682.

[Roberson et al., 2005] Roberson, R. S., Kussick, S. J., Vallieres, E., Chen, S.-y. J., and Wu, D. Y. (2005). Escape from Therapy-Induced Accelerated Cellular Senescence in p53-Null Lung Cancer Cells and in Human Lung Cancers. *Cancer Research*, 65(7):2795–2803.

[Romá-Mateo et al., 2012] Romá-Mateo, C., Sanz, P., and Gentry, M. S. (2012). Deciphering the role of malin in the lafora progressive myoclonus epilepsy. *IUBMB Life*, 64(10):801–808.

[Rooney et al., 2015] Rooney, J., Ryde, I., Sanders, L., Howlett, E., Germ, K., Mayer, G., Greenamyre, J., and Meyer, J. (2015). PCR Based Determination of Mitochondrial DNA Copy Number in Multiple Species. *Methods Mol. Biol.*, pages 23–38.

[Ros et al., 2009] Ros, S., García-Rocha, M., Domínguez, J., Ferrer, J. C., and Guinovart, J. J. (2009). Control of liver glycogen synthase activity and intracellular distribution by phosphorylation. *Journal of Biological Chemistry*, 284(10):6370–6378.

[Rossell, 2009] Rossell, D. (2009). GaGa: A parsimonious and flexible model for differential expression analysis. *Annals of Applied Statistics*, 3(3):1035–1051.

[Rousset et al., 1981] Rousset, M., Zweibaum, A., and Fogh, J. (1981). Presence of glycogen and growth-related variations in 58 cultured human tumor cell lines of various tissue origins. *Cancer Research*, 41(March):1165–1171.

[Saez et al., 2014] Saez, I., Duran, J., Sinadinos, C., Beltran, A., Yanes, O., Tevy, M. F., Martínez-Pons, C., Milán, M., and Guinovart, J. J. (2014). Neurons have an active glycogen metabolism that contributes to tolerance to hypoxia. *Journal of Cerebral Blood Flow & Metabolism*, 34(6):945–955.

[Salama et al., 2014] Salama, R., Sadaie, M., Hoare, M., and Narita, M. (2014). Cellular senescence and its effector programs. *Genes and Development*, 28:99–114.

[Salminen and Kaarniranta, 2012] Salminen, A. and Kaarniranta, K. (2012). Amp-activated protein kinase (ampk) controls the aging process via an integrated signaling network. *Ageing research reviews*, 11(2):230–241.

[Salmon and Flatt, 1985] Salmon, D. and Flatt, J. (1985). Effect of dietary fat content on the incidence of obesity among ad libitum fed mice. *International journal of obesity*, 9(6):443–449.

[Samanta and Datta, 2012] Samanta, D. and Datta, P. (2012). Alterations in the Smad pathway in human cancers. *Frontiers in Bioscience*, 1(17):1281–1293.

[Sazanov, 2015] Sazanov, L. A. (2015). A giant molecular proton pump: structure and mechanism of respiratory complex I. *Nature Reviews Molecular Cell Biology*, 16(6):375–388.

[Schmidt et al., 2002] Schmidt, M., Fernandez de Mattos, S., van der Horst, A., Klompmaker, R., Kops, G. J. P. L., Lam, E. W.-F., Burgering, B. M. T., and Medema, R. H. (2002). Cell cycle inhibition by FoxO forkhead transcription factors involves downregulation of cyclin D. *Molecular and cellular biology*, 22(22):7842–52.

[Schulze and Harris, 2012] Schulze, A. and Harris, A. L. (2012). How cancer metabolism is tuned for proliferation and vulnerable to disruption.

[Seo et al., 2008] Seo, Y. H., Jung, H. J., Shin, H. T., Kim, Y. M., Yim, H., Chung, H. Y., Lim, I. K., and Yoon, G. (2008). Enhanced glycogenesis is involved in cellular senescence via GSK3/GS modulation. *Aging Cell*, 7(6):894–907.

[Seoane et al., 2004] Seoane, J., Le, H.-v., Shen, L., Anderson, S. A., and Massague, J. (2004). Integration of Smad and Forkhead Pathways in the Control of Neuroepithelial and Glioblastoma Cell Proliferation. *Cell*, 117:211–223.

[Serrano et al., 1997] Serrano, M., Lin, A. W., McCurrach, M. E., Beach, D., and Lowe, S. W. (1997). Oncogenic ras provokes premature cell senescence associated with accumulation of p53 and p16(INK4a). *Cell*, 88(5):593–602.

[Seyfried and Huysentruyt, 2013] Seyfried, T. N. and Huysentruyt, L. C. (2013). On the origin of cancer metastasis. *Critical reviews in oncogenesis*, 18(1-2):43.

[Shahwan et al., 2005] Shahwan, A., Farrell, M., and Delanty, N. (2005). Progressive myoclonic epilepsies: a review of genetic and therapeutic aspects. *Lancet Neurol*, 4(4):239–248.

[Shanmugam et al., 2009] Shanmugam, M., Mcbrayer, S. K., and Rosen, S. T. (2009). Targeting the Warburg Effect in Hematological Malignancies: from PET to Therapy. *Current Opinion in Oncology*, 21(6):531–536.

[Shulman and Rothman, 2001] Shulman, R. G. and Rothman, D. L. (2001). The "glycogen shunt" in exercising muscle: A role for glycogen in muscle energetics and fatigue. *Proceedings of the National Academy of Sciences of the United States of America*, 98(2):457–461.

[Silljé et al., 1999] Silljé, H. H. W., Paalman, J. W. G., Ter Schure, E. G., Olsthoorn, S. Q. B., Verkleij, A. J., Boonstra, J., and Verrips, C. T. (1999). Function of trehalose and glycogen in cell cycle progression and cell viability in Saccharomyces cerevisiae. *Journal of Bacteriology*, 181(2):396–400.

[Sinadinos et al., 2014] Sinadinos, C., Valles-Ortega, J., Boulan, L., Solsona, E., Tevy, M. F., Marquez, M., Duran, J., Lopez-Iglesias, C., Calbó, J., Blasco, E., Pumarola, M., Milán, M., and Guinovart, J. J. (2014). Neuronal glycogen synthesis contributes to physiological aging. *Aging Cell*, 13(5):935–945.

[Smith and Pereira-smith, 1996] Smith, J. R. and Pereira-smith, O. M. (1996). Replicative Senescence : Implications for in Vivo Aging and Tumor Suppression. 273(5271):63–67.

[Stapleton et al., 2010] Stapleton, D., Nelson, C., Parsawar, K., Mcclain, D., Gilbert, R., Barker, E., Rudd, B., Brown, K., Hendrix, W., Donnell, P. O., and Parker, G. (2010). Analysis of hepatic glycogen-associated proteins. *Proteomics*, 10(12):2320–2329.

[Stincone et al., 2015] Stincone, A., Prigione, A., Cramer, T., Wamelink, M., Campbell, K., Cheung, E., Olin-Sandoval, V., Grüning, N.-M., Krüger, A., Tauqeer Alam, M., et al. (2015). The return of metabolism: biochemistry and physiology of the pentose phosphate pathway. *Biological Reviews*, 90(3):927–963.

[Storer et al., 2013] Storer, M., Mas, A., Robert-Moreno, A., Pecoraro, M., Ortells, M. C., Di Giacomo, V., Yosef, R., Pilpel, N., Krizhanovsky, V., Sharpe, J., and Keyes, W. M. (2013). XSenescence is a developmental mechanism that contributes to embryonic growth and patterning. *Cell*, 155(5):1119–1130.

[Sullivan et al., 2012] Sullivan, M. A., OConnor, M. J., Umana, F., Roura, E., Jack, K., Stapleton, D. I., and Gilbert, R. G. (2012). Molecular insights into glycogen α-particle formation. *Biomacromolecules*, 13(11):3805–3813.

[Tagliabracci et al., 2008] Tagliabracci, V. S., Girard, J. M., Segvich, D., Meyer, C., Turnbull, J., Zhao, X., Minassian, B. A., DePaoli-Roach, A. A., and Roach, P. J. (2008). Abnormal metabolism of glycogen phosphate as a cause for Lafora disease. *Journal of Biological Chemistry*, 283(49):33816–33825.

[Tagliabracci et al., 2011] Tagliabracci, V. S., Heiss, C., Karthik, C., Contreras, C. J., Glushka, J., Ishihara, M., Azadi, P., Hurley, T. D., Depaoli-Roach, A. A., and Roach, P. J. (2011). Phosphate incorporation during glycogen synthesis and Lafora disease. *Cell Metabolism*, 13(3):274–282.

[Tagliabracci et al., 2007] Tagliabracci, V. S., Turnbull, J., Wang, W., Girard, J.-M., Zhao, X., Skurat, A. V., Delgado-Escueta, A. V., Minassian, B. A., Depaoli-Roach, A. A., and Roach, P. J. (2007). Laforin is a glycogen phosphatase, deficiency of which leads to elevated phosphorylation of glycogen in vivo. *Proceedings of the National Academy of Sciences of the United States of America*, 104(49):19262–6.

[Takahashi et al., 1999] Takahashi, S., Satomi, a., Yano, K., Kawase, H., Tanimizu, T., Tuji, Y., Murakami, S., and Hirayama, R. (1999). Estimation of glycogen levels in human colorectal cancer tissue: relationship with cell cycle and tumor outgrowth. *Journal of gastroenterology*, 34(4):474–80.

[Taub, 2004] Taub, R. (2004). Liver regeneration: from myth to mechanism. *Nature Reviews Molecular Cell Biology*, 5(10):836–847.

[Thannickal and Fanburg, 2000] Thannickal, V. J. and Fanburg, B. L. (2000). Reactive oxygen species in cell signaling. *American Journal of Physiology-Lung Cellular and Molecular Physiology*, 279(6):L1005–L1028.

[Thorgeirsson, 1996] Thorgeirsson, S. (1996). Hepatic stem cells in liver regeneration. *The FASEB Journal*, 10(11):1249–1256.

[Tremain et al., 2000] Tremain, R., Marko, M., Kinnimulki, V., Ueno, H., Bottinger, E., and Glick, A. (2000). Defects in TGFβ signaling overcome senescence of mouse keratinocytes expressing v-rasHa. *Oncogene*, 19(13):1698–1709.

[Tsukuma et al., 1993] Tsukuma, H., Hiyama, T., Tanaka, S., Nakao, M., Yabuuchi, T., Kitamura, T., Nakanishi, K., Fujimoto, I., Inoue, A., Yamazaki, H., et al. (1993). Risk factors for hepatocellular carcinoma among patients with chronic liver disease. *New England journal of medicine*, 328(25):1797–1801.

[Van Der Vos and Coffer, 2008] Van Der Vos, K. E. and Coffer, P. J. (2008). FOXO-binding partners: It takes two to tango. *Oncogene*, 27(16):2289–2299.

[van der Windt et al., 2012] van der Windt, G. J., Everts, B., Chang, C.-H., Curtis, J. D., Freitas, T. C., Amiel, E., Pearce, E. J., and Pearce, E. L. (2012). Mitochondrial respiratory capacity is a critical regulator of cd8+ t cell memory development. *Immunity*, 36(1):68–78.

[Vander Heiden et al., 2009] Vander Heiden, M., Cantley, L., and Thompson, C. (2009). Understanding the Warburg effect: The metabolic requirements of cell proliferation. *Science*, 324(5930):1029–1033.

[Ventura et al., 2007] Ventura, A., Kirsch, D. G., McLaughlin, M. E., Tuveson, D. A., Grimm, J., Lintault, L., Newman, J., Reczek, E. E., Weissleder, R., and Jacks, T. (2007). Restoration of p53 function leads to tumour regression in vivo. *Nature*, 445(7128):661–665.

[Wamelink et al., 2008] Wamelink, M., Struys, E., and Jakobs, C. (2008). The biochemistry, metabolism and inherited defects of the pentose phosphate pathway: a review. *Journal of inherited metabolic disease*, 31(6):703–717.

[Wang et al., 2003] Wang, W., Yang, X., de Silanes, I. L., Carling, D., and Gorospe, M. (2003). Increased amp: Atp ratio and amp-activated protein kinase activity during cellular senescence linked to reduced hur function. *Journal of Biological Chemistry*, 278(29):27016–27023.

[Warburg, 1956] Warburg, O. (1956). On the Origin of Cancer Cells On the Origin of Cance. *Source: Science, New Series*, 123(123):309–314.

[Ward and Thompson, 2012] Ward, P. S. and Thompson, C. B. (2012). Metabolic Reprogramming: A Cancer Hallmark Even Warburg Did Not Anticipate.

[Wiley et al., 2016] Wiley, C. D., Velarde, M. C., Lecot, P., Liu, S., Sarnoski, E. A., Freund, A., Shirakawa, K., Lim, H. W., Davis, S. S., Ramanathan, A., Gerencser, A. A., Verdin, E., and Campisi, J. (2016). Mitochondrial dysfunction induces senescence with a distinct secretory phenotype. *Cell Metabolism*, 23(2):303–314.

[Wong, 2011] Wong, R. S. (2011). Apoptosis in cancer: from pathogenesis to treatment. *Journal of Experimental & Clinical Cancer Research*, 30:87.

[Wu et al., 2007] Wu, C.-H., van Riggelen, J., Yetil, A., Fan, A. C., Bachireddy, P., and Felsher, D. W. (2007). Cellular senescence is an important mechanism of tumor regression upon c-Myc inactivation. *Proceedings of the National Academy of Sciences*, 104(32):13028–13033.

[Yang et al., 2009] Yang, J., Wahdan-Alaswad, R., and Danielpour, D. (2009). Critical role of Smad2 in tumor suppression and transforming growth factor-beta-induced apoptosis of prostate epithelial cells. *Cancer research*, 69(6):2185–90.

[Yang et al., 2010] Yang, L., Pang, Y., and Moses, H. L. (2010). Tgf-β and immune cells: an important regulatory axis in the tumor microenvironment and progression. *Trends in immunology*, 31(6):220–227.

[Zhang and Cuervo, 2008] Zhang, C. and Cuervo, A. M. (2008). Restoration of chaperone-mediated autophagy in aging liver improves cellular maintenance and hepatic function. *Nature medicine*, 14(9):959.

[Zhu et al., 2009] Zhu, A., Romero, R., and Petty, H. R. (2009). An enzymatic fluorimetric assay for glucose-6-phosphate: Application in an in vitro Warburg-like effect. *Analytical Biochemistry*, 388(1):97–101.

[Zirin et al., 2013] Zirin, J., Nieuwenhuis, J., and Perrimon, N. (2013). Role of Autophagy in Glycogen Breakdown and Its Relevance to Chloroquine Myopathy. 11(11).

[Zois et al., 2014] Zois, C. E., Favaro, E., and Harris, A. L. (2014). Glycogen metabolism in cancer. *Biochemical Pharmacology*, 92(1):3–11.

[Zois and Harris, 2016] Zois, C. E. and Harris, A. L. (2016). Glycogen metabolism has a key role in the cancer microenvironment and provides new targets for cancer therapy. *Journal of Molecular Medicine*, 94(2):137–154.

[Zong et al., 2016] Zong, W.-X., Rabinowitz, J. D., and White, E. (2016). Molecular Cell Review Mitochondria and Cancer. *Molecular Cell*, 61:667–676.

[Zou et al., 2012] Zou, Y., Bao, Q., Kumar, S., Hu, M., Wang, G. Y., and Dai, G. (2012). Four waves of hepatocyte proliferation linked with three waves of hepatic fat accumulation during partial hepatectomy-induced liver regeneration. *PLoS ONE*, 7(2).

[Zwerschke et al., 2003] Zwerschke, W., Mazurek, S., Ockl, P. S. T., Utter, E. H., and Eigenbrodt, E. (2003). Metabolic analysis of senescent human fibroblasts reveals a role for AMP in cellular senescence. 411:403–411.